# Optimal Control and Multibody Dynamic Modelling of Human Musculoskeletal Systems

by

Mohammad Sharif Shourijeh

A thesis
presented to the University of Waterloo
in fulfillment of the
thesis requirement for the degree of
Doctor of Philosophy
in
Systems Design Engineering

Waterloo, Ontario, Canada, 2013

I hereby declare that I am the sole author of this thesis. This is a true copy of the thesis, including any required final revisions, as accepted by my examiners.

I understand that my thesis may be made electronically available to the public.

**Abstract**

Musculoskeletal dynamics is a branch of biomechanics that takes advantage of interdisciplinary models to describe the relation between muscle actuators and the corresponding motions of the human body. Muscle forces play a principal role in musculoskeletal dynamics. Unfortunately, these forces cannot be measured non-invasively. Measuring surface EMGs as a non-invasive technique is recognized as a surrogate to invasive muscle force measurement; however, these signals do not reflect the muscle forces accurately. Instead of measurement, mathematical modelling of the musculoskeletal dynamics is a well-established tool to simulate, predict and analyse human movements. Computer simulations have been used to estimate a variety of variables that are difficult or impossible to measure directly, such as joint reaction forces, muscle forces, metabolic energy consumption, and muscle recruitment patterns.

Musculoskeletal dynamic simulations can be divided into two branches: inverse and forward dynamics. Inverse dynamics is the approach in which net joint moments and/or muscle forces are calculated given the measured or specified kinematics. It is the most popular simulation technique used to study human musculoskeletal dynamics. The major disadvantage of inverse dynamics is that it is not predictive and can rarely be used in the cause-effect interpretations. In contrast with inverse dynamics, forward dynamics can be used to determine the human body movement when it is driven by known muscle forces.

The musculoskeletal system (MSS) is dynamically under-determinate, i.e., the number of muscles is more than the degrees of freedom (dof) of the system. This redundancy will lead to infinite solutions of muscle force sets, which implies that there are infinite ways of recruiting different muscles for a specific motion. Therefore, there needs to be an extra criterion in order to resolve this issue. Optimization has been widely used for solving the redundancy of the force-sharing problem. Optimization is considered as the missing consideration in the dynamics of the MSS such that, once appended to the under-determinate problem, "human-like" movements will be acquired. "Human-like" implies that the human body tends to minimize a criterion during a movement, e.g., muscle fatigue or metabolic

energy. It is commonly accepted that using those criteria, within the optimization necessary in the forward dynamic simulations, leads to a reasonable representation of real human motions.

In this thesis, optimal control and forward dynamic simulation of human musculoskeletal systems are targeted. Forward dynamics requires integration of the differential equations of motion of the system, which takes a considerable time, especially within an optimization framework. Therefore, computationally efficient models are required. Musculoskeletal models in this thesis are implemented in the symbolic multibody package MapleSim® that uses Maple® as the leverage. MapleSim® generates the equations of motion governing a multibody system automatically using linear graph theory. These equations will be simplified and highly optimized for further simulations taking advantage of symbolic techniques in Maple®. The output codes are the best form for the equations to be applied in optimization-based simulation fields, such as the research area of this thesis.

The specific objectives of this thesis were to develop frameworks for such predictive simulations and validate the estimations. Simulating human gait motion is set as the end goal of this research. To successfully achieve that, several intermediate steps are taken prior to gait modelling. One big step was to choose an efficient strategy to solve the optimal control and muscle redundancy problems. The optimal control techniques are benchmarked on simpler models, such as forearm flexion/extension, to study the efficacy of the proposed approaches more easily. Another major step to modelling gait is to create a high-fidelity foot-ground contact model. The foot contact model in this thesis is based on a nonlinear volumetric approach, which is able to generate the experimental ground reaction forces more effectively than the previously used models.

Although the proposed models and approaches showed strong potential and capability, there is still room for improvement in both modelling and validation aspects. These cutting-edge future works can be followed by any researcher working in the optimal control and forward dynamic modelling of human musculoskeletal systems.

**Acknowledgements**

I would like to thank my supervisor, Professor John McPhee who guided me throughout this work.

I'm also grateful to Motion Research Group past and present researchers who helped me push my research ahead whenever it was stuck.

I must also acknowledge MapleSoft for valuable discussions and meetings.

## Dedication

To my family...

# Table of Contents

# List of Tables

# List of Figures

# Nomenclature

| | |
|---|---|
| $\alpha_p$ | muscle fiber pennation angle |
| $\bar{f}^{ce}(l)$ | normalized force-length relationship for contractile element (CE) |
| $\bar{f}^{ce}(v)$ | normalized force-velocity relationship for CE |
| $\boldsymbol{\lambda}$ | column matrix of Lagrange multipliers |
| $\boldsymbol{\Phi}$ | column matrix of kinematic constraints |
| $\boldsymbol{\Phi_q}$ | Jacobian matrix |
| $\Delta$ | time shift in the Fourier series |
| $\delta$ | deformation |
| $\dot{\delta}$ | rate of deformation |
| $\dot{A}$ | muscle activation heat rate |
| $\dot{B}$ | muscle basal metabolic rate |
| $\dot{E}$ | rate of metabolic energy consumption |
| $\dot{H}$ | muscle heat rate |

$\dot{h}$ muscle heat rate per unit mass

$\dot{h}_A$ muscle activation heat rate per unit mass

$\dot{h}_M$ muscle maintenance heat rate per unit mass

$\dot{h}_{SL}$ muscle shortening/lengthening heat rate per unit mass

$\dot{M}$ muscle maintenance heat rate

$\dot{M}_{fast}$ a parameter in the maintenance heat rate

$\dot{M}_{slow}$ a parameter in the maintenance heat rate

$\dot{S}$ muscle shortening/lengthening heat rate

$\epsilon^t$ tendon strain

$\epsilon^t_{toe}$ tendon characteristic threshold

$\epsilon^m_0$ passive muscle strain

$\epsilon^t_0$ tendon characteristic strain

$\epsilon_{HE}$ constraint violation tolerance for hyper-extension in gait

$\epsilon_{per}$ constraint violation tolerance for gait periodicity

$\epsilon_{symP}$ constraint tolerance for gait bilateral symmetry condition

$\epsilon_{tr}$ tracking constraint tolerance in optimization

$\eta$ nonlinearity exponent of the foundation in the hyper-volumetric contact model

$\Gamma_i$ share of muscle $i$ in the net muscle moment

$\hat{f}$ normalized asymptotic eccentric force in the muscle model

| | |
|---|---|
| $\lambda$ | Lagrange multiplier |
| $\mathcal{H}$ | nonlinearity exponent of the volume in the hyper-volumetric contact model |
| $\mathcal{L}$ | Lagrangian |
| $\mu$ | weighting factor in the augmented objective function |
| $\mu_f$ | friction asymptotic coefficient |
| $\nabla$ | gradient |
| $\nabla^2$ | Hessian |
| $\omega_d$ | desired angular speed |
| $\phi_A$ | ankle joint angle |
| $\phi_H$ | hip joint angle |
| $\phi_K$ | knee joint angle |
| $\phi_P$ | phalangeal joint angle |
| $\phi_T$ | torso orientation |
| $\phi_{df}$ | decay function in the activation heat rate |
| $\psi$ | difference between the simulated and desired generalized coordinate |
| $\psi_H$ | a variable in the maintenance heat rate |
| $\rho_m$ | muscle density |
| $\sigma_m$ | muscle specific tension |
| $\tau$ | motion period |

$\tau_\phi$ a decay time constant in the activation heat rate

$\tau_{fall}$ fall time constant in activation dynamics

$\tau_{rise}$ rise time constant in activation dynamics

$\mathbf{M}$ mass matrix

$\mathbf{Q}$ column matrix of quadratic velocity terms and generalized forces

$\mathbf{q}$ column matrix of generalized coordinates

$\mathbf{Q}^{(c)}$ reaction forces corresponding to the kinematic constraints

$\tilde{f}^t$ tendon force normalized to muscle maximum isometric force

$\tilde{f}^{pe}$ parallel elastic (PE) element force normalized to muscle maximum isometric force

$\tilde{l}^{ce}$ muscle CE length normalized by muscle optimal fiber length

$\tilde{v}^{ce}$ muscle CE speed normalized by muscle optimal fiber length

$\xi$ scaling factor in the heat rate model

$a$ muscle activation

$A_f$ shape parameter in the muscle model

$a_h$ pseudo-damping of the hyper-volumetric model

$A_i$ coefficients of sin terms in Fourier series

$a_S$ spring pseudo-damping

$a_V$ volumetric pseudo-damping

$A_{rel}$ parameter in the CE force-velocity relation

$B_i$ coefficients of cos terms in Fourier series

$B_{rel}$ parameter in the CE force-velocity relation

$D$ damping

$dx$ relaxation parameter for characteristic points of the contact model in local $x$

$dy$ relaxation parameter for characteristic points of the contact model in local $y$

$f^{ce}$ muscle CE force

$f^{ce}_{isom}$ force-length relation normalized to muscle maximum isometric force

$f^{pe}$ the force-length relationship for the PE

$f^{t}$ tendon force

$f_d$ desired frequency

$f_f$ friction force

$f_n$ normal contact force

$f_{CD}$ contraction dynamics function

$f_{fast}$ fraction of fast twitch fibers

$f_{FS}$ Fourier series parametrization function

$F^m_{max}$ muscle maximum isometric force

$f_{PN}$ polynomial parametrization function

$f_{slow}$ fraction of slow twitch fibers

$g_{eq}$ equality constraint in the analytical muscle force-sharing

$GRF_x$ horizontal ground reaction force

$GRF_y$ vertical ground reaction force

$i$ index of muscle

$J$ objective function

$j$ time instant index

$K$ stiffness

$k^t$ tendon stiffness

$k^{pe}$ parameter in the PE force-length relation

$K_0$ shape parameter for the tendon equation

$K_1$ shape parameter for the tendon equation

$K_2$ shape parameter for the tendon equation

$k_h$ pseudo-stiffness of the hyper-volumetric model

$k_S$ spring stiffness

$k_V$ volumetric stiffness

$k_{lin}$ slope of the linear part in the tendon force-length relation

$L$ spring length

$l^m$ muscle length

$l^{ce}$ muscle CE length

$l^{ce}_{opt}$ optimal length of muscle fiber

$l^{tm}$ length of the tendon-muscle unit

$L_0$ spring rest length

$L_l$ left step length

$L_r$ right step length

$l_{slack}$ tendon slack length

$m$ muscle mass

$N$ muscle-related function in the objective function

$n$ number of muscles

$n_S$ nonlinearity exponent of the spring force-length relation

$P$ exponent in activation effort objective function

$p(s)$ foundation pressure distribution

$PCSA$ muscle physiological cross sectional area

$q$ generalized coordinate

$r$ muscle moment arm

$R_V$ radius of the contact element sphere

$S_i$ weighting factor in the objective function

$s_i$ slack variable corresponding to muscle $i$

$T$ joint torque

$T^m_{net}$ net muscle moment

$T_{Passive}$ passive joint torque

$t_{stim}$ a variable in the activation heat rate

$TrErr$ tracking error

$u$ muscle neural excitation

$u_{fast}$ contribution of fast twitch fibers to the total muscle excitation

$u_{slow}$ contribution of slow twitch fibers to the total muscle excitation

$V$ muscle volume

$v^{tm}$ rate of $l^{tm}$

$V_h$ deformed hyper-volume

$v_n$ normal speed

$v_s$ shape parameter in the friction model

$v_{cn}$ normal speed of the centroid of the deformed volume

$v_{ct}$ tangential speed of the centroid of the deformed volume

$v_{max}$ maximum CE velocity

$width$ parameter in the CE force-length relation

$x$ state variable

$X_{cop}$ centre of pressure location

$X_{tor}$ longitudinal position of torso center of mass in the global frame

$Y_{tor}$ vertical position of torso center of mass in the global frame

$v^{ce}$ rate of $l^{ce}$

AD activation dynamics

BH body height

BM body mass

CD contraction dynamics

CE contractile element of the muscle-tendon unit

CF cost function

DAE differential algebraic equation

DO dynamic optimization

dof degree of freedom

EID extended inverse dynamics

EMG electromyogram

FD forward dynamics

FF fully forward simulation design

FS Fourier series

FSO forward static optimization

ID inverse dynamics

IFM inverse forward simulation design starting at muscle force

IFT inverse forward simulation design starting at joint torque

MBS multibody system

MSO modified static optimization

MVC maximum voluntary contraction

OCP optimal control problem

ODE ordinary differential equation

PDE partial differential equation

PE parallel elastic element of the muscle-tendon unit

SE series elastic element of the muscle-tendon unit

SO static optimization

# Chapter 1

# Introduction

## 1.1 Background

Biomechanics is a field that uses the capabilities of mechanical engineering to study biological problems. The human body is a very complex multi-disciplinary system including mechanical, chemical, electrical, and other components that are working together simultaneously.

Human movement study is a branch of biomechanics which takes advantage of interdisciplinary models to simulate, predict, and analyze different movements of humans. Computer simulations have been used to estimate a variety of variables that are difficult or impossible to measure directly, such as joint forces, muscle forces, metabolic energy consumption, and muscle recruitment patterns. Among a variety of human movements, gait is recognized as a fundamental yet complex movement that has been challenging for researchers to model, especially for predictive muscle driven simulations with any degree of accuracy.

Inverse dynamics is the approach in which net joint moments and/or muscle forces are calculated given the measured or specified kinematics. It is the most popular simulation

technique used to study human musculoskeletal systems. The major disadvantage of inverse dynamics is that it is not predictive and can rarely be used in cause-effect interpretations. In contrast with inverse dynamics, forward dynamics can be used to determine the human body movement when it is driven by muscle forces. Forward dynamic simulations look for "human-like" motions, [22, 23]. For instance in gait, "human-like" implies that the gait of a human tends to minimize the metabolic energy cost per unit distance, [24, 25]. It is commonly assumed that using metabolic energy per unit distance traveled as the objective function, within the optimization necessary in the forward dynamic gait simulations, will lead to a reasonable representation of real human gait, [26].

Many human multibody models are torque-actuated and use joint torques as the driver of the dynamic system. These models suffer from serious shortcomings:

- They do not reflect the physiological aspects of the human body by excluding muscle models, e.g. muscle fatigue or the delay existing in muscle activation dynamics.
- These models may lead to unphysiological results for joint torques that seem fine, but actually can not be produced by real muscles.
- They are not able to provide valid estimations of joint reaction forces because of the absence of muscle actuators.

## 1.2 Motivations and Applications

Many biomechanical studies in movement dynamics are devoted to pure experiments. Using experiments only involves some considerable restrictions:

1. Muscle forces and also joint forces, as critical components of human movement studies, can not be measured non-invasively. There are some cadaveric studies, e.g., by [27], in which the Achilles force and ligament strain are measured within the

stance phase of a gait cycle. However, as the measurements are performed on cadavers, these forces reflect the contribution of the passive muscle force only.

2. It is very hard to discover the cause-effect relations of these dynamic systems by using only measurements. As a well-known example, by examining electromyogram (EMG) data, one can find out when a specific muscle is active; however, no one can say what motion will be yielded given these EMG data.

Muscle-actuated dynamic simulations complement the experimental studies by providing researchers with estimations of muscle and joint forces and body motion. These simulations present cause-effect relations and allow researchers to conduct "what if" studies, e.g., by changing the neural excitation of some muscles, how would the resulting motion change?

Additionally, in our research group, there were two PhD students working on biomechanical applications. One worked on torque-actuated models and the development of more efficient balance controllers for gait, where the other one studied foot-contact models. Thus, there was a motivation to develop a higher fidelity model that integrated these available sub-models, to add the vital missing element, i.e., a muscle model, and also to design an efficient framework for solving the muscle redundancy. The integrated model is a complete musculoskeletal model, which is able to produce forward dynamic simulations of human gait.

Since dynamic simulations of musculoskeletal systems involve optimization techniques, many studies have been focused on finding more efficient and/or more exact approaches to solve the muscle redundancy, which exists in the human musculoskeletal system. Additionally, as the model is called by the optimization routine many times, there is ongoing research to make the simulations faster by taking advantage of model reduction, symbolic and analytical techniques.

Dynamic modelling of human musculoskeletal systems, including the solution for individual muscle forces, has several applications in the following areas:

- Pathologic studies: for instance, these simulations may help surgeons to examine the possible improvements in patient movements before and after tendon transfer surgery.
- Rehabilitation engineering: simulations help to evaluate the design and effectiveness of prostheses and assistive devices.
- Sports biomechanics: dynamic simulations provide athletes with knowledge to improve sports performance and reduce the incidence of injuries.
- Ergonomics: finding individual muscle forces leads to more efficient design of accessibilities to avoid early fatigue.

## 1.3 Challenges

There are serious challenges in the dynamic modelling of human musculoskeletal systems, summarized as the following:

1. Muscle forces cannot be measured non-invasively; therefore, there is no direct way to validate the calculated muscle forces. The common approach researchers take is to compare the results for neural excitations with EMGs; however, even if these two match each other very well, it does not imply that the model has predicted the muscle forces accurately [14].
2. Optimization processes are always challenging. If global optimizers are to be used, there will be a high computation cost. On the other hand, if one uses gradient-based methods, a reasonably good initial guess for the solution will be required. Moreover, defining the constraints within the optimization problem is very challenging and may lead to infeasibilities.
3. There are limited data on muscle parameters, which is a great restriction for modelling of the human body.

4. Most of the time, subject-specific simulations are required for comparison of the model results to experimental data from different subjects. To this goal, simulation speed would be vital; therefore the model simulation must run within a reasonable time using available computers.

## 1.4 Thesis Outline

In this thesis, a dynamic musculoskeletal model will be developed to predict human gait motion as the end goal. This model includes a muscle-redundant dynamic system, which involves solving an optimization problem for individual muscle forces. For a successful gait modelling, there exist several pre-requisites, such as an efficient muscle force-sharing approach, an accurate and efficient foot contact model, and a balance control strategy, that will be discussed in this thesis. In chapter 2, the literature review for musculoskeletal modelling is presented. In chapter 3, different approaches are introduced for solving the optimal control and muscle redundancy problems. Chapter 4 discusses a novel foot contact model within human gait simulations. In chapter 5, forward dynamic simulation of human gait is described. Finally, chapter 6 presents the conclusions of this thesis and future work.

# Chapter 2

# Literature Review

The literature review begins with a review of some muscle models. Then it continues with the muscle redundancy problem and popular approaches in solving that. Afterwards, a review of literature foot contact models is presented, and eventually a section on multibody dynamics of the human musculoskeletal systems is included.

## 2.1 Muscle Models

Muscle modelling is one of the most challenging parts in the simulation of musculoskeletal systems. Indeed, a major difference between industrial robots and the human body is the muscle recruitment during the movements. Muscle, as a living part of the system, is a combination of chemical, electrical and mechanical systems. A muscle model should describe the relation and interaction of neural and mechanical systems of human movement. A good muscle model must be non-task-specific and able to simulate different body movements without any modification of its parameters.

There are three fundamental models available in the literature, and other models are developed based on these models. The first model is built on the basis of input-output

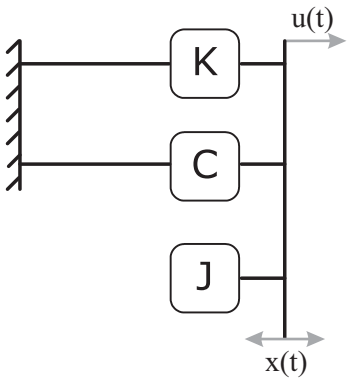


Figure 2.1: Schematic representation of second-order model

analysis of a specific task and is basically formed by a simple second-order ODE (Ordinary Differential Equation). The second model is the fundamental study done by Hill [28]. This model leads to a nonlinear system of ODEs. The third model focuses on the microscopic details of the contraction mechanism and is expressed by PDEs (Partial Differential Equations). These three different categories of muscle models will be reviewed in the following, and advantages and disadvantages of each will be discussed in detail.

### 2.1.1 Second-Order Models

These models simply consist of elastic, damping, and inertial elements. The schematic representation of these models is depicted in Figure 2.1.

The basic formulation of the model is as follows:

$$J\ddot{x}(t) + C\dot{x}(t) + Kx(t) = Gu(t) \tag{2.1}$$

where $K$, $C$, and $J$ are the stiffness, damping, and inertia of the muscle, and $G$ is a gain. Equation 2.1 may be rearranged as:

$$\ddot{x}(t) + 2\xi\dot{x}(t) + \omega_n^2 x(t) = \frac{G}{J}u(t) \tag{2.2}$$

where $\xi$ is the damping ratio and $\omega_n$ is the natural frequency of the system, $x(t)$ can be either the joint angle or torque, and $u(t)$ can be either the neural input or external load actuating the system. As a result, the muscle joint structure can be considered as a second-order ODE with parameters that will change as a function of task and also range of motion [29]. This second-order model assumes the muscle joint structure as a black box and tries to approximate the contents of the system as a linear ODE for a specific task and range of performance.

Many early researchers used this type of model to analyze human movements, such as [30, 31]. The main advantage of this type of model is its mathematical simplicity, whereas for example using Hill-type models within a complete muscle-joint system will lead to higher-order equations.

### 2.1.2 Hill-Type Models

The second type of model is based on the fundamental studies of Hill [28] on isolated muscles. The classic model is lumped-parameter and includes a contractile element in series with a series elastic element. The basic model has been used for complicated dynamic simulations including different muscle coordination [32]. These models are called phenomenological since they are based on the analysis of input-output relations from experiments.

One of the most popular Hill-type muscle models is the three-element model. It includes a contractile element (CE), a parallel elastic element (PE), and a series elastic element (SE). The CE is basically an actuator or a force generator and is representative of the active part of muscle. It accounts for muscle fibers and contraction. The PE models the tissue parallel to muscle fibers and is parallel to the CE element. The SE acts as whatever is in series with the CE, usually a tendon.

This model has been modified by many researchers, not only for isolated muscle, such as [33,34], but also for muscle joint systems, like [34]. The model includes solving ODEs. All

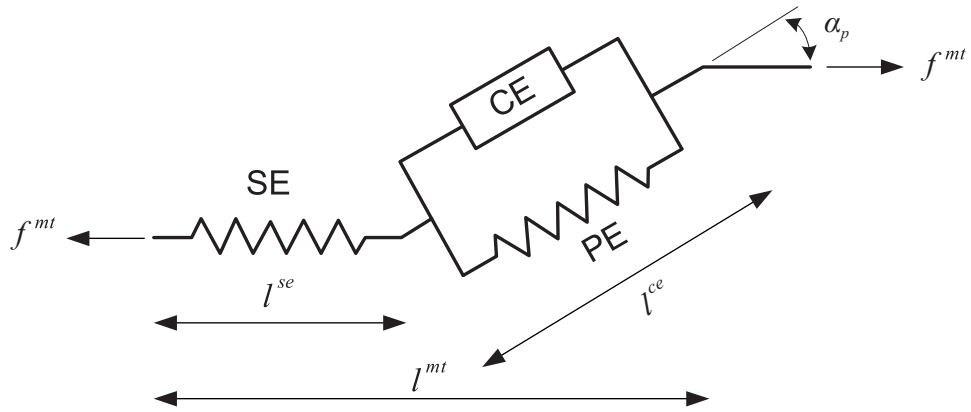


Figure 2.2: A Hill-type muscle model with three elements

of the elements in the model are inherently nonlinear; the formulations of these nonlinear elements can be different. The PE and SE force expressions are usually parabolic or exponential functions of muscle fiber or tendon length, respectively. For instance, the exponential relation for tendon force $f^t$ based on [35] is as follows:

$$\frac{df^t}{dl^t} = K_1 f^t + K_2 \tag{2.3}$$

where $l^t$ is tendon length, $K_1$ and $K_2$ are some shape constants. Equation 2.3 can be integrated and rearranged using suitable boundary conditions [34]:

$$F = \frac{F_0}{e^{X_0}}(e^{\frac{K_0}{X_0}x} - 1) \tag{2.4}$$

where $F$ and $x$ are the force and extension of SE, respectively; $F_0$ and $X_0$ are maximum force and extension, and $K_0$ is a constant of curve shape.

The most complicated component is the CE that is a function of muscle fiber length, velocity, and excitation. There are two high level dynamics occurring in the CE element: activation and contraction dynamics, which are discussed in the following.

**Activation Dynamics**

Activation dynamics is the relation between the normalized neural excitation signal $u(t)$

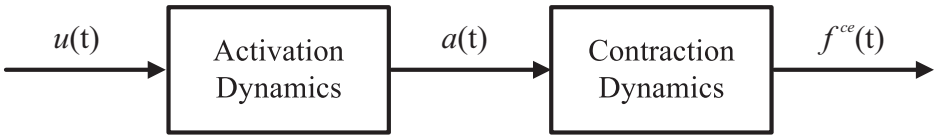


Figure 2.3: Diagram of excitation signal to CE force

and the activation signal $a(t)$, as depicted in Figure 2.3, during muscle contraction and force generation, where $u(t)$ reflects the number of motor units recruited as well as relevant firing rates [32]. As muscle fibers are excited, Calcium ions will bind to troponin, and this results in the ability of cross-bridge interaction; this state of muscle is called an activation. For a maximally excited muscle, $u$ is unity and all of the motor units are fully excited at the maximum of their firing rate. At steady-state conditions and when the muscle fiber is at a specific length (called optimal fiber length) and the contraction is isometric, the maximum contraction force $F^m_{max}$ will be generated. Activation dynamics is usually modelled through a first-order ODE, which can be linear or quadratic in terms of u(t). The following relation shows a first-order ODE model presented by [1]:

$$\dot{a}(t) = (u(t) - a(t))(t_1 u(t) + t_2) \tag{2.5}$$

with

$$t_2 = 1/\tau_{fall}$$

$$t_1 = 1/\tau_{rise} - t_2$$

where $u$ and $a$ are the muscle excitation and activation, respectively, $\tau_{fall}$ is the deactivation time constant, and $\tau_{rise}$ is the activation time constant. It should be added that both excitation and activation signals are normalized and therefore bounded between 0 and 1.

**Contraction Dynamics**

The force generated by muscle fibers has two separate dependencies: force-length and force-velocity. Schematic representations of these two relations are depicted in Figure 2.4 (a) and (b). It is notable that these two graphs are for maximal activation, i.e., $a = 1$ [5].

In general, the CE force can be formulated as follows:

$$f^{ce} = f^{ce}(l^{ce}, v^{ce}, a) \tag{2.6}$$

where $l^{ce}$ and $v^{ce}$ are muscle fiber length and velocity, respectively. The general form of the force-velocity relation of contractile element for concentric contraction during maximal activation based on [28] is the following hyperbolic equation:

$$(f^{ce} + AF^{m}_{max})(v + Av_{max}) = AF^{m}_{max}v_{max}(1 + A) \tag{2.7}$$

where $f^{ce}$ is the CE force, $v$ is the CE velocity, $A$ is a constant that defines the hyperbola shape, $v_{max}$ is the maximum CE velocity (x-intercept), and $F^{m}_{max}$ is the maximum isometric force (y-intercept).

There are different studies in the literature on how to scale the CE force from maximal activation to the entire range of activation signal. A few researchers simply multiply the force-length-velocity relations by $a(t)$, e.g. [36], and some consider a more complicated scaling, see e.g. [3, 7, 37, 38]. If the simple scaling is applied, the general muscle total force can be written as:

$$f^{m} = \left\{F^{m}_{max}\bar{f}^{ce}(l)\bar{f}^{ce}(v)a(t) + f^{pe}(l)\right\}\cos(\alpha_p) \tag{2.8}$$

where $f^{m}$ is the muscle force, $F^{m}_{max}$ is the maximum isometric force the muscle can generate, $\bar{f}^{ce}(l)$ is the normalized force-length relationship for the CE, $\bar{f}^{ce}(v)$ is the normalized force-velocity relationship, $a(t)$ is the activation value bounded between 0 and 1, $f^{pe}(l)$ is the force-length relationship for the PE, and $\alpha_p$ is the pennation angle (the angle that the tendon makes to the muscle fibers, as depicted in Figure 2.2).

### 2.1.3 Huxley-Type Models

The last model is famous due to the classic research done by Huxley (1957). This model focuses on the microstructure of the contraction mechanism. It models the cross-bridge and

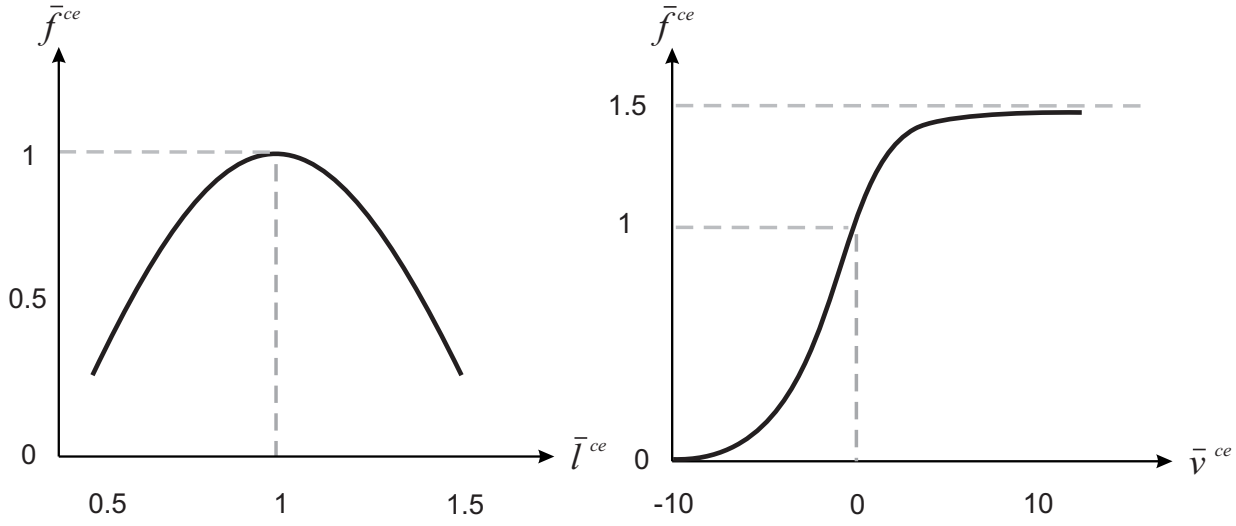


Figure 2.4: Schematic dynamics of the CE element, (a) force-length relation; (b) force-velocity relation

contraction using distribution functions, which involves solving PDEs. Figure 2.5 shows the idea of the Huxley model; the sliding element will join another in series and eventually those are attached to a tendon represented as the elastic element at both ends.

To write constitutive equations simply, the number of states of the attach-detach mechanism may be restricted to two, i.e., a cross-bridge is either attached or detached and there is no other state in between:

$$\left(\frac{\partial n}{\partial t}\right) - v(t)\left(\frac{\partial n}{\partial x}\right) = f(x) - [f(x) + g(x)]\, n \tag{2.9}$$

where $n(x,t)$ is the distribution function and accounts for the fraction of attached cross bridges, $x$ is the distance from the sarcomere equilibrium position, $f(x)$ and $g(x)$ are attachment and detachment rate functions, respectively, and $v(t)$ is the contraction velocity of a half-sarcomere. Rate parameters $f(x)$ and $g(x)$ may typically be linear functions of $x$.

Once the distribution function $n(x,t)$ is specified, the macroscopic parameters can be calculated based on different moments of $n(x,t)$. For instance, if the cross-bridge is assumed

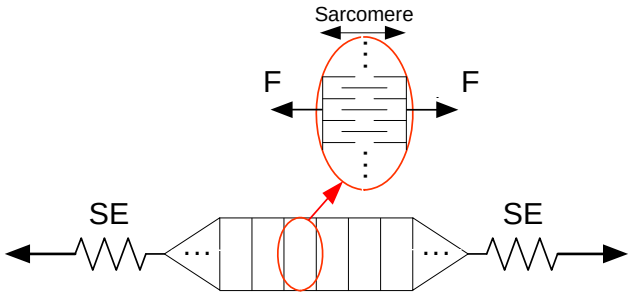


Figure 2.5: Huxley-based model showing the cross-bridge concept

to have a linear force-displacement relation, muscle force per unit area will be:

$$S(t) = \frac{P}{A} = aC \int_{-\infty}^{\infty} xn(x,t)dx \tag{2.10}$$

where $a$ is the state of activation, and $C$ is a parameter depending on the contractile microstructure.

As modifications have been made over the years, this model has evolved. This evolution has usually been toward increasing the number of rate parameters [39, 40]. Although these studies have been done to improve our understanding of the contraction mechanism, they do not clarify the necessity and biomechanical significance of all parameters of the model.

Since this model is mathematically complicated, only simulations of very stereotypical motions like iso-velocity contractions are simple to perform. Furthermore, there is not enough information for model parameter determination, especially for rate parameters; therefore, as mentioned, this model has not been used for human motion simulations [29].

A simpler Huxley-based model was presented by [41], called the DM (Distribution Moment) model. This model still has the basic specifications of the Huxley model, but, assuming a normal distribution function for $n(x,t)$, the model is able to simulate eccentric contractions fairly well through a system of ODEs instead of PDEs. This model could reduce complications and computations of Huxley model for a specific application.

### 2.1.4 Discussion on Different Muscle Models

A second-order model has serious limitations [29]:

1. It inherently has one input location.
2. Secondary inputs like neural co-activation may be taken into account only by changing parameter values of the system rather than affecting the system as direct inputs.
3. Values of model parameters will change as the task changes or even when the range of motion of a similar task varies.

For different tasks, using the same biomechanical system, completely different values for the second-order model will be found. Consequently, second-order models have been developed and used for one specific purpose, and that is to calculate model parameter values so that in terms of a specified input, it curve-fits the output. Overall, second-order models are not considered good representatives for muscle joint systems.

Unlike the second-order model, Hill-based lumped parameter models (with for instance three elements), using appropriate nonlinear functions for CE force-length and force-velocity relations, are able to simulate human muscle-actuated systems with different combinations of neural input signal [29, 32]. Hill-based models are very useful for human muscle-driven simulations and they are task-independent, i.e., they can model different tasks without changing model parameters.

Huxley-based models have been rarely used for simulations of human movements. In addition to their complexity, there is no good source for model-required parameters.

## 2.2 Muscle Redundancy and Solutions

### 2.2.1 Introduction

The musculoskeletal system is a complex system and is actuated by muscles redundantly during different movements; this is because the number of recruited muscles is more than the degrees of freedom of the dynamic system [10]. Moreover, some muscles are bi-articular joint (2-joint) muscles, i.e., they span more than one joint, such as the gastrocnemius muscle which spans both knee and ankle joints. This leads to a more complicated dynamic system. In such a system, to find individual muscle forces, the resultant joint moment can not be distributed to each muscle force directly [42]. In order to solve this indeterminacy, an optimization problem can be posed. In general, objective functions of these optimization problems are supposed to model some physiological criteria, which are minimized during a movement [43].

In this section, different methods that have been presented in the literature for solving the muscle redundancy, or force-sharing, are introduced and at the end, advantages and disadvantages of each are discussed in detail.

### 2.2.2 Static Optimization (SO)

In this approach, the goal is to find muscle forces as optimization variables such that an instantaneous objective function is minimized. SO has low computation cost, which makes it interesting and popular; however, it includes some drawbacks. In the static optimization approach, the objective function is minimized at each time step; therefore it does not allow using a time-integral objective function such as metabolic energy. Different expressions for objective functions have been presented [42, 44]. The most popular type of cost functions used in SO is of a polynomial-type:

$$J_j = \sum_{i=1}^{n} \left( \frac{f_{ij}^m}{N_i} \right)^P \tag{2.11}$$

where $n$ is the total number of muscles considered, $f_{ij}^m$ is the $i^{th}$ muscle force at time step $j$, $N_i$ may have different forms such as muscle maximum strength or physiological cross-sectional area (PCSA) for muscle $i$, and $P$ is the polynomial order. References [44–46] have discussed how changing the objective function would affect results of muscle forces in detail. Researchers have used different orders of polynomial: for instance, [43, 47] used $P$=1, [48–50] used $P$=2, and Crowninshield and Brand [43] used $P$=3. The last one has been considered widely since it claims to model muscle fatigue:

$$J_j = \sum_{i=1}^{n} \left( \frac{f_{ij}^m}{PCSA_i} \right)^3 \tag{2.12}$$

Rasmussen et al. [51] showed that by increasing $P$ in the polynomial criterion, the results of the force-sharing problem would converge to the results of the following expression:

$$J_j = \max \left( \frac{f_{ij}^m}{N_i} \right)^P, \; i = 1, 2, ..., n \tag{2.13}$$

If Equation 2.13 is applied as the objective function, the technique is called a min/max optimization.

### 2.2.3 Modified Static Optimization (MSO)

In static optimization, applying different objective functions may lead to unphysiological values for muscle forces as the optimization variables. This problem can be resolved by adding contraction and activation dynamics to the optimization process [14]. The goal of the modified static optimization method is to find neural excitations of muscles at each time step $u_{ij}$ that minimize an instantaneous objective function and satisfy some constraints and bounds. The major constraints, which are non-linear in terms of the decision variables, are first the equality constraints of the equations of motion, and second

the additional constraints that guarantee the neural excitations are bounded between 0 and 1, i.e., $0 \leq u_{ij} \leq 1$ where $i$ is the muscle number, and j is the time step number. MSO can apply objective functions usable in SO and also those written as forms of instantaneous activations or excitations. For example, the instantaneous activation effort can be written as:

$$J_j = \sum_{i=1}^{n} S_i a_{ij}^P \tag{2.14}$$

where $S_i$ is a muscle-related property, such as muscle volume, and $a_{ij}$ is the activation corresponding to muscle $i$ at time instant $j$.

As in SO, extra physiological bounds may be added on muscle force and activation which makes the search space smaller and produces smoother results; however, it may result in infeasibilities.

Although MSO is a modification of SO, it requires finite difference derivatives of the muscle force and activation in computing the muscle speed, activation, and excitation, which potentially leads to numerical issues, such as instability and truncation errors.

### 2.2.4 Extended Inverse Dynamics (EID)

This approach was presented by Ackermann [14] and was used for an inverse dynamics simulation of human gait. The major advantage of EID over static optimization is in the time-history inclusion. In EID, a time-integral function can be used, whereas in SO an instantaneous objective function must be applied. In other words, since EID is based on minimizing a function of the entire movement, the objective function can be a desired time-integral expression, like metabolic energy, which has been adopted as a criterion in human movements [22, 24, 25]. Using such an approach will increase computation time of the optimization process compared to SO and MSO. In addition to the possibility of using a time-integral function to optimize, EID also includes contraction and activation dynamics, and therefore does not lead to unrealistic results in comparison with SO. On the other hand, EID does not include numerical integrations of differential equations as will be seen

in Dynamic Optimization in the following section. This approach is called Extended Inverse Dynamics as it is used within inverse dynamics and it is based on inverting contraction and activation dynamics.

Constraints of EID include equality constraints, i.e., equations of motion over the motion interval, and inequality constraints as bounds on neural excitations. The optimization problem searches for the muscle forces at all time steps of motion, which minimize a time-integral cost function, for instance, metabolic energy expenditure, under given constraints.

### 2.2.5 Dynamic Optimization (DO)

This approach is based on optimal control of a musculoskeletal system, driven by neural excitations through forward dynamics, in order to determine a motion trajectory. Since many numerical integrations of equations of motion are required, dynamic optimization involves a high computation cost [11].

Different studies have investigated muscle recruitment and coordination of human movements using neural excitation as the control signal within an optimal control problem, such as [52, 53].

Pandy et al. [54] introduced a different approach for solving such a problem. They converted this optimal control problem to a parametrized optimization problem. This method parametrized histories of neural excitations at time steps, and then a nonlinear programming problem was solved. This method was used successfully in some studies, for example [55], where the objective function was the normalized metabolic energy, i.e., metabolic energy per unit of distance travelled. All of these studies focused on gait modelling, and could simulate optimal gait speed, optimal motion and optimal energy expenditure very well.

One of the advantages of Dynamic Optimization over Static Optimization is that the cost function can be calculated over the motion period, which is very desirable; for instance the objective function can be metabolic expenditure or those introduced for SO and MSO

but in an integral form instead of a discrete form. Another advantage is that DO includes the time-history of the control variables and system states. Therefore, it does not result in unphysiological abrupt changes in controls as in SO.

As mentioned, dynamic optimization is very computationally costly. For instance, for a 2-D model of gait simulation, this method required many CPU days in 2003 [16]. In cases that reference motions are specified, in a forward dynamics manner, the optimization problem must minimize the energy as well as the tracking error. In this case, as a multi-objective optimization problem, one approach is converting the cost function to a linear combination of time-integral function (e.g. metabolic energy) and the error between simulated and prescribed motions. This will reduce the quality of results, since using different weights as multipliers of two objective functions will change the results and interpretations.

Anderson and Pandy in [55] showed that if the goal is to find estimations of muscle forces and joint contact forces during normal gait, dynamic and static optimizations will lead to remarkably similar results. They used a 23-dof model with 54 muscles and simulated an entire normal gait cycle to show this.

### 2.2.6 Analytical approach for solving the muscle redundancy

This section describes an analytical approach with limited applications to distribute the muscle moment to muscle individual forces. The contents of this section are mostly from [56] in which this approach is presented with no bounds on the muscle forces. Especially with absence of lower bounds on muscle forces, the forces will easily become negative, which is incorrect. There are some other works that have added the bounds on muscle forces and numerically solved the rest of the approach, for instance [57], which does not seem satisfying for the initial logic of the analytical approach.

Assume the goal is to minimize the following objective function in a 1-dof system:

$$J(F_i) = \sum_{i=1}^{n} \left( \frac{F_i}{N_i} \right)^P \text{ subject to } g_{eq}(F_i) \triangleq T_{net}^m - \sum_{i=1}^{n} r_i F_i = 0 \tag{2.15}$$

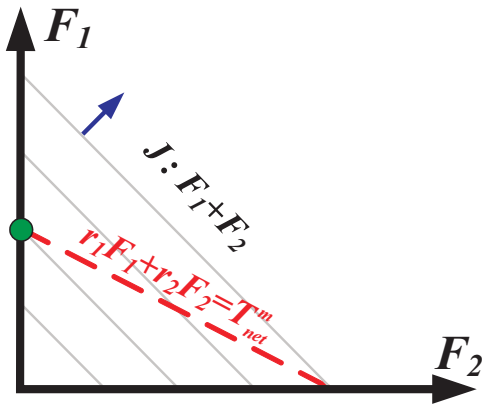


Figure 2.6: Case when $P = 1$ for two flexor muscles and positive $T^m_{net}$

where $P$ is the polynomial order of the objective function, $n$ is the number of muscles, $F$ is the muscle force, $N$ is a muscle property function such as physiological cross-sectional area (PCSA), maximum force capacity, etc., $g_{eq}$ is the equality constraint imposed to the problem, $r$ is the muscle moment arm about the joint and $T^m_{net}$ is the net muscle moment. Note that the system assumed here is a 1-dof, so all muscles are single-articular.

**Convention:** $r_i$ is positive when the muscle is a flexor and negative when it acts as an extensor.

For the case that $P$ is unity, assuming all $r_i$ and $T^m_{net}$ to be positive, it is a linear programming problem that the global minimum value for $J$ occurs when only the muscle with the greatest moment arm is recruited. For an example, assume a system with only two flexors where $r_1 > r_2$ and net muscle moment $T^m_{net} > 0$. As shown in Figure 2.6, the optimal solution would be the circle, where the feasible line of equality constraint intersects the minimum line of objective function contour that would be on the far left side of the constraint line. The arrow on the contour shows the ascent direction of the function.

For higher values of $P$, one can write the Lagrangian as follows:

$$\mathcal{L} = J + \lambda g_{eq} \tag{2.16}$$

where $\lambda$ is called the Lagrange multiplier. To find the optimal solution, the gradients of the Lagrangian in terms of the decision variables and Lagrange multiplier are required to be zero.

$$\frac{\partial \mathcal{L}}{\partial F_i} = P\frac{F_i^{P-1}}{N_i^P} - \lambda r_i \equiv 0,\ i = 1..n \tag{2.17}$$

$$\frac{\partial \mathcal{L}}{\partial \lambda} = g_{eq} \equiv 0 \tag{2.18}$$

Rearrange Equation 2.17 for the Lagrange multiplier, as follows:

$$\lambda = P\frac{F_i^{P-1}}{r_i N_i^P} \tag{2.19}$$

For $i \neq j$, as the Lagrange multiplier is unique, one can write

$$P\frac{F_i^{P-1}}{r_i N_i^P} = P\frac{F_j^{P-1}}{r_j N_j^P} \tag{2.20}$$

which implies the following:

$$\frac{F_i}{F_j} = \left(\frac{r_i}{r_j}\right)^{\frac{1}{P-1}} \left(\frac{N_i}{N_j}\right)^{\frac{P}{P-1}} \tag{2.21}$$

Equation 2.21 provides a nice property of the global optimal solution that the ratio of two muscle forces is a function of the ratio of the moment arms and muscle property function. By replacing the force ratios in the equality constraint, one can derive the optimal force expression, as follows:

$$F_j = \frac{\left(r_j N_j^P\right)^{\frac{1}{P-1}}}{\sum_{i=1}^{n} \left(r_i N_i\right)^{\frac{P}{P-1}}} T_{net}^m \tag{2.22}$$

which can be re-written in the simpler following form:

$$F_j = \frac{T_{net}^m}{r_j \sum_{i=1}^{n} \left(\frac{r_i}{r_j}\frac{N_i}{N_j}\right)^{\frac{P}{P-1}}} = \Gamma_j T_{net}^m \tag{2.23}$$

where $\Gamma_j$ represents the percentage of $T_{net}^m$ in $F_j$, function of given parameters. As a special case that muscle property functions are unity, the expression for the optimal muscle force

$j$ will be the following:

$$F_j = \frac{r_j^{\frac{1}{P-1}}}{\sum_{i=1}^{n} r_i^{\frac{P}{P-1}}} T_{net}^m \tag{2.24}$$

### 2.2.7 Discussion

Static optimization is desirable due to its simplicity and low computation time, but it neglects contraction and activation dynamics, which may cause non-physiological results. Moreover, SO does not allow using a time-integral objective function like metabolic energy, which results in instantaneous variations of muscle forces.

MSO resolves the first drawback of SO, i.e., it includes contraction and activation dynamics. Its optimization process includes a loop from neural excitation to motion kinematics which avoids reaching unrealistic results by setting bounds for neural excitations. However, MSO like SO still needs to solve the optimization loop at each time step and a time-integral cost function may not be used in this approach. MSO is interesting since it is simple and needs low computation cost like SO.

Extended Inverse Dynamics is limiting since it is developed to be used for inverse dynamic simulations. Advantages of EID are counted as:

- It allows using a time-integral cost function.
- It includes muscle activation and contraction dynamics.
- It has significantly less computation cost with respect to DO.

It is notable that EID has much more cost of computation with respect to SO because of using a non-instantaneous cost function.

Dynamic optimization is prohibitive due to its computation cost. However, it contains contraction and activation dynamics as well as a time-integral objective function. It can

be used for both forward and inverse dynamics. It was shown that dynamic and static optimizations will lead to similar results of muscle force estimation during normal gait [55].

Analytically solving the muscle redundancy problem is an efficient approach in terms of time and accuracy; however, it can be deployed in limited cases, and it has a few serious shortcomings:

- It can only apply an objective function that is an explicit function of decision variables.
- Considering lower and upper bounds for muscle forces as the optimization variables is a major challenge for this approach.
- Solving a system that includes muscle dynamics seem to be cumbersome.

In this thesis, Section 3.5 presentes the solution of a system with bounds on muscle forces using Maple®.

In the above, five major groups of approaches to solve the force-sharing and muscle coordination were introduced. There exist some other approaches which can be categorized in the mentioned groups. For instance, CMC (Computed Muscle Control) [58], which is based on Static Optimization, includes a control algorithm to control the system dynamics to track a measured kinematics. This approach is restrictive because it can not be used in a predictive forward dynamic simulation that there is no measured motion. Additionally, as CMC is based on SO, it cannot be used with a time-integral objective function.

Among the discussed approaches, SO, MSO, and EID can not be applied in forward dynamic simulations, and only DO is able to be implemented in both forward and inverse dynamics. There would be a trade-off to choose a method for a specific application, computation cost versus possibility of using a time integral cost function, and also inclusion of activation and contraction dynamics.

## 2.3 Foot Contact Modelling

Foot contact modelling is an essential piece in the forward dynamic simulations of gait since ground reaction forces are not measured a priori, as opposed to inverse dynamics. Contact forces affect the muscle, ligament, and joint reaction forces. Therefore, it plays a crucial role in understanding gait simulations, injury biomechanics, and design of prosthetics [13, 22, 38, 59–61]. Muscle forces, along with gravity and ground reaction forces on the feet during the stance phase, produce the required force for human movements. Therefore, a suitable foot contact model in terms of both efficiency and quality of results will be crucial in human gait modelling.

Many studies have included foot contact models in human gait simulations; however, none as yet can accurately produce the ground reaction forces. Previous studies (except [26] and finite element models) have modelled the foot-ground interaction by means of point contact elements, i.e., discrete springs and dampers [12, 55, 62–64]. The point contact elements result in sharp contact forces that lead to inadequate reproduction of ground reaction forces (GRFs). For instance, Peasgood et al. [22] and Wojtyra [64] predicted ground reaction forces that do not match the measured quantities well. Also in [22, 55, 62], high frequency oscillations are reported at initial contact instants. One might circumvent this issue by increasing the number of contact elements as in [63], but this results in longer simulation time. Also, the more the number of contact elements, the more the number of parameters, and therefore the more time required for parameter identification.

A nonlinear foot contact model was presented by Sandhu and McPhee [13]. This model was claimed to be volumetric; however, they did not compute any closed-form volume. They discretized the foundation to nonlinear spring-damper elements, and calculated the contact forces by adding the forces of those elements, which is more somewhat similar to the study by Gilchrist and Winter [62].

The foot model presented by Millard et al. [26] consists of two segments with three spheres where the metatarsal joint was assumed to be a passive joint with a rotational

spring and damper. A volumetric foot contact model was based on the work by Gonthier et al. [65], which assumes a linear elastic foundation, i.e. small deformations. This does not seem well-suited for modelling of the foot since the heel pad soft tissue undergoes a significantly large deformation in impact with the ground, which is reported to be up to 12 mm for a subject with 22.8 mm heel pad thickness [26]. The gait simulation results reported by those authors for the ground reaction forces did not sufficiently match the experimental data.

In this thesis, chapter 4 is dedicated to foot contact modelling, and a modification of current models for application in human gait simulations are presented.

## 2.4 Dynamics of the Human Body as a Multi-Body System

Analysis of human movement requires the understanding and usage of multi-body dynamics formulations. In this section, the structure of dynamic equations for a multi-body system is studied. The human musculoskeletal system is an over-actuated system, i.e., the number of actuators (muscles) is more than what is needed to drive the degrees of freedom of the dynamic system. In another statement, this muscle-actuated system is redundant in the sense that one can choose a different number of muscles to drive a specific joint with the same degrees of freedom. Therefore, the dynamic system is indeterminate, which means the number of unknowns is more than the number of equations. In general, this problem is solved through an optimization process in which the unknown variables are muscle forces or muscle activations (See Section 2.2). Activations can be applied either as a discrete (in a finite number of time steps) or continuous function. The activation can be parametrized in terms of muscle force using a Hill muscle model, which was presented in Section 2.1.2 in detail.

To analyze these biomechanical models, multi-body dynamic equations are required.

In deriving the equations of motion for a specific height and weight, anthropometric data are used for bio-fidelity of the model [10].

A biomechanical model can be driven by two different groups of actuators: joint torque actuators and muscle actuators. If the goal is to calculate the net joint torque of the model, only joint actuators are considered and the dynamic system is not redundant. However, if the analysis looks for muscle forces, muscle actuators must be taken into account which makes the model redundant, i.e., the number of unknowns is more than the available known equations. It should be noted that redundancy of the model is not dependent on whether the analysis is inverse or forward dynamics, but it is a nature of the system.

### 2.4.1 Formulations of Multi-Body Systems

A multi-body system is a set of rigid or flexible bodies and joints that are driven by forces and moments. Bodies are connected with joints that restrict the degrees of freedom. The human body is an example of a multi-body system in which the bones are the bodies, and muscles and soft tissues are considered as elements containing internal force. A multi-body system may be constrained or unconstrained. Kinematic constraints can be written as a set of algebraic equations:

$$\mathbf{\Phi}(\mathbf{q}, t) = 0 \tag{2.25}$$

where $\mathbf{q}$ is the column matrix of generalized coordinates, and $t$ is the time. For instance, body joints are time-independent constraints, whereas a prescribed trajectory of a joint is an example of a time-dependent constraint.

For an unconstrained multi-body system, the equations of motion can be written in the following from:

$$\mathbf{M}\ddot{\mathbf{q}} = \mathbf{Q} \tag{2.26}$$

where $\mathbf{Q}$ is the column matrix of quadratic velocity terms and generalized forces on the system and $\mathbf{M}$ is the mass matrix, which contains masses and moments of inertia of all rigid bodies.

By combining Equations 2.25 and 2.26, the equations of motion for a multi-body system with kinematic constraints can be yielded as a set of differential-algebraic equations (DAEs) via the Lagrange multiplier method:

$$\left\{ \begin{array}{c} \mathbf{M}\ddot{\mathbf{q}} + \mathbf{\Phi}_{\mathbf{q}}^{T}\boldsymbol{\lambda} = \mathbf{Q} \\ \mathbf{\Phi} = 0 \end{array} \right\} \tag{2.27}$$

where $\mathbf{\Phi}_{\mathbf{q}} = \frac{\partial \mathbf{\Phi}}{\partial \mathbf{q}}$ is the Jacobian matrix. In Equation 2.27, $\boldsymbol{\lambda}$ is the column matrix of Lagrange multipliers which corresponds to the reaction forces of joints, or more generally kinematic constraints. Then, the reaction forces corresponding to the kinematic constraints can be expressed as:

$$\mathbf{Q}^{(c)} = -\mathbf{\Phi}_{\mathbf{q}}^{T}\boldsymbol{\lambda} \tag{2.28}$$

In this research project, the equations due to the multibody system will be in the form of ODEs only as given by Equation 2.26. In biomechanical human body modelling, as long as no kinematics constraint is present, the equations will be in the form of Equation 2.26. For example, even in gait modelling that there is a double-support phase, if the contact is not considered through kinematic constraints, multibody equations will still be pure ODEs.

### 2.4.2 Symbolic Musculoskeletal Modelling with Maple®

The numerical optimization methods involved in this work may require tens or hundreds of dynamic simulations. Thus, it is critical to formulate and solve the multi-body equations as efficiently as possible.

Dynamic equations governing a multi-body system can be expressed numerically or symbolically. Numerical techniques produce matrices which are meaningful only at a specific instant of time; as a result the equations must be reformulated at each time step of the analysis. Although numerical approaches are used in most popular simulation packages such as MSC.ADAMS, they suffer from the relatively slow process in reformulating equations of motion.

Symbolic formulation techniques produce sets of equations that describe the system motion over the entire time, thereby increasing the simulation speed. Prior to the simulation, symbolic expressions can be greatly simplified through different ways such as simplification of trigonometric expressions, removing repeated calculations, and removing multiplications by zero and one. For example, in many multi-body applications, some parameters have zero values; all of these values are treated similarly to the non-zero values in a numerical process, which causes time loss. A symbolic package such as Maple® performs the simplifications as well as code optimization to reduce computation time. These simplifications lead to simulations five to ten times faster than those simulated through numerical approaches [66].

Finally, unlike the numerical model, a symbolic approach allows the user to apply the equations of motion in a meaningful and faster way in design and analysis of the multi-body system [67, 68]. However, symbolic formulation techniques may produce large expressions for a complex system. Large systems may need more memory for a symbolic simulation. However, an efficient package like Maple® using a suitable formulation process can overcome this drawback.

In this thesis, musculoskeletal models will be implemented in MapleSim® (physical modelling toolbox of Maple®), and will take advantage of symbolics, possible simplifications, and code optimization [69]. It is to be noted that MapleSim® automatically generates simplified equations of motion governing a multi-body system using graph theory. Afterwards, the optimized and simplified equations of motion and other model expressions can be exported to another package like MATLAB® to perform the optimization needed for the force-sharing problem. Figure 2.7 illustrates the schematic flowchart of such a process. The modelling begins from an implemented muscle model in MapleSim®, which will be inserted into the multi-body system. Dynamic equations will be generated automatically and transferred to Maple® afterward. Different types of simplifications will be automatically performed on those dynamic expressions using Maple® commands. Then using the Maple® ability for code optimization, a highly efficient code will be exported to MATLAB®. Once the code is imported in MATLAB®, the optimization process needed

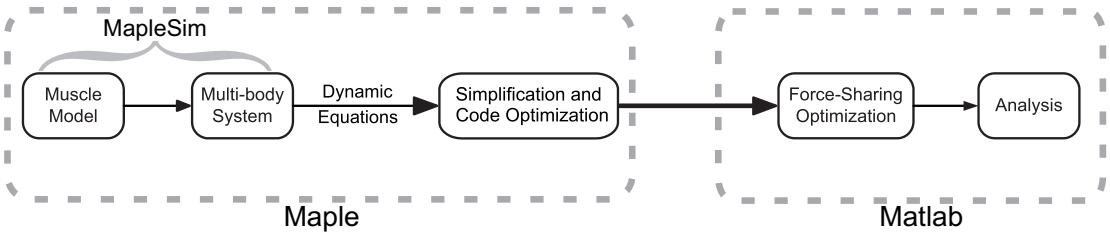


Figure 2.7: Work flow from MapleSim® to MATLAB®

for the force-distribution or the optimal control problem will be performed.

### 2.4.3 Solution Approaches of Equations of Motion

There are two approaches to solve the equations of motion: forward and inverse dynamics. In forward dynamics, forces and moments are known, and the motion and kinematics of bodies are unknown. In inverse dynamics, given the kinematics of the multi-body system (MBS), the goal is to find the corresponding forces and moments. In general, to perform a forward dynamics approach on a MBS, a set of DAEs in Equation 2.27 are required to be solved.

In inverse dynamics, the motion is generally specified from measurements using video imaging techniques [70, 71]. The following assumptions are required in doing an inverse dynamics analysis:

1. The prescribed motion is completely known.

2. The motion is consistent with the kinematic constraints of the defined model.

The column matrix $\mathbf{Q}$ can be separated into unknown and known terms $\mathbf{Q}_{unknown}$ and $\mathbf{Q}_{known}$, respectively. Let the unknown forces be considered as follows [18]:

$$\mathbf{Q}_{unknown} = \mathbf{C}^T \mathbf{F}_{unknown} \tag{2.29}$$

where $\mathbf{C}$ is a matrix mapping the force space to the space of generalized forces. Now, the first row of Equation 2.27 can be written in the following form:

$$\mathbf{\Phi}_{\mathbf{q}}^{T}\boldsymbol{\lambda} - \mathbf{C}^{T}\mathbf{F}_{unknown} = -\mathbf{M}\ddot{\mathbf{q}} + \mathbf{Q}_{known} \tag{2.30}$$

This equation will have a unique solution if the number of unknown forces and independent kinematic constraints is equal to the number of coordinates in the model. Otherwise, Equation 2.30 will not yield a unique solution due to the redundancy. It is to be noted that since there is no closed kinematic chain, and no constraint equation, in musculoskeletal models, the term $\mathbf{\Phi}_{\mathbf{q}}^{T}\boldsymbol{\lambda}$ will be zero.

### 2.4.4 Kinematic Relations due to Muscles

In early models of musculoskeletal systems, muscles were considered as single lines, i.e., one single line connects the origin and insertion of the muscle, which is not a valid assumption in general. Muscles have different paths of effect; some can be assumed as a straight line, called two point muscles, but for most of muscles there is not a reasonable line that can model the force line of effect through the muscle. In Figure 2.8, two typical muscles are depicted to show this statement better. Semimembranosus (SM) is a two point muscle within the knee joint range of motion; however, the Tensor Fasciae Latea (TFL) has a more complicated geometry and can be modelled as a multi-linear path muscle passing through some via points [18]. According to Figure 2.8, SM as a two-point muscle is a bi-articular joint muscle; therefore length and velocity of the tendon-muscle unit can be written as follows:

$$l_{SM}^{tm} = l_{SM}^{tm}(\theta_1, \theta_2) \text{ and } v_{SM}^{tm} = v_{SM}^{tm}(\theta_1, \theta_2, \dot{\theta}_1, \dot{\theta}_2) \tag{2.31}$$

where $\theta$, $\dot{\theta}$ are joint angle and angular speed, respectively.

As shown in Figure 2.8, the TFL can be divided to three straight lines 1, 2, and 3, in which each segment can be treated as a two-point muscle, e.g., the length and velocity of $\text{TFL}_1$ will be functions of $\theta_1$, $\dot{\theta}_1$, respectively. Consequently, given the origins and insertions

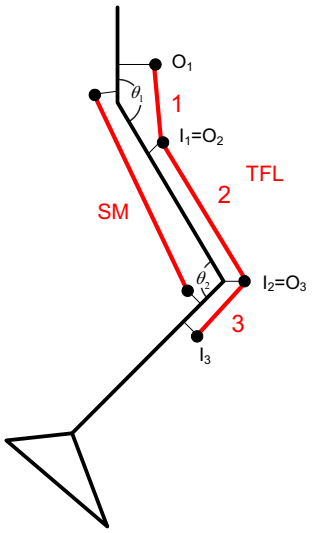


Figure 2.8: Different force effect paths of two typical muscles, SM and TFL [18]

of muscles, above relations can be used to calculate the tendon-muscle lengths ($l^{tm}$) and velocities ($v^{tm}$) at different system kinematics.

## 2.5 Chapter Summary

In this chapter, a literature review for modelling of human musculoskeletal systems was presented. The chapter started with muscle modelling where three major muscle models in the literature were introduced, and advantages and disadvantages of each were brought up. The chapter was continued with muscle redundancy solutions; SO and DO were discussed as main approaches and also popular objective functions were presented. Eventually, a section was dedicated to multibody formulation of musculoskeletal system dynamics.

The next chapter introduces the proposed techniques to solve the optimal control problem and also muscle redundancy involved in human musculoskeletal modelling.

# Chapter 3

# Optimal Control of Musculoskeletal Systems

In this chapter, a few approaches to solve the optimal control and muscle redundancy problems of human musculoskeletal systems are addressed. In each section, the approach is introduced, an example is presented, and a discussion of the efficacy, advantages, and disadvantages of the approach is given.

## 3.1 Introduction

When the goal is to find the optimal time-history of functions of interest, such as muscle forces or activations, one must solve a Dynamic Optimization (DO) or an Optimal Control Problem (OCP). DO, in spite of high computation cost, results in more realistic results as it considers all the time-course in the optimization procedure and solves for the time-history of the decision signals. Therefore, in contrast to SO, DO takes into account the effect of previous time instants on the current instant of simulation.

In the books by [72–74], several approaches for solving a general optimal control problem are presented, including linear quadratic regulator (LQR) control, linear quadratic

Gaussian (LQG) control, variational approaches such as direct collocation (DC), model predictive control (MPC), and parametrization. For all techniques, pros and cons are involved. It should be noted that not all of those approaches are applicable to musculoskeletal modelling; for instance, LQR and LQG are for linear systems only, MPC normally works in linear or linearized systems with quadratic optimization form only, and DC requires a complicated implementation and thus has been scarcely applied recently [75].

Local parametrization has been used by a few researchers, e.g., [14,76]. Locally parametrizing the control signals or state variables sounds like a promising approach as it captures the local dynamics of the system as long as the local considered windows are small enough, which is relative. However, by increasing the number of parametrization windows, the scale of the optimization problem, and therefore CPU time, increases significantly, which is a serious challenge.

The main focus in the next two sections of this chapter is to introduce the global parametrization approach and proposed functions. Using a control signal parametrization method, the OCP is converted to a nonlinear optimization problem by using parametric pattern functions as the control inputs, the neural excitations. Different parametrization functions might be used, based on the information of the system, degree of nonlinearity, and a priori data. Global and local parametrization might be utilized. For instance, different orders of polynomials can be used for the global control parametrization [77], or splines as local functions within finite windows of the simulation [76, 78]. Although global parametrizing, compared to local parametrization, seems to be possibly missing some local dynamics of the system, this approach will provide good sub-optimal results in general. Also, for applications with no drastic changes in the control signals (a priori knowledge of the system behaviour is required), global parametrization will still output reasonable results. In addition, global parametrization will reduce the number of decision variables considerably, which results in significant reduction of the CPU time.

## 3.2 Polynomial Global Parametrization

### 3.2.1 Introduction

In this section, a model for forward dynamic simulation of the rapid tapping motion of an index finger is presented. The model consists of a 1-dof horizontal pendulum with two muscles (one as flexor and the other as extensor). The goal of this analysis is to solve the force-sharing problem during a desired motion, as well as to investigate the maximum motion frequency that the assumed muscles can achieve for the finger. The pattern of each muscle excitation signal is assumed to be a sixth-order polynomial function of time. The first reason for assuming such a pattern is that filtered, rectified, and normalized EMG signals are quite smooth and can be curve-fitted by a suitable continuous mathematical function such as a polynomial, and the second is that assuming a continuous and continuously differentiable function like a polynomial will help the optimizer to meet the nonlinear constraints on the excitation signal within the optimization problem definition. Thirdly, assuming a parametric continuous function may lead possibly to symbolic simplifications and analytical solutions.

### 3.2.2 Example: Finger Tapping

The muscle model is a three-element Hill model based on [3]. The activation and contraction dynamics expressions employed for this model are presented in Appendix A.3.

The following assumptions are made for the finger modelling and simulation:

1. The maximum isometric force $F^m_{max}$ is assumed to be 100 N for both the extensor and the flexor muscles. It seems reasonable for the flexor muscle since it is supposed to act as a resultant of all flexor muscles. For the sake of similarity of the flexor and the extensor, the same value is assumed for both.

2. Anthropometric properties of the index finger, including length, mass and moment of inertia are taken from [79]. The composite moment of inertia is calculated given the moments of inertia of the three phalanges of the index finger.

3. Muscle moment arms are assumed to be constant during the motion because of small finger rotation amplitude, and both radii are assumed to be 10 mm, which agrees with the dimensions of metacarpophalangeal joint [80].

4. The desired motion is defined as follows:

$$\theta_d(t) = 0.21 \sin(\omega_d t) \tag{3.1}$$

where 0.21 rad is the amplitude of the considered motion according to [81], and $\omega_d = 2\pi f_d$ in which $f_d$ is the frequency of the sinusoidal defined motion.

**Optimization Problem Description**

The control signals are globally parametrized by 6th-order polynomials:

$$u = p_6 t^6 + p_5 t^5 + p_4 t^4 + p_3 t^3 + p_2 t^2 + p_1 t + p_0 \tag{3.2}$$

Therefore, the optimizer job is to look for the optimal coefficients of the two control signals, for a total of 14 variables. A set of nonlinear constraints will be imposed to the problem to meet the bounds on the neural excitations, i.e., $0 \leq u \leq 1$.

The objective function for simulating this model is defined as a linear combination of two cost functions $J = \mu J_1 + (1 - \mu) J_2$:

$$J = \frac{\mu}{\tau} \sum_{j=1}^{2} \int_0^\tau a_j^2 \, dt + \frac{1-\mu}{\tau \max(\theta_d^2)} \int_0^\tau (\theta_s - \theta_d)^2 \, dt \tag{3.3}$$

where the first term in the objective functional describes a physiological objective function (activation effort) based on [50], whereas the second term accounts for the tracking job. In

Equation 3.3, $\tau = 1/f_d$ is the motion period, $j$ is the muscle index, and $\theta_s$ is the simulated joint angle. The weight factor $\mu$ indicates the relative importance of the physiological term against the tracking error. Since in this simulation, tracking of the motion is much more important, the weight factor is assumed to be 0.1, which implies higher significance of the tracking error. It must be noted that the objective functional is written so that each term in dimensionless.

Finally, Sequential Quadratic Programming (SQP) as implemented in the fmincon function in the Optimization Toolbox of Matlab® is used as the optimizer. For the initial guess needed in SQP, results of the same case using a Genetic Algorithm as the optimizer were used. Consequently, the optimization approach applied to solve for the muscle redundancy is a hybrid method.

**Results and Discussion**

Different sets of simulations are run. The major focus is on motion frequency variation; to be brief, only the plots regarding some frequencies are shown. Another set of simulations is performed to examine the effect of gravity, and a separate one is done to see the finger mass effect. Also, it is investigated how the optimization weight factor affects the results.

The first set of results are presented in Figures 3.1 to 3.3. Each figure includes one set of simulations and consists of four plots: $\theta_d$ and $\theta_s$ (desired and simulated motions), excitations, activations, and muscle forces. Figures 3.1 to 3.3 are dedicated to motion frequency variations. In this investigation, the focus is on how increasing the motion frequency affects the results. The purpose is to find the maximum frequency that this biomechanical system can follow. Motion frequency is started from 2(Hz) (Figure 3.1) and increased to 3, 4, 5, 6 (Figure 3.2), and 7 Hz (Figure 3.3), where it was observed that the system is not able to produce the desired motion any more. In this case, values of the total cost function increased significantly, see Table 3.1, and the created motion differs from the desired motion definitely.

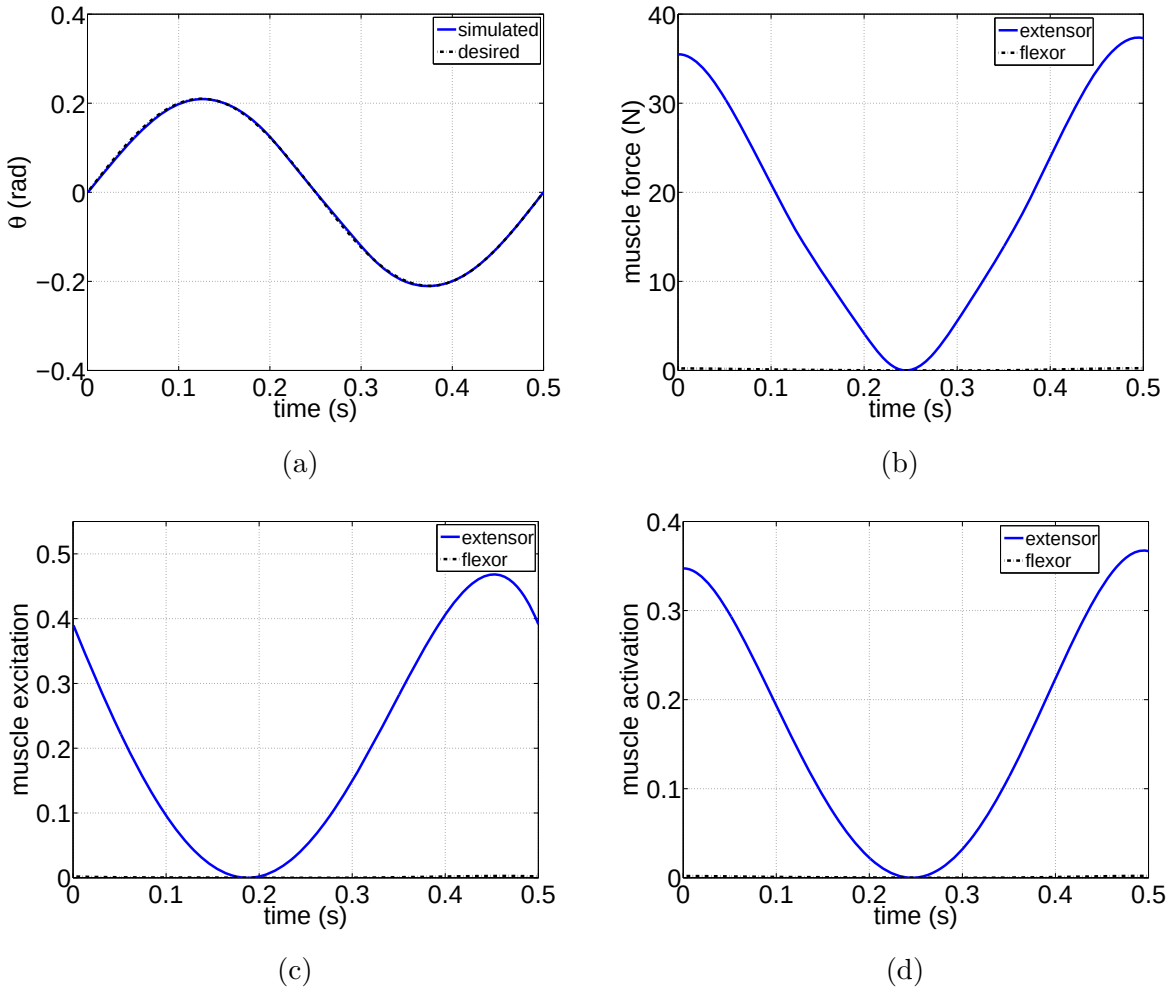


Figure 3.1: Simulation results with $f_d$=2 Hz: (a) desired and simulated joint angle $\theta$, (b) muscle forces, (c) muscle excitations, and (d) muscle activations

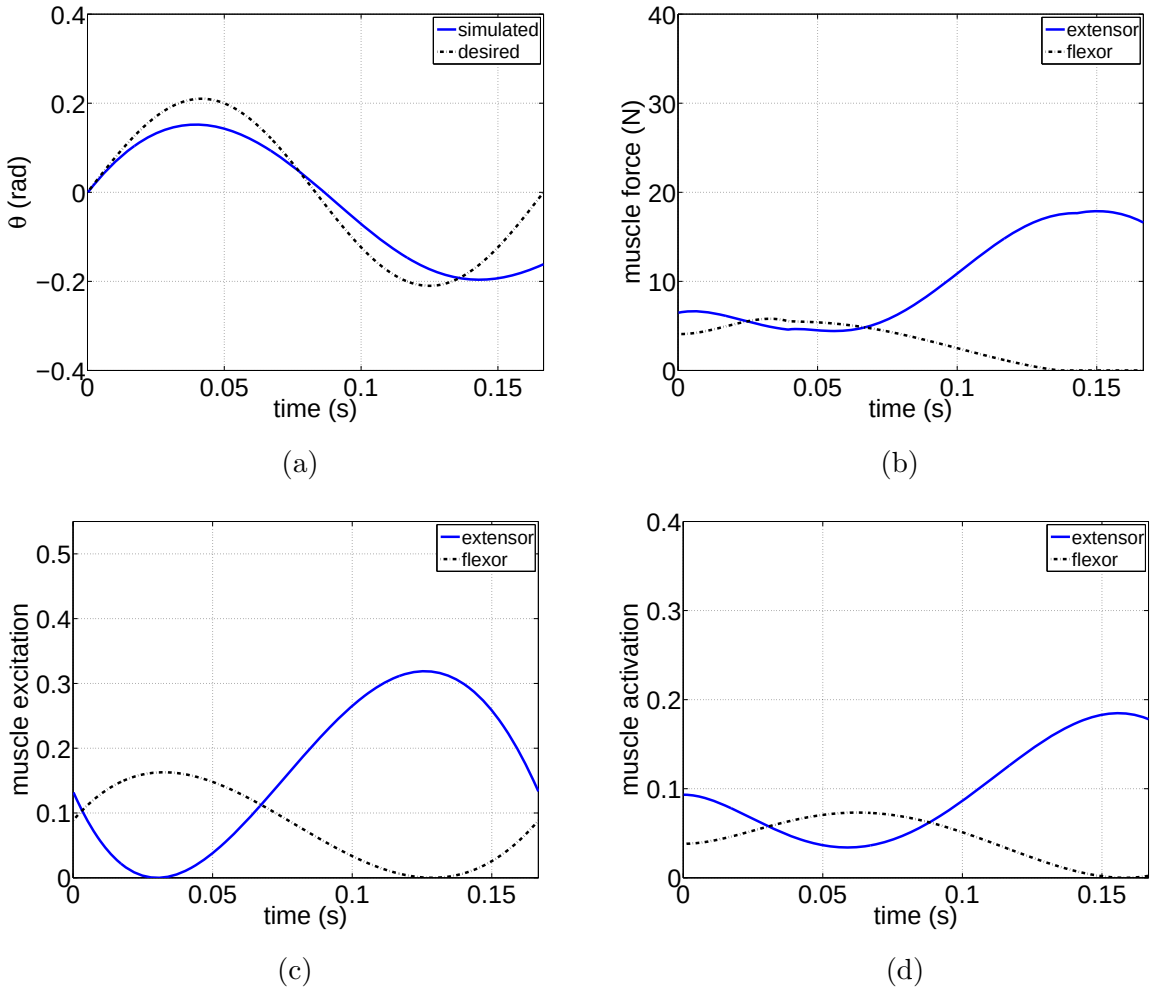


Figure 3.2: Simulation results with $f_d$=6 Hz: (a) desired and simulated joint angle $\theta$, (b) muscle forces, (c) muscle excitations, and (d) muscle activations

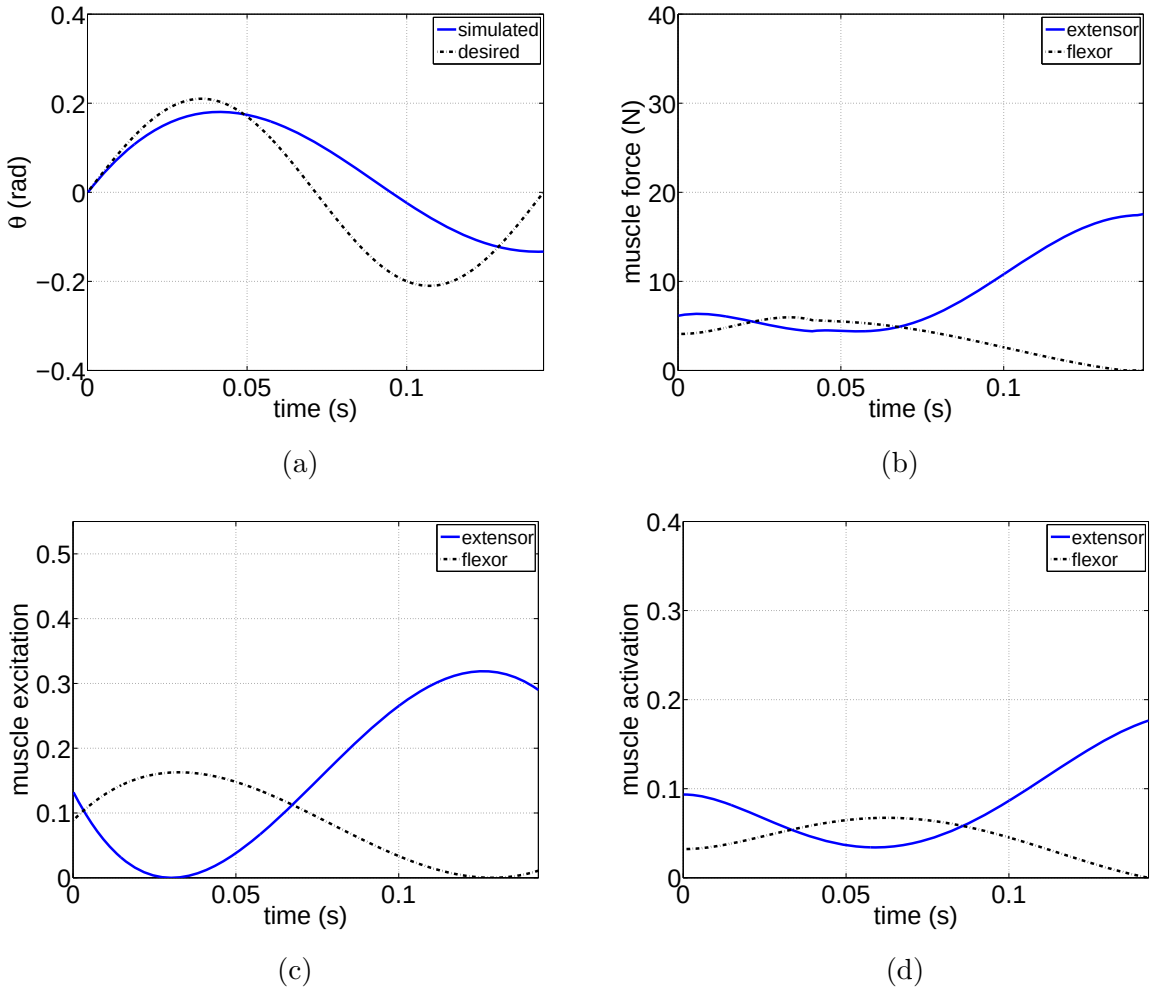


Figure 3.3: Simulation results with $f_d$=7 Hz: (a) desired and simulated joint angle $\theta$, (b) muscle forces, (c) muscle excitations, and (d) muscle activations

Table 3.1: Variation of motion frequency and cost function values

| Frequency(Hz) | $J$ | $J_1$ | $J_2$ |
|---|---|---|---|
| 2 | 0.041 | 0.101 | 0.035 |
| 4 | 0.196 | 0.145 | 0.201 |
| 5 | 0.211 | 0.176 | 0.215 |
| 6 | 0.898 | 0.109 | 0.986 |
| 7 | 1.553 | 0.097 | 1.714 |

It must be mentioned that, in general, what activation dynamics does, based on the first order model, is to make a time delay between neural excitation and activation signals; moreover, a small scaling also occurs between these two signals [1]. When $f_d$=2 (Figure 3.1), the simulated and the desired motions are the same, i.e., $J_2$ is relatively small as seen in Table 3.1. Excitation values of the extensor are much more than those of the flexor, due to the fact that the muscles are uni-articular joint muscles (they span only one joint) and theoretically no coactivation will occur [56]. It implies that at this frequency, the extensor and the gravity perform the extension and flexion without any requirement to the flexor. The flexor muscle has negligible values of excitation, which again is related to the help of gravity and absence of co-activation.

As the motion frequency is increased from 2 Hz, the ability of the finger to follow the desired motion decreases, as can be observed from increased $J_2$ values in Table 3.1. Also the cost of activations to track the desired motion is increased, resulting in more activation (greater $J_1$ value).

Table 3.1 implies that as the motion frequency increases from 2 to 5 Hz, the demand of cost ($J_1$) increases, and the error of tracking, $J_2$, increases as well. From 6 Hz on, it is observed that although the total cost function increases, the physiological cost required for motion tracking, $J_1$, decreased; it means that in this case, increasing the muscle activations does not help to better imitate the desired trajectory. By looking at Figures 3.2 and 3.3,

it is seen that the optimization process has found the simulated trajectories at the least activation efforts, although those trajectories do not look similar to the desired ones.

There are a number of studies in the literature on finding the maximal frequency or speed at which a finger can move. Kuboyama et al. [82] mentions 6.46 Hz while [83] reports 6.92±0.56 Hz. The results of this study imply that this maximal frequency is around 6 Hz which is close to the available values in the literature. These mentioned references have measured the desired value experimentally, so the maximal motion frequency extracted from the results of this study predicts the experiments quite well.

The reason why the model is not able to track the desired motion is that at high motion frequencies, the required contraction velocity is more than the velocity at which muscle can produce the force to satisfy the equations of motion. Figure 2.4(b), which shows the force-velocity relationship schematically, implies that when the concentric contraction velocity increases, the force production ability decreases. Therefore, the muscle can move faster only if it can produce enough force to satisfy the equations of motion. At around 6 Hz, as the maximal frequency, muscle must contract with the maximum velocity of 79.2 mm/s, which will lead to small force generation ability. Since the muscle can not create enough force at such a velocity in order to satisfy the equations of motion, it is not able to move at this velocity and can not track the desired motion.

A separate study is also done to investigate the sensitivity of the simulation outputs to the finger mass. To this goal, finger mass is reduced to 50%, and the optimal control problem is resolved for this case at $f_d$=2. The quality of the motion tracking was the same as the one shown in Figure 3.1(a). Optimal muscle excitations, activations, and forces of this case are depicted in Figure 3.4. These results can be compared to those of the same case but with 100% finger mass, illustrated in Figure 3.1. The excitation values in the case with 50% mass are less, which is reasonable, and the values are approximately scaled compared to those of the case with 100% mass. This can also be observed by comparing the activations and forces of two cases better. Based on that, the modelling framework is able to simulate the system response even with a large change in model mass, which is

necessary for subject-specific simulations.

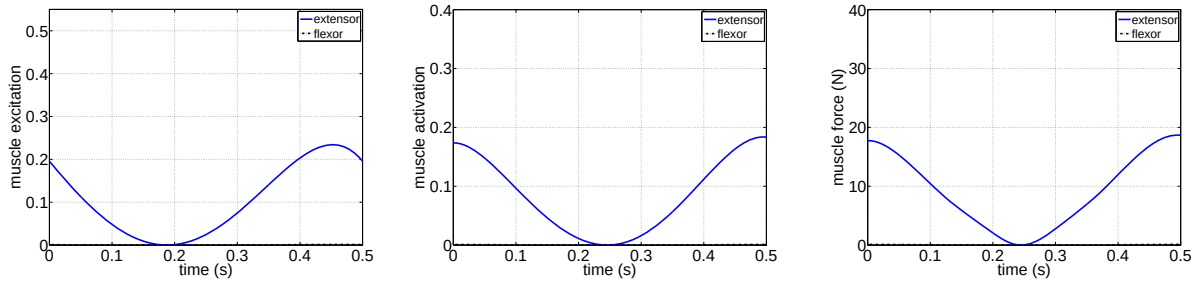


(a) (b) (c)

Figure 3.4: Optimal results for $f_d$=2 Hz and 50% of index finger mass: (a) excitations, (c) activations, and (d) forces

## 3.3 Fourier Series Global Parametrization

The aim of this section is to introduce a Fourier series (FS) based parametrization function for the muscle excitations, which are the control signals in musculoskeletal dynamics. The Fourier series patterns implemented here are similar to those presented by Peasgood et al. [22], but deployed for joint angles. Here, the optimal control is converted to a parametric optimization problem that looks for the optimal coefficients of the control vector, a set of muscle excitations. Although desired control signals are approximated with finite-term patterns, this approach is potentially efficient as it reduces the number of optimization variables considerably, especially compared to the alternative case that discrete control node values are the search variables as in [54], or control signals are locally parametrized. In other words, in a global parametrization approach, the variables are a few function coefficients, in contrast to the many control nodes at the simulation time instances, which are the variables in the alternative approach. Finally, numerical optimization is used to solve the muscle redundancy problem.

Fourier series terms are chosen here to approximate the excitation signals globally,

where these functions consist of the first $2K+1$ terms of a FS as follows:

$$u(t) = A_0 + \sum_{k=1}^{K} [A_k \sin(\frac{2\pi kt}{\tau}) + B_k \cos(\frac{2\pi kt}{\tau})] \tag{3.4}$$

where $K$ is assumed to be 5 according to [22], resulting in 11 coefficients for each muscle neural state. Then, the optimization algorithm seeks the optimal set of coefficients for excitation parametrized functions to minimize the objective functional and satisfy the constraints. At each iteration of optimization, after constructing the excitation functions, the system dynamics including muscle activation and contraction dynamics, and system equations will be integrated to find the relevant state vector of that iteration. It should be highlighted that neural excitations must be bounded between 0 and 1. These bounds will be in the form of nonlinear constraints imposed to the optimization framework.

### 3.3.1 Objective Functions

Two major objective functions, which are variously used in the literature, are used here: activation effort and metabolic energy.

#### Activation Effort

The first type of objective function group is the one that computes the amount of activation effort of the muscles to perform a motion. It can be formulated as the following:

$$J = \frac{1}{\sum S_i} \frac{1}{\tau} \sum_{i=1}^{n} S_i \int_0^{\tau} a_i^P dt \tag{3.5}$$

where $a_i$ is the muscle activation, $\tau$ is the motion period, $S_i$ is a weighting factor for muscle $i$, $n$ is the number of muscles considered in the model, and $P$ is an exponent. This type of objective function has been used by many researchers with different weighting factors and exponents, either in discrete form for SO or integral form for DO, such as [43, 75, 84, 85]. It should be noted that $J$ is dimensionless.

**Metabolic Energy**

Metabolic energy expenditure of the muscles can be also considered as another form of the objective function. There are different phenomenological models in the literature for computing the heat rate produced by a muscle during contraction. Here, the model utilized for formulating the metabolic energy rate, which includes the muscle mechanical power, activation heat rate, maintenance heat rate, and the shortening/lengthening heat rate, is based on [7]. These equation are presented in Appendix B. Based on these, the objective function can be written as follows:

$$J = \frac{1}{\sum \max(\dot{E}_i)} \frac{1}{\tau} \sum_{i=1}^{n} \int_0^{\tau} \dot{E}_i dt \tag{3.6}$$

where $\dot{E}$ is the muscle metabolic energy rate. The objective function computes the total metabolic energy consumed by the musculoskeletal system from time 0 to $\tau$ of the motion. Again, the presented objective function is non-dimensionalized. A similar objective function is used by [55] except they divided it by the distance travelled in a human gait simulation.

### 3.3.2 Example: Forearm Modeling

A two-dimensional forearm model is studied as an example. The skeletal model consists of a forearm and hand while the wrist angle is assumed to be constant. The upper arm is also assumed to be kept beside the torso. Thus, the only dof is due to the elbow joint, which was assumed to be a revolute joint. Mass, inertia and center of mass position of the rigid body is according to anthropometric data reported in [10] assuming 80 kg for the body mass and 1.8 m for body height.

Seven muscles are considered in the model: Brachioradialis (BRD), Biceps Long Head (BICLH), Biceps Short Head (BICSH), Brachialis (BRA), Triceps Long Head (TRILH), Triceps Lateral Head (TRILT), and Triceps Medial Head (TRIMH). Muscle models are of

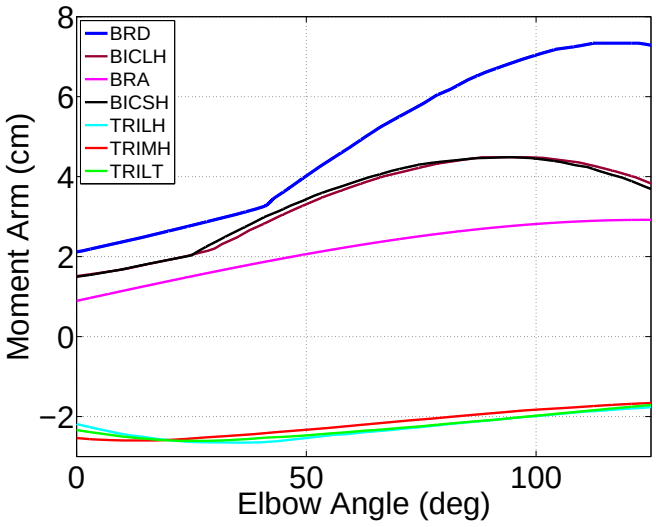


Figure 3.5: Moment arms plotted versus the elbow flexion angle. The moment arm data for all muscles is adopted from [8] except BRA, which is from [19].

the three-element Hill type according to [3]. The three components in the muscle model are the contractile element (CE), the parallel elastic element (PE), and the serial elastic element (SE). Muscle parameters are presented in Table 3.2. Additionally, muscle moment arms are implemented as functions of the elbow flexion angle; all moment arm data are taken from the model presented by Garner and Pandy [8] except that for the BRA muscle, which is adopted from the model by Murray et al. [19]. These moment arms are plotted against the elbow angle in Figure 3.5.

A motion tracking forward dynamic analysis is performed. To this goal, the desired elbow flexion angle motion was measured a priori, and the average motion considering the number of subjects and trials was calculated. Therefore, a motion tracking constraint is imposed to the optimization to produce a motion which is close to the average measured data. To this goal, a nonlinear constraint is adjoined to the optimization objective function as the following:

$$\left\|(\theta^{sim} - \theta^{exp})\right\|_{\infty} \leq \epsilon_{tr} \tag{3.7}$$

Table 3.2: Parameters of the model, adopted from [8]: muscle fiber optimal length $l^{ce}_{opt}$, muscle maximum isometric force $F^{m}_{max}$, tendon slack length $l_{slack}$, fiber pennation angle $\alpha_p$, and muscle volume $V$

| Muscle | $l^{ce}_{opt}$(cm) | $F^{m}_{max}$(N) | $l_{slack}$(cm) | $\alpha_p$(deg) | $V$(cm$^3$) |
|---|---|---|---|---|---|
| BRD | 27.03 | 101.58 | 6.04 | 5.00 | 83.19 |
| BICLH | 15.36 | 392.91 | 22.93 | 10.00 | 182.92 |
| BICSH | 13.07 | 461.76 | 22.98 | 10.00 | 182.92 |
| BRA | 10.28 | 853.90 | 1.75 | 15.00 | 256.96 |
| TRILH | 15.24 | 692.21 | 19.05 | 15.00 | 290.67 |
| TRIMH | 6.17 | 1268.87 | 19.64 | 15.00 | 237.28 |
| TRILT | 4.90 | 619.67 | 12.19 | 15.00 | 92.04 |

where $\epsilon_{tr}$ is the tracking constraint violation tolerance, and $\theta^{sim}$ and $\theta^{exp}$ are the simulated and experimental elbow joint angles, respectively. The constraint violation tolerance for motion tracking was chosen to be 0.1 rad. Other sets of constraints on the optimization problem include the following:

$$0 \leq u \leq 1 \tag{3.8}$$

where the chosen tolerances for these constraints are 1e-6. Each muscle excitation $u_i$ as a function of time was parametrized with the 11-term Fourier series, so the total number of control parameters in the model is 77. As explained earlier, two groups of objective functions $J$ are considered here, activation effort and metabolic energy. For the activation effort, two different weighting factors $S_i$ (unity and muscle volume) and exponents $P$ (2 and 3) are investigated, resulting in four forms of activation efforts. Consequently, five objective functions, as summarized in Table 3.3, and five sets of results are presented in this study. Muscle volume data are adopted from [8], which are presented in Table 3.2.

The equations of motion were written as first order ordinary differential equations

Table 3.3: Five different objective functions

| | Activation Effort | | Metabolic Energy |
|---|---|---|---|
| | $P = 2$ | $P = 3$ | |
| $S_i = 1$ | $J_1$ | $J_2$ | $J_5$ |
| $S_i = V_i$ | $J_3$ | $J_4$ | |

integrated with contraction and activation dynamics as presented below:

$$\dot{l}^m(t) = f_{CD}(l^m, l^{mt}, \dot{l}^{mt}, a) \tag{3.9}$$

where $l^m$, $\dot{l}^m$, $f_{CD}$, $l^{mt}$, $\dot{l}^{mt}$, and $a$ are muscle length, muscle velocity, contraction dynamics function, tendon-muscle length and velocity, and muscle activation, respectively. The activation and contraction dynamics expressions are presented in Appendix A.3. All the musculoskeletal dynamic equations were derived in the following form in MapleSim®:

$$\dot{x} = f(x, u, t) \tag{3.10}$$

where $x$ includes elbow joint angle and velocity, seven $l^m$ and seven $a$, resulting in a total of 16 states in the state vector of the dynamical system.

### 3.3.3 Experimental Design

The experiments included motion capture using Optotrak™and surface EMG using a Delsys™wireless system. The motion capture goal was to measure the elbow angle by attaching three markers on the wrist, elbow and shoulder of the subject. The surface EMGs of three muscle groups were measured: BRD, BIC, and TRI. The EMG signals, recorded at 2000 Hz, were high-pass filtered, full-wave rectified, normalized to subject's MVC (maximum voluntary contraction), and zero-lag low-pass filtered. The high-pass filter was done by means of a Butterworth 10th order at 20 Hz, where the low-pass filter

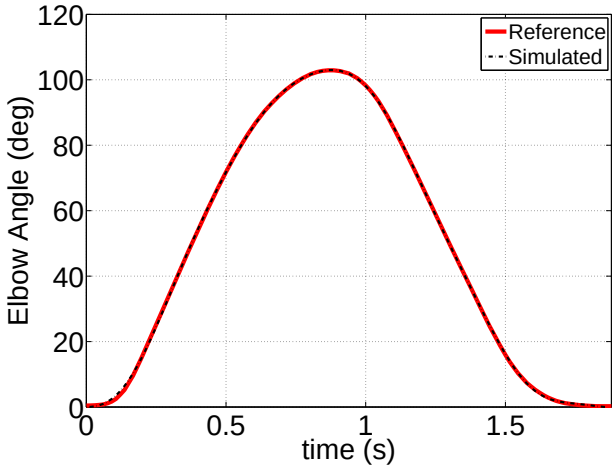


Figure 3.6: Simulated versus average measured forearm motion

was a Butterworth 3rd order at 5 Hz. Three male subjects, ages from 27-29, heights from 1.78-1.88 m, and body weights from 77-85 kg, were tested. To account for the repeatability of the experimental data, three trials were performed per each subject resulting in a total of 9 trials. The subjects were asked to perform the elbow flexion/extension at their own self-selected speeds. The average forearm motion $\theta^{exp}$ (with a period of nearly 1.9 s) was then tracked by the simulation.

### 3.3.4 Convergence Study

For each objective function, three different random initial points were obtained by solving the constrained optimization problem using a Genetic Algorithm (GA) in MATLAB®. Afterwards, these three solutions were used to run a Sequential Quadratic Programming (SQP) solver to take advantage of normally faster gradient-based algorithms. From those three runs, the best one was chosen to be the raw optimum. Using this new solution as a new initial guess, Pattern Search function as a Direct Search (DS) routine was then run to ensure the globality of the solution. If the objective function value of the DS was less, it was put into the SQP again. This cycle was repeated until the change in the objective function

was less than 1e-6 and the constraint violation values satisfied the defined tolerances, where the result was accepted as the global optimum.

### 3.3.5 Results

The results in Figure 3.6 show that the model has followed the desired trajectory very well. The reason why only one simulation graph is presented for the motion is that the quality of motion tracking for all five cases of objective function were quite similar.

The optimal muscle excitations using objective functions $J_1$ and $J_2$ (Figures 3.7(a,b)), and $J_3$ and $J_4$ (Figures 3.8(a,b)) express that in this type of motion, elbow flexors mostly do the defined job. During extension, joint flexors are active and control the limb that is under extension by gravity. Only at the beginning and the end of the period of the motion, elbow extensors are slightly active due to the fact that zero angle of elbow is not the angle providing the resting length for extensors. In the case that metabolic energy $J_5$ was used as the objective function, only one flexor and one extensor were recruited, as shown in Figure 3.9, which is not in agreement with the measured EMGs.

For activation effort cases $J_1$ to $J_4$, the patterns of the four flexor excitations are very similar. The values of the excitations are between 0 and 0.06, which show that for this type of motion, small muscle activity is required. To examine the model validity, simulation results of the muscle excitations using $J_4$ as the objective function are presented in Figure 3.10 and compared against measured EMGs for three muscle groups. The results show that there is a reasonable correlation between the measured and simulated values.

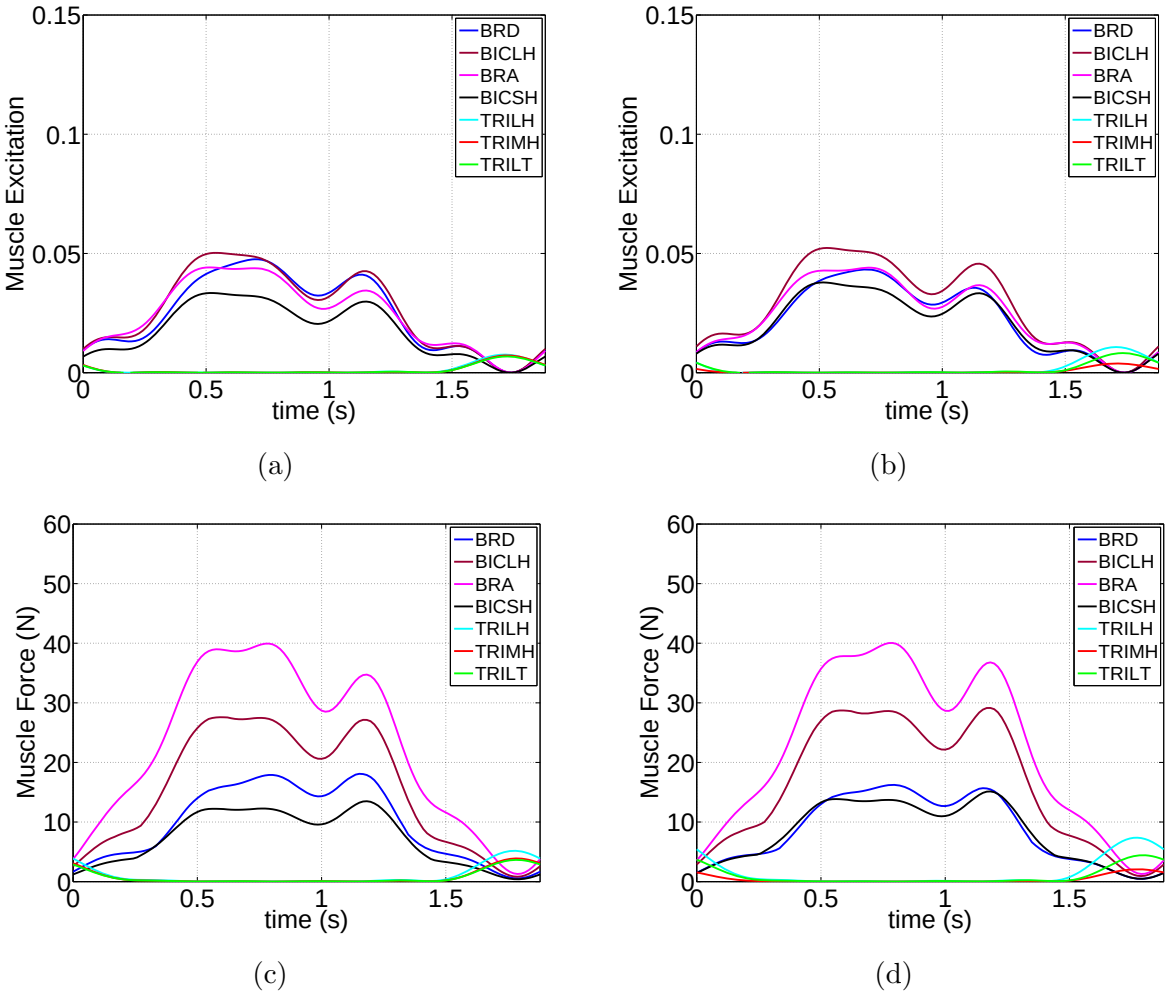


Figure 3.7: Optimal muscle excitations and forces: (a,c) with $J_1$ and (b,d) with $J_2$

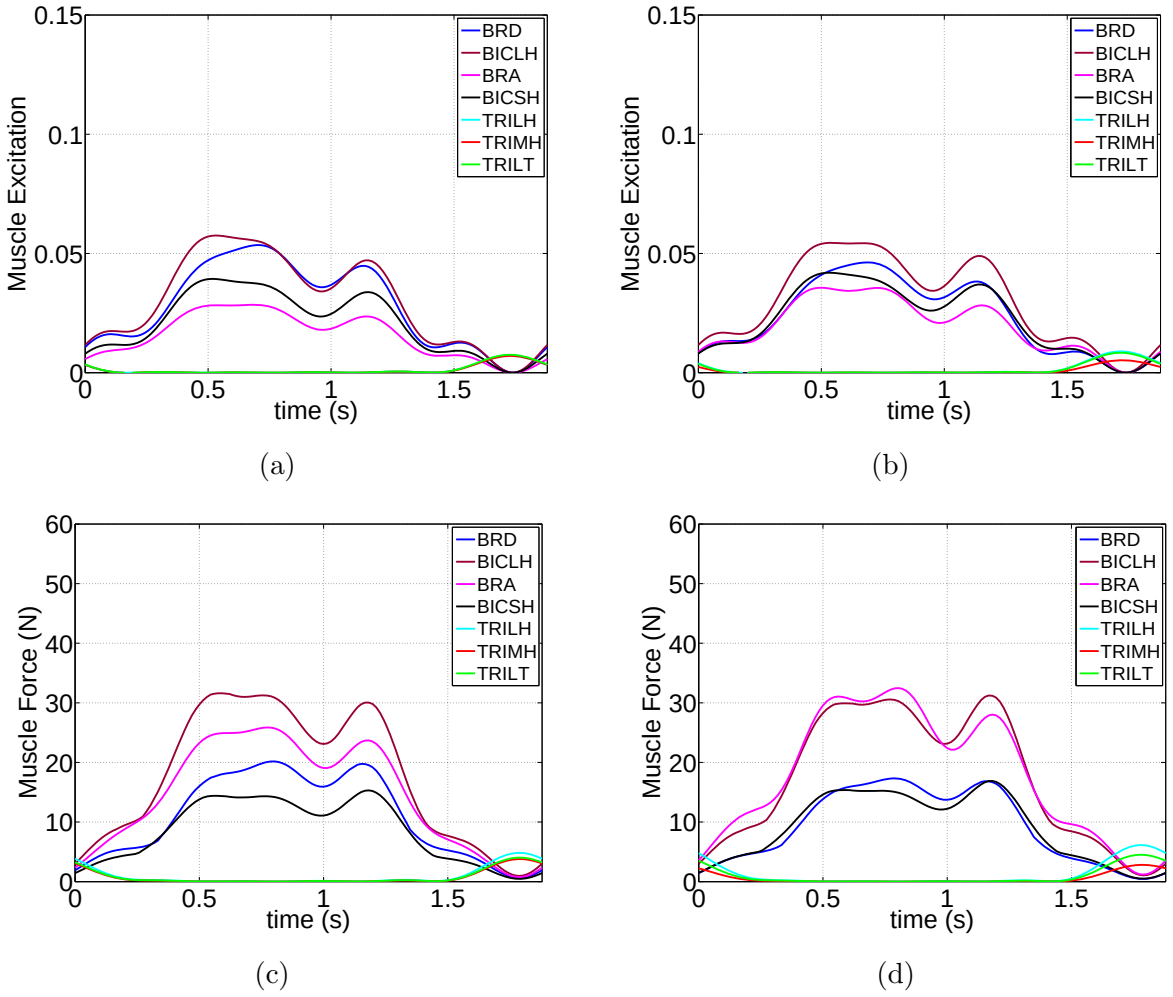


Figure 3.8: Optimal muscle excitations and forces: (a,c) with $J_3$ and (b,d) with $J_4$

### 3.3.6 Discussion

Although in this section, a Fourier series was applied to a periodic example, this FS function can be utilized for non-periodic motions as well. Consider Equation 3.4. If $\tau$ is set to the motion period, the created function will be periodic in that time course; however, if $\tau$ is

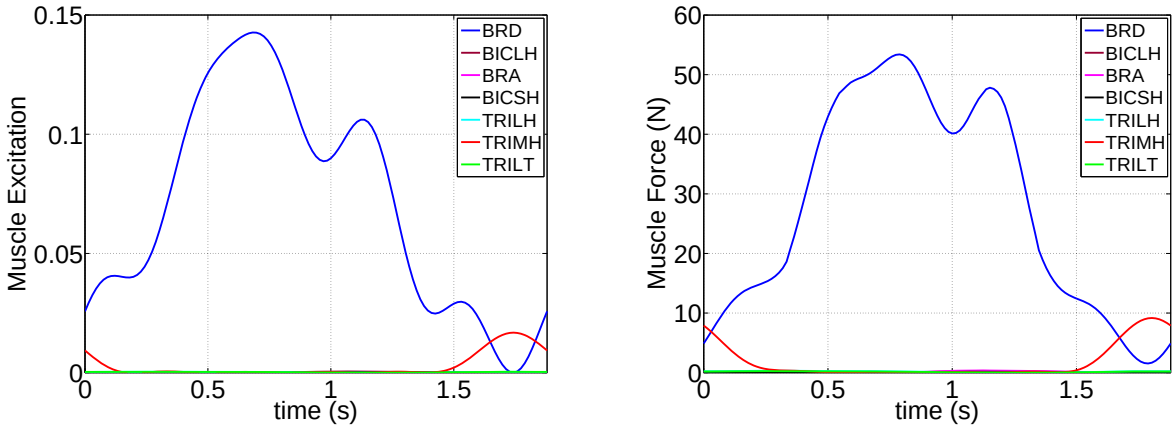


(a) (b)

Figure 3.9: Optimal muscle excitations and forces with $J_5$ as the objective function

free to be less than or greater than the motion duration, then the parametrization function is able to produce non-periodic patterns in that duration. In that case, the FS period $\tau$, which is different from the motion duration, will enter the optimization procedure as an additional parameter.

Optimal control problems can be converted to nonlinear parameter optimization problems using parametric pattern functions for the control signals. Choosing a suitable pattern function depends on the conditions of the problem. FS-based functions are smooth which can approximate the neural excitations in human movements. The number of FS terms utilized for each control input can be debatable and depends on the type of movement; it might be determined by having tentative before-hand information about the motion and the corresponding excitation signals.

The presented results show that the simulation results are in a fairly good agreement with the experimental data. Therefore, parametrizing the control signals with Fourier series terms is a suitable strategy in musculoskeletal simulations. Forearm motion was chosen to show the efficiency of the approach; however, for future work, more complicated motions such as human gait or running can be showcased.

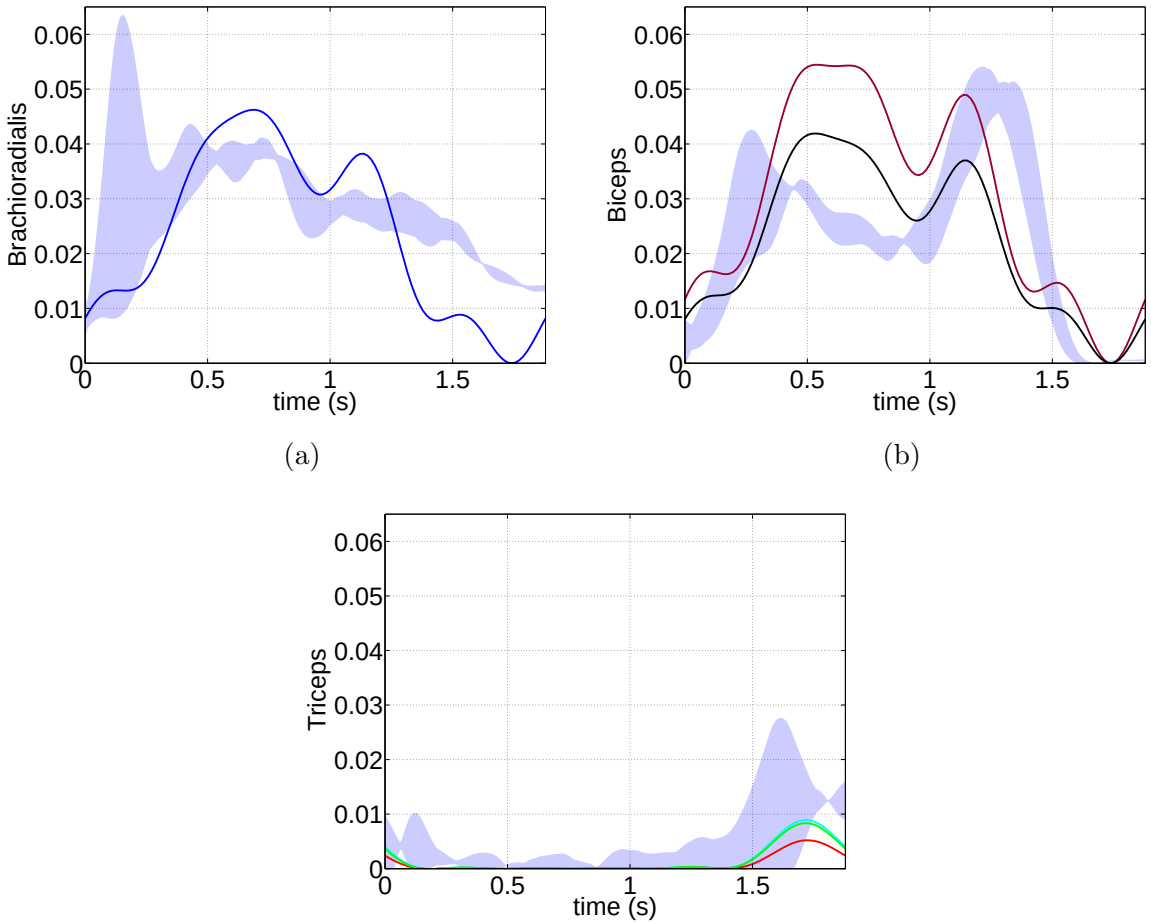


(a) (b) (c)

Figure 3.10: Comparison of the simulation results for muscle excitation $u$ (solid line, in case activation effort $J_4$ is minimized) against normalized EMGs (grey band) depicted as mean $\pm 1$ standard deviation

In Sections 3.2 and 3.3, parametrization was found to be a promising approach in Dynamic Optimization of human musculoskeletal systems. In terms of the quality of the optimal results, one can say that global parametrization provides reasonable results; however, this approach may lead to over-prediction of antagonistic coactivations.

Another aspect of any approach to solve muscle redundancy would be the time efficiency. The finger tapping example with two muscles using 6th order polynomials (total 14 parameters) took a total CPU time of fifteen minutes to find the global optimum. On the other hand, the forearm simulation with seven muscles using 11-term Fourier series (total 77 parameters) took nearly half an hour on the same machine to reach optimality. Additionally, calling the finger tapping model takes 0.4 seconds to run, whereas the forearm function takes 0.9 seconds. Given the aforementioned information, one can conclude that the optimizer had an easier job finding the optimal point for the forearm model. This can be associated with the type of the parametrization function. To explain that, consider the general form for a polynomial (PN) of order $n$:

$$f_{PN} = a_0 + a_1 t + a_2 t^2 ... + a_n t^n \tag{3.11}$$

with

$$\frac{\partial f_{PN}}{\partial a_n} = t^n$$

As can be interpreted from the Equation 3.11, the sensitivity of the approximated function with respect to the parameters is unbounded and increases drastically with time and corresponding order of the polynomial term. Now, consider a Fourier series function with $2K + 1$ terms. The sensitivities can be written as:

$$f_{FS} = A_0 + \sum_{k=1}^{K} [A_k \sin(\frac{2\pi kt}{\tau}) + B_k \cos(\frac{2\pi kt}{\tau})] \tag{3.12}$$

with

$$\frac{\partial f_{FS}}{\partial A_k} = \sin(\frac{2\pi kt}{\tau})$$

and

$$\frac{\partial f_{FS}}{\partial B_k} = \cos(\frac{2\pi kt}{\tau})$$

As can be noticed from comparing the sensitivities of the polynomial and FS functions, the sensitivity of polynomial coefficients blows up easily as the order of corresponding term

increases; however, the FS sensitivity remains bounded regardless of the value for $K$, which is a nice feature of an FS function.

The other interesting characteristic of the FS is that it provides a reasonable path for the optimization solver in finding the optimal coefficients. Consider simply the curve-fitting process using numerical optimization. No matter what high frequency is added to the function, the coefficients of the lower frequencies remain the same as long as the lowest frequency is kept constant, which is the case for periodic motions. As an example, an optimal excitation of the BICSH is set as the target, on which different orders of Fourier series with eleven, seven, and three terms are tested. The comparison of the FS functions is shown in Figure 3.11(a), and the optimal coefficients of the three cases are presented in Table 3.4(a). As can be seen from the coefficient values, when increasing the term from three to seven and eleven, the low frequency coefficients remain the same, which reduces the effort of the optimizer significantly.

This property of the Fourier series does not exist for polynomials. To show this as it was done for the FS, the similar target pattern is curve-fitted with three different orders of polynomials: 4th, 8th, and 10th. Figure 3.11(b) shows that the 11-term FS provides a much better fit than the comparable polynomial. The coefficient values of these three polynomial functions are presented in Table 3.4(b), which shows that, by increasing the order of a polynomial, coefficients of the lower order terms change considerably.

To examine this difference between FS and PN functions in solving a musculoskeletal problem, the forearm example is resolved by parametrizing the muscle excitations with 11-term polynomials. This can support the claim above. As the number of parameters for each muscle control and total number of parameters in the optimization is the same in both FS and PN approaches, the results and computational efficiencies are comparable. By parametrizing all muscle controls with 10th-order polynomials, the optimal control problem was solved again with $J_4$ as the objective function, and the optimal results of the motion tracking and the excitations are depicted in Figure 3.12. The final objective value functions for FS and PN functions are 0.10 and 0.12, respectively, which confirms

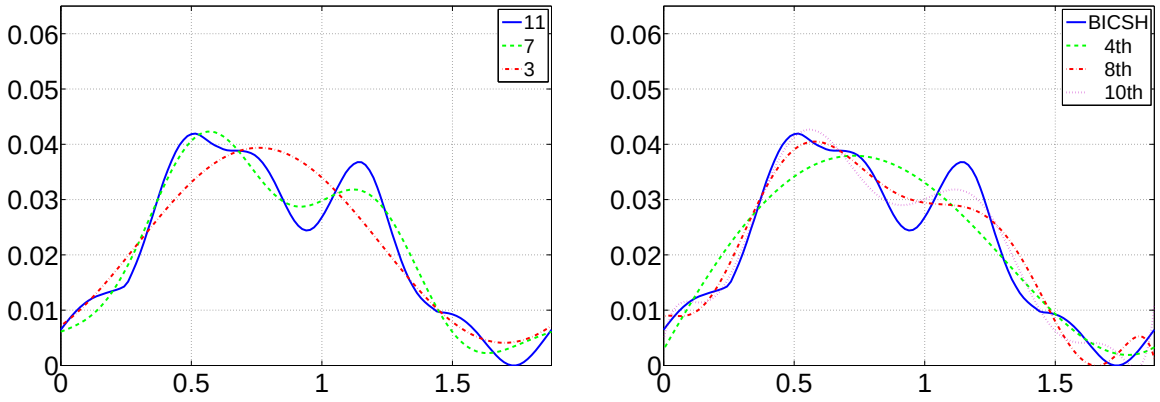


(a) (b)

Figure 3.11: Curve-fitting the results for an optimal BICSH excitation with (a) three Fourier series functions with 11, 7, and 3 terms and (b) 10th, 8th, and 4th order polynomials

that the results of the FS case are better. Also, by comparing the motion tracking in Figure 3.12(a) and Figure 3.6, one can observe that the motion tracking quality is better for the case when Fourier series was used as the parametrization function. Furthermore, the PN function leads to slightly more antagonistic coactivation between the flexors and extensors; see Figures 3.12(b) and 3.8(b).

An important aspect of comparing the two cases of FS and PN is the computational efficiency. It should be noted that both simulations were done on the same machine. The CPU time for the simulation with 11-term polynomial functions was fifty minutes, whereas the CPU time for the case using FS patterns was thirty minutes. These CPU times are those required to reach the global optimum, as discussed in Section 3.3.4. Therefore, Fourier series provide relatively better results and faster simulations in globally parametrizing the control signals in the optimal control of musculoskeletal systems.

Table 3.4: Optimal coefficients of the (a) three Fourier series functions with 11, 7, and 3 terms and (b) 10th, 8th, and 4th order polynomials curve-fitting an optimal BICSH excitation

(a)

| Coefficient | 11 | 7 | 3 |
|---|---|---|---|
| $A_0$ | 0.0217 | 0.0217 | 0.0217 |
| $A_1$ | 0.0100 | 0.0100 | 0.0100 |
| $B_1$ | -0.0145 | -0.0145 | -0.0145 |
| $A_2$ | 0.0019 | 0.0019 | - |
| $B_2$ | -0.0043 | -0.0043 | - |
| $A_3$ | -0.0028 | -0.0028 | - |
| $B_3$ | 0.0032 | 0.0032 | - |
| $A_4$ | 0.0015 | - | - |
| $B_4$ | -0.0012 | - | - |
| $A_5$ | 0.0021 | - | - |
| $B_5$ | 0.0024 | - | - |

(b)

| Coefficient | 10th | 8th | 4th |
|---|---|---|---|
| $P_0$ | 1.283 | 0.009 | 0.003 |
| $P_1$ | -10.537 | 0.014 | 0.083 |
| $P_2$ | 34.854 | -0.428 | -0.017 |
| $P_3$ | -57.844 | 4.359 | -0.060 |
| $P_4$ | 46.283 | -12.641 | 0.024 |
| $P_5$ | -7.438 | 16.959 | - |
| $P_6$ | -14.539 | -11.793 | - |
| $P_7$ | 10.029 | 4.127 | - |
| $P_8$ | -2.277 | -0.575 | - |
| $P_9$ | 0.210 | - | - |
| $P_{10}$ | 0.005 | - | - |

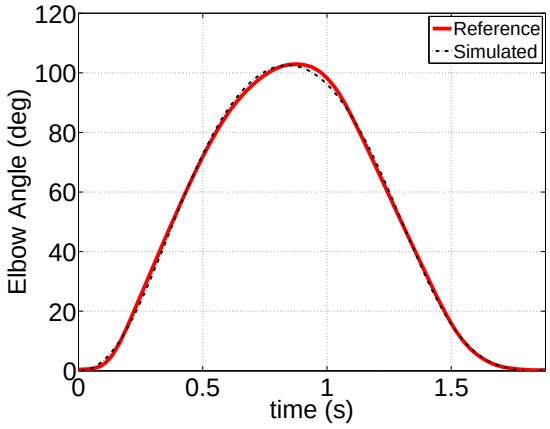


(a)

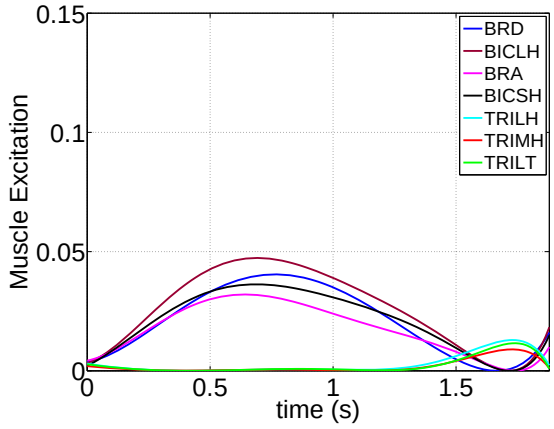


(b)

Figure 3.12: Optimal control of the forearm model by parametrizing the excitations with 11-term polynomials

## 3.4 Using Static Optimization in Forward Dynamic Simulation of Human Musculoskeletal Models

This section describes possible and efficient ways that static optimization can be used for forward dynamics (FD) of musculoskeletal simulations. Static Optimization (SO) is a suitable approach in solving the muscle redundancy in inverse dynamics (ID). In other words, given all the state values of the system, it can easily solve the under-determinate problem of assigning a share of each muscle to the torque of the joint(s) it is spanning. The major issue with SO is that it is an instantaneous optimization. In another statement, it freezes time and solves the under-determinacy of the system as a nonlinear optimization, not an optimal control problem (OCP). The outcome of that is the independency of the results from one instant of time to another, which is prone to result in abrupt changes of the values of interest [55, 86]. These instantaneous changes are mostly unphysiological. Another issue with SO is that due to the nature of the technique, a time-integral cost function (CF) like metabolic energy rate cannot be used.

In forward dynamics, the equations of motion need to be integrated. These equations, that in the best case are in the form of Ordinary Differential Equations (ODE), are highly nonlinear and require a good solver. Most of these ODE solvers are variable step, i.e., they return and correct their step size to reduce the integration error. In FD, if realistic results are desired regardless of the computation cost, DO is a suitable choice; however, DO needs a high and somewhat unacceptable simulation time. Then the question is: would it be possible to take advantage of SO speed in FD? More simply, would it be possible to use SO for FD?

### 3.4.1 Implementing SO for FD

To answer these questions, a forearm model with seven muscles is considered; the model properties are the same as those presented in Section 3.3. First, we run SO to find the

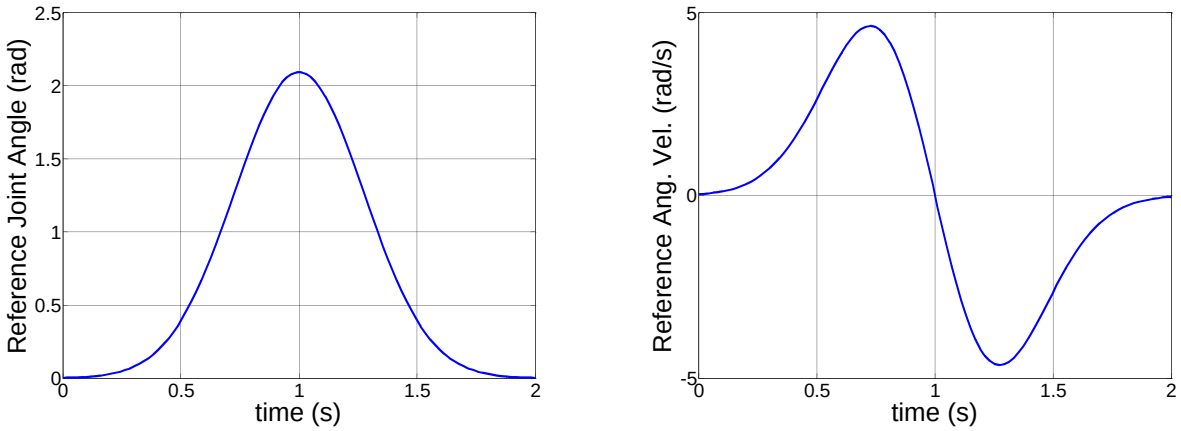


Figure 3.13: Reference joint angle and angular speed used for inverse dynamics in SO and tracking forward dynamics in FSO

optimal solutions for muscle forces given the motions. As there is no integration error involved in SO, as long as the optimization convergence is assured, we can set these results as the reference base for comparison. The reference motion is a Gaussian curve over 2 s, with a peak value of 120 degrees of the joint angle, as shown in Figure 3.13. The objective function used for SO is as follows:

$$J_j = \sum_{i=1}^{n} F_{ij}^P \tag{3.13}$$

where index $i$ and $j$ refer to the muscle index and the time instant of simulation, respectively, $F$ is a muscle force and exponent $P$ is the polynomial order of the objective function that can be 1, 2, 3, or 10. There is one equality constraint on the problem that assures the dynamic consistency of the results, as follows:

$$\sum_{i=1}^{n} r_{ij} F_{ij} = T_{net,j}^m \tag{3.14}$$

where $r_{ij}$ is the moment arm of muscle $i$ at time $j$; these moment arms are assumed to be constant, based on the average data reported in [9]. $T_{net,j}^m$ is the total joint torque due to muscles calculated from inverse dynamics at each instant of time. Additionally, there are a set of box bounds on the optimization variables (muscle forces) to guarantee their values

Table 3.5: Moment arms for this forearm model, based on average values of [9]

| Muscle | BRD | BICLH | BICSH | BRA | TRILH | TRIMH | TRILT |
|---|---|---|---|---|---|---|---|
| $r$(cm) | 5.40 | 2.73 | 3.70 | 2.10 | 2.00 | 2.58 | 2.00 |

are non-negative and do not go beyond their physiological maximum force capacity, $F^m_{max}$. The results for the optimal forces from SO for different exponent values are presented in Figure 3.14. The corresponding CPU time is also mentioned. The idea of using SO in FD is that it needs to be implemented as in ID, but we need to come up with a way of integrating the ODEs as it is forward dynamics. Consequently, integration of the state equations should be done instantaneously. In other words, starting from initial conditions of the states, we use any solver to calculate the state values for the next time step using a discrete state space form of the system. As a result, at each integration, there would be only two control points involved in total, where the values of one are already known. It should be noted that integration points will be more than two as the solver might create several interpolations; however we will only use the first and the last.

At each instant of simulation, the framework needs to track the target motion as well. At each instant of time, in addition to solving the muscle redundancy, a motion tracking must be done through either motion tracking constraints or as follows:

$$J_j = \mu_1 \sum_{i=1}^{n} F_{ij}^P + \mu_2 TrErr_j \tag{3.15}$$

Assuming $q$ to be the joint angle, different forms of tracking error can be used as follows:

$$TrErr_j = \left(q_j^{sim} - q_j^{des}\right)^2 \tag{3.16}$$

$$TrErr_j = \left(q_j^{sim} - q_j^{des}\right)^2 + \left(\dot{q}_j^{sim} - \dot{q}_j^{des}\right)^2 \tag{3.17}$$

$$TrErr_j = \left(q_j^{sim} - q_j^{des}\right)^2 + \left(\dot{q}_j^{sim} - \dot{q}_j^{des}\right)^2 + \left(\ddot{q}_j^{sim} - \ddot{q}_j^{des}\right)^2 \tag{3.18}$$

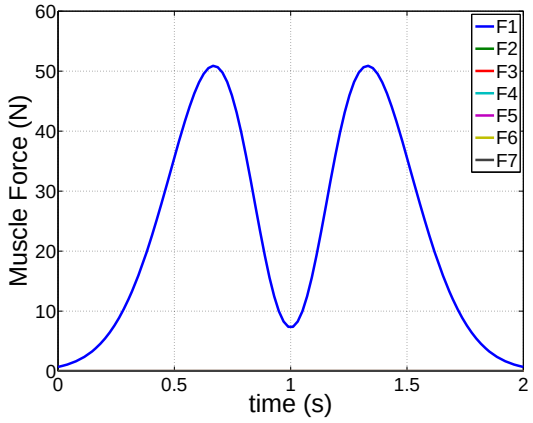


(a) Muscle forces with SO, $P = 1$

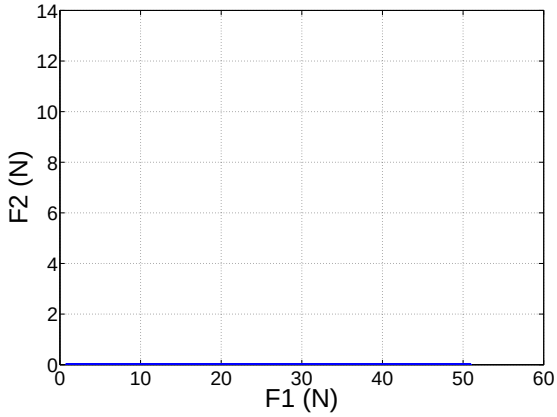


(b) Sample force ratio with SO, $P = 1$

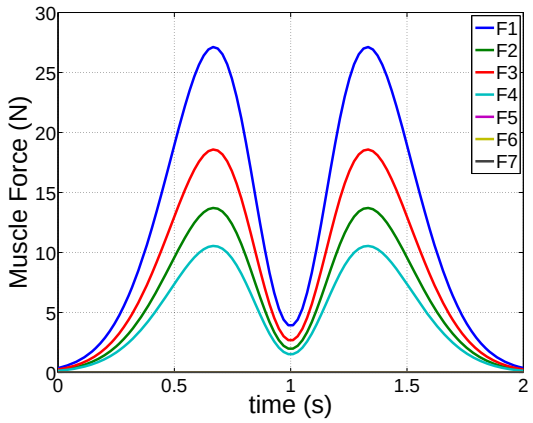


(c) Muscle forces with SO, $P = 2$

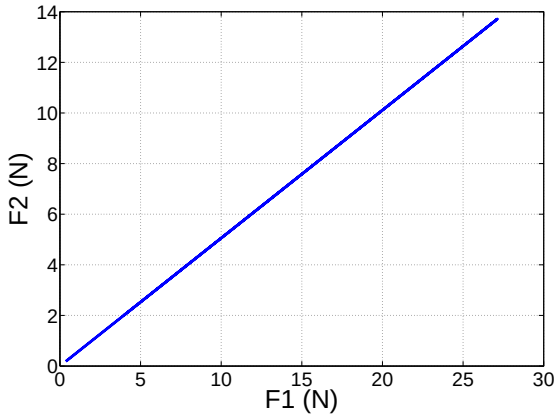


(d) Sample force ratio with SO, $P = 2$

Figure 3.14: Results of SO for two different values of the exponent $P$, (a,b) $P = 1$ (CPU time: 8 s), and (c,d) $P = 2$ (CPU time: 6 s)

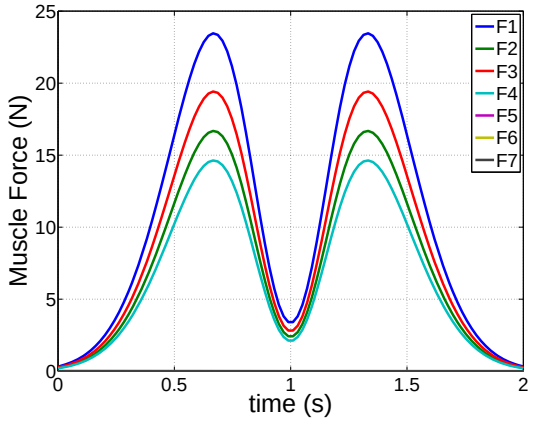


(a) Muscle forces with SO, $P = 3$

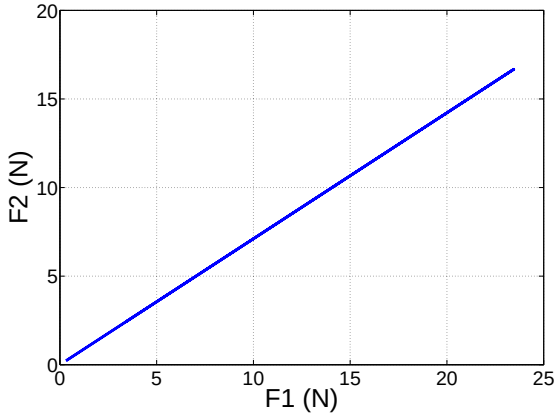


(b) Sample force ratio with SO, $P = 3$

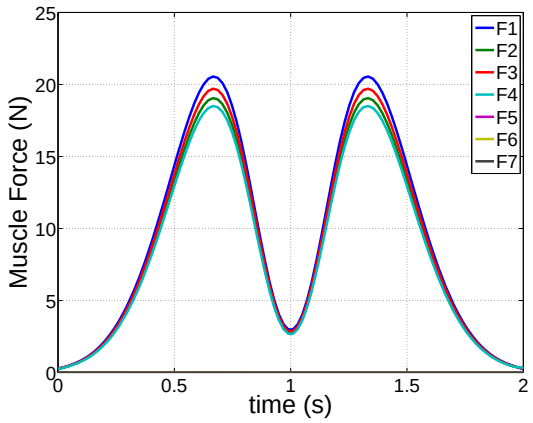


(c) Muscle forces with SO, $P = 10$

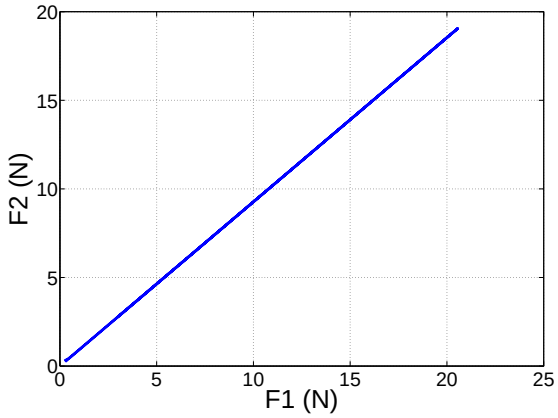


(d) Sample force ratio with SO, $P = 10$

Figure 3.15: Results of SO for two different values of the exponent $P$, (a,b) $P = 3$ (CPU time: 7 s), and (c,d) $P = 10$ (CPU time: 31 s)

Equation 3.16 sets the joint angle as the target only, whereas Equations 3.17 and 3.18 include joint angular velocity and acceleration, respectively as well. This is very similar to the Baumgarte constraint violation stabilization (CVS) approach [87], as the idea of both is to minimize the expression above. In Equation 3.17, the joint angle is controlled with a Proportional-Derivative (PD) controller and is assisting the acceleration level of the errors between the simulated and desired values. This PD controller is similar to the Computed Muscle Control (CMC) approach [58].

A modification to improve the Baumgarte CVS is to add an integral term to the controller to build up a Proportional-Integral-Derivative (PID) expression [88]. If $\psi = q_j^{sim} - q_j^{des}$, then the modified instantaneous tracking error, which again can be implemented as either constraints or a sub-objective function, will be the following:

$$\ddot{\psi} + \alpha\dot{\psi} + \beta\psi + \gamma \int_0^{t_j} \psi dt \tag{3.19}$$

At each instant of forward integration $t_j$, the integral term, calculates the area under the curve of the joint angle error from the beginning of the simulation. This integral term can resolve the probable sudden changes of the integrated states in Equation 3.18 as this integral term adds a time-history of errors to the static optimization problem. Furthermore, this modification decreases the steady state error, as a PID advantage over PD, compared to the case Equation 3.18 is applied as the tracking term.

### 3.4.2 Results and Comparison between FSO and SO

For comparison, two popular cases of $P = 2$ and $P = 3$ are presented in Figures 3.16 and 3.17. FSO was simulated on 100 uniformly distributed control points with a variable step integrator (based on RK45). For each case, four plots are demonstrated, which are joint angle and angular velocity, optimal muscle forces and force space plot of first muscle force versus second one. The corresponding CPU times are also presented for comparison with SO. The FSO results are nearly the same as those of SO. Also the simulation periods acquired for FSO until convergence are more than SO, but considerably better than the

similar case with dynamic optimization. It should be added that a DO with Fourier series parametrization excluding the muscle dynamics takes approximately half an hour to converge to global optimum, which is not comparable to the FSO CPU time.

## 3.5 Analytical Muscle Force Sharing Solution with Maple®

In this section, solving the muscle redundancy problem analytically using Maple is investigated. This approach provides some nice properties, including its time efficiency; however, it involves a few shortcomings that will be discussed.

A case study with no bounds on the muscle forces was presented in Section 2.2.6. The goal here is to add lower bounds on the muscle forces and investigate the possibility of solving the optimization problem with different objective functions using Maple®.

### 3.5.1 Analytical Approach with only Lower Bounds on the Muscle Forces

Assume the same objective function and equality constraint due to the net muscle torque again, as in Equation 2.15. In addition, another constraint or bound can be adjoined to the problem, which is due to the fact that muscle forces cannot be negative:

$$F_i \geq 0 \tag{3.20}$$

To make the equations less lengthy, only two muscles are considered and $P$ is assumed to be 2 and 3 in this section. First $P = 2$ is investigated.

**Case $P$=2:** The objective function and the torque constraint will be given by:

$$J(F_i) = \left(\frac{F_1}{N_1}\right)^2 + \left(\frac{F_2}{N_2}\right)^2 \text{ subject to } g_{eq}(F_i) \triangleq T^m_{net} - r_1F_1 - r_2F_2 = 0 \tag{3.21}$$

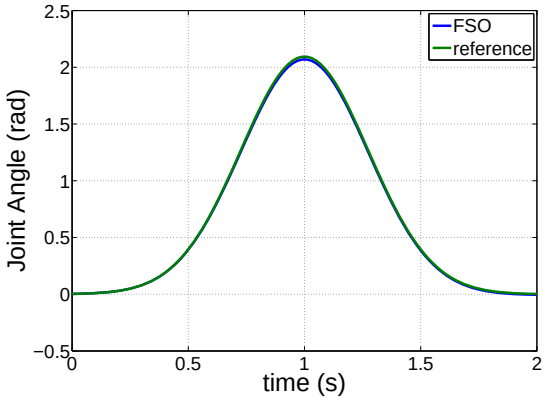


(a) Joint angle

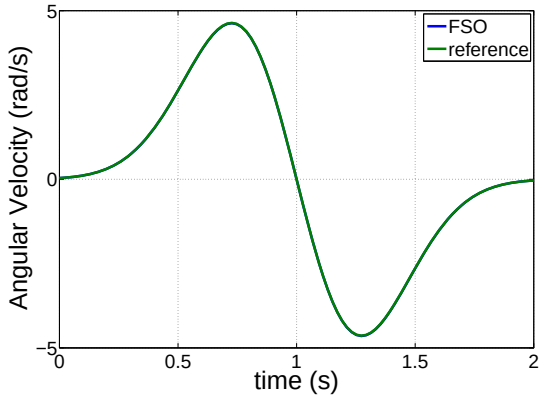


(b) Joint Ang. Vel.

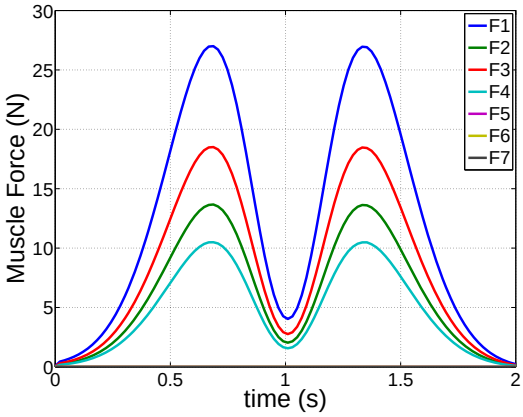


(c) FSO Muscle forces

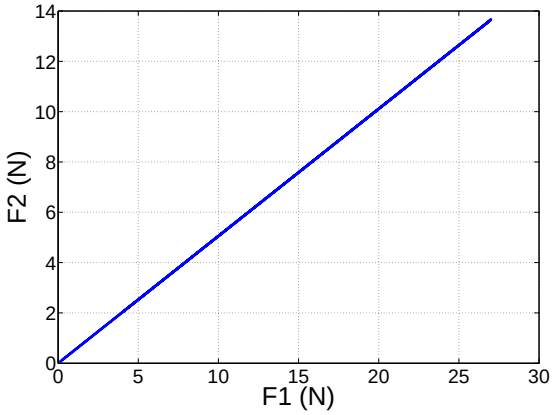


(d) Sample FSO force ratio

Figure 3.16: Results of FSO for the exponent $P = 2$. CPU time= 20 s

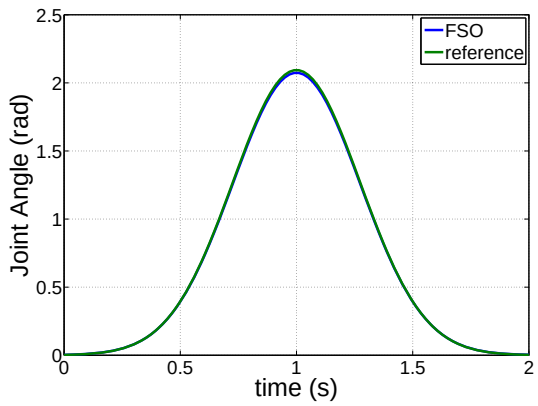


(a) Joint angle

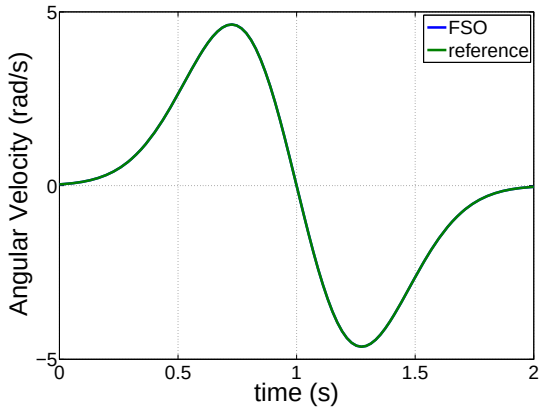


(b) Joint Ang. Vel.

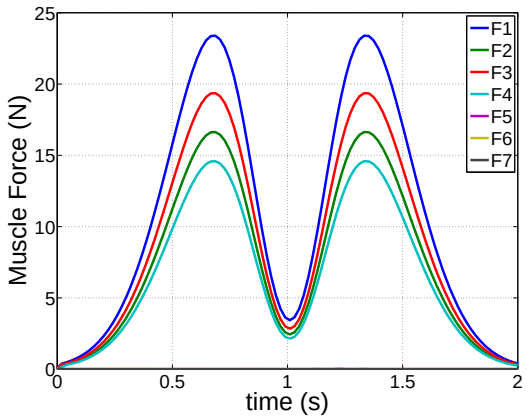


(c) FSO Muscle forces

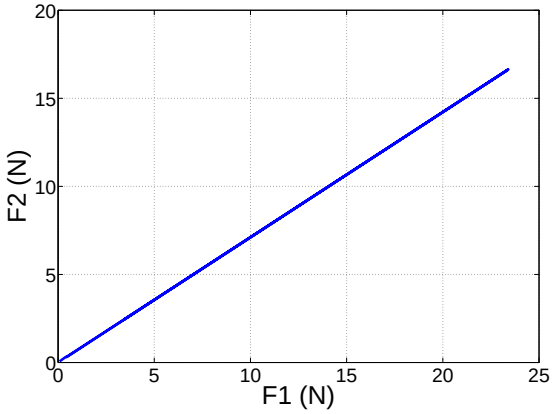


(d) Sample FSO force ratio

Figure 3.17: Results of FSO for the exponent $P = 3$. CPU time= 29 s

To append the inequality constraint on the forces, it is converted to an equality constraint using the idea of a slack variable $s_i$:

$$s_i^2 - F_i = 0 \tag{3.22}$$

As the variable $s_i$ is always non-negative, it assures the non-negativity of the muscle forces. Then, the Lagrangian can be written as:

$$\mathcal{L} = J + \lambda g_{eq} + \mu_1 \left(s_1^2 - F_1\right) + \mu_2 \left(s_2^2 - F_2\right) \tag{3.23}$$

$$\mathcal{L} = \left(\frac{F_1}{N_1}\right)^2 + \left(\frac{F_2}{N_2}\right)^2 + \lambda \left(T_{net}^m - r_1 F_1 - r_2 F_2\right) + \mu_1 \left(s_1^2 - F_1\right) + \mu_2 \left(s_2^2 - F_2\right) \tag{3.24}$$

where $\mu_i$ are those Lagrange multipliers associated with inequality constraints converted to equality ones. For more simplicity, assume $N_1$ and $N_2$ to be unity as well. The gradient and the Hessian of the Lagrangian with respect to the decision variables, the Lagrange multipliers and the slack variables, are:

$$\nabla\mathcal{L} = \left\{2F_1 - \mu_1 - \lambda r_1, 2F_2 - \mu_2 - \lambda r_2, s_1^2 - F_1, s_2^2 - F_2, T_{net}^m - F_1 r_1 - F_2 r_2, 2\mu_1 s_1, 2\mu_2 s_2\right\} \tag{3.25}$$

$$\nabla^2\mathcal{L} = \{2, 2, 0, 0, 0, 2\mu_1, 2\mu_2\} \tag{3.26}$$

To find the global minimum of the problem, the gradients are required to be equal to zero and solved while the Hessian needs to be non-negative. From Karush-Kuhn-Tucker (KKT) optimality conditions, see e.g. [73], $\mu_1$ and $\mu_2$ need to be zero or positive. Also from KKT complementary slackness condition and multiplier sign condition, if $s_i$ is non-zero, $\mu_i$ should be zero, whereas when $s_i$ is zero, $\mu_i$ would be non-negative.
From the first two components of the gradient vector, forces can be derived as:

$$F_1 = \frac{1}{2}(\mu_1 + \lambda r_1) \text{ and } F_2 = \frac{1}{2}(\mu_2 + \lambda r_2) \tag{3.27}$$

Now, by substituting expressions in Equation 3.27 into the three equality constraints (which are equal to the third, fourth and fifth component of the gradient vector, respectively),

three subsequent expressions will be yielded:

$$\left\{-\frac{1}{2}\mu_1 - \frac{1}{2}\lambda r_1 + s_1^2, -\frac{1}{2}\mu_2 - \frac{1}{2}\lambda r_2 + s_2^2, T_{net}^m - \left(\frac{1}{2}\mu_1 + \frac{1}{2}\lambda r_1\right) r_1 - \left(\frac{1}{2}\mu_2 + \frac{1}{2}\lambda r_2\right) r_2\right\} \tag{3.28}$$

Then by adding last two components of the gradient vector to the components shown in Equation 3.28, one can equal those to zero and solve them for $\mu_1$, $\mu_2$, $\lambda$, $s_1$, and $s_2$. Due to the multiple branches of solution, this was done taking advantage of the Polynomial-Ring command in Maple® that outputs all the different possibilities of the solution. The following are all four branches of solution:

$$\begin{aligned}
&\left\{2s_1^2 - \lambda r_1, 2s_2^2 - \lambda r_2, \mu_1, \mu_2, (r_1^2 + r_2^2)\lambda - 2T_{net}^m\right\} \\
&\left\{2s_1^2 - \lambda r_1, s_2, \mu_1, \mu_2 + \lambda r_2, r_1^2\lambda - 2T_{net}^m\right\} \\
&\left\{s_1, 2s_2^2 - \lambda r_2, \mu_1 + \lambda r_1, \mu_2, r_2^2\lambda - 2T_{net}^m\right\} \\
&\left\{s_1, s_2, \mu_1 + \lambda r_1, \mu_2 + \lambda r_2, 2T_{net}^m\right\}
\end{aligned} \tag{3.29}$$

To get the final expressions for the original problem, components of each branch need to be equalled to zero from the last to the first. In the following, the explanations on all the four branches are presented. First, the last branch is discussed which is the simplest.

**Branch four:** It is the trivial solution, and means that total muscle torque is zero and $s_1$ and $s_2$ are zero too, which results in zero values for forces no matter whether the muscles are flexor or extensor.

For branches one to three, for better understanding, let us assume $T_{net}^m > 0$ ; the other case when net muscle moment is negative will be discussed after.

**Branch one:**

$$\lambda = \frac{2T_{net}^m}{r_1^2 + r_2^2},\ \mu_1 = 0,\ \mu_2 = 0,\ s_1^2 = \frac{\lambda r_1}{2},\ s_2^2 = \frac{\lambda r_2}{2} \tag{3.30}$$

It can be feasible only if $r_1$ and $r_2$ are positive, i.e., both muscles are flexors. It should be noted that the zero values for $\lambda_1$ and $\lambda_2$ in this branch meets the condition of non-negativity of Hessian elements and also KKT conditions. The optimal forces for this branch will be

the following:

$$F_1^{opt} = \frac{T_{net}^m r_1}{r_1^2 + r_2^2},\ F_2^{opt} = \frac{T_{net}^m r_2}{r_1^2 + r_2^2} \tag{3.31}$$

**Branch two:**

$$\lambda = \frac{2T_{net}^m}{r_1^2},\ \mu_1 = 0,\ \mu_2 = -\lambda r_2,\ s_1^2 = \frac{\lambda r_1}{2},\ s_2 = 0 \tag{3.32}$$

The value for $\lambda$ shows that only the first muscle has contribution to the net torque; $\mu_1$ is zero; $s_2$ is zero; $\mu_2$ should be non-negative that occurs only if $r_2$ is negative, i.e., this branch is considering a case that muscle one is a flexor, whereas muscle two is an extensor. Optimal muscle forces are:

$$F_1^{opt} = \frac{T_{net}^m}{r_1},\ F_2^{opt} = 0 \tag{3.33}$$

**Branch three:** This branch is similar to branch two, but muscle one is an extensor and muscle two is a flexor. Optimal muscle forces are:

$$F_1^{opt} = 0,\ F_2^{opt} = \frac{T_{net}^m}{r_2} \tag{3.34}$$

It should be added that if $T_{net}^m$ is negative, in branch one, both muscles with negative moment arms are active; in branch two, extensor muscle one is active, whereas in branch three, extensor muscle two is active only. Note that these branches are in agreement with the unconstrained problem presented in [56].

**Case $P$=3:** Similar to the case $P = 2$, the system has two muscles and the optimization framework is imposed to non-negativity inequality constraint of forces. The branches of solution for this case are:

$$\begin{aligned}
&\left\{T_{net}^m - r_1 s_1^2 - r_2 s_2^2,\ \lambda r_1 - 3s_1^4,\ \lambda r_2 - 3s_2^4,\ \sqrt{3\mu_1 + 3\lambda r_1} - 3s_1^2,\ \sqrt{3\mu_2 + 3\lambda r_2} - 3s_2^2\right\} \\
&\left\{T_{net}^m - r_2 s_2^2,\ \lambda r_2 - 3s_2^4,\ \sqrt{3\mu_1 + 3\lambda r_1} - 3s_1^2,\ \sqrt{3\mu_2 + 3\lambda r_2} - 3s_2^2,\ s_1\right\} \\
&\left\{T_{net}^m - r_1 s_1^2,\ \lambda r_1 - 3s_1^4,\ \sqrt{3\mu_1 + 3\lambda r_1} - 3s_1^2,\ \sqrt{3\mu_2 + 3\lambda r_2} - 3s_2^2,\ s_2\right\} \\
&\left\{T_{net}^m,\ \sqrt{3\mu_1 + 3\lambda r_1} - 3s_1^2,\ \sqrt{3\mu_2 + 3\lambda r_2} - 3s_2^2,\ s_1,\ s_2\right\}
\end{aligned} \tag{3.35}$$

Again, assuming $T_{net}^m > 0$ and a little bit of calculation and simplification, each of the four branches of solution can be analysed:

**Branch one:** From component five and three, knowing $s_2$ is non-zero, $\mu_2$ will be zero. Similarly, from components four and two, knowing $s_1$ is non-zero, $\mu_1$ will have to be zero. As $s_1$ and $s_2$ are not zero in this branch, zero values for $\mu_i$ meets the KKT condition. Now, putting all components to zero and solving for $\lambda$, the following solution will be acquired:

$$\lambda = \frac{3{T_{net}^m}^2}{\left(r_1^{3/2} + r_2^{3/2}\right)^2} \tag{3.36}$$

Consequently, the corresponding optimal muscle forces of branch one are:

$$F_1^{opt} = \frac{r_1^{1/2} T_{net}^m}{r_1^{3/2} + r_2^{3/2}},\ F_2^{opt} = \frac{r_2^{1/2} T_{net}^m}{r_1^{3/2} + r_2^{3/2}} \tag{3.37}$$

which is in agreement with the solution with no bound on muscle forces, Equation 2.24.

**Branch two:** $s_1$ and $\mu_2$ will be zero and the optimal muscle force will be the following:

$$F_1^{opt} = 0,\ F_2^{opt} = \frac{T_{net}^m}{r_2} \tag{3.38}$$

**Branch three:** $s_2$ and $\mu_1$ will be zero and the optimal muscle force will be the following:

$$F_1^{opt} = \frac{T_{net}^m}{r_1},\ F_2^{opt} = 0 \tag{3.39}$$

**Branch four:** This branch is the trivial solution: $s_1$ and $s_2$ will be zero, and $\mu_1$, $\mu_2$, and $\lambda$ can have any value.

### 3.5.2 Example: Forearm Modelling

To show the efficiency of the analytical approach, a forearm simulation is run. The model specifications are the same as those presented in Section 3.3. Muscle moment arms and the reference motion is the same as that mentioned in Section 3.4. In this way, our results can be compared to those of the numerical SO presented in Section 3.4. The net muscle torque

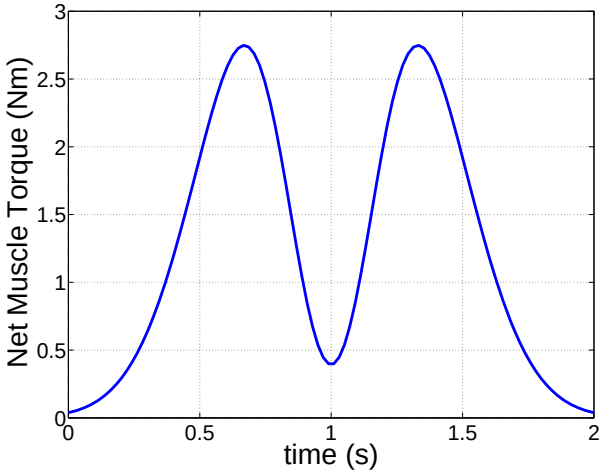


Figure 3.18: Muscle net torque at the elbow joint for the specified Gaussian motion

is plotted in Figure 3.18. As the net muscle torque is positive throughout the course of motion, based on the description above, only muscles with positive moment arms (elbow flexors) contribute, and extensors will be off. For $P = 2$, Equation 3.31 shows the optimal muscle forces, but for only two flexors; however, there are four flexors in this example. A generalization based on inductive reasoning and compatible with the analytical solution for the unconstrained case can be made as follows:

$$F_j = \frac{r_j^{\frac{1}{P-1}}}{\sum_{i=1}^{n} r_i^{\frac{P}{P-1}}} T_{net}^m \tag{3.40}$$

From Equation 3.40, which is a duplicate of Equation 2.24, and that the extensors have zero contribution, the optimal muscle forces can be computed. In Figure 3.19, the results from the analytical force sharing for the flexors is depicted for case $P = 2$. Note that $n$ is the number of muscles contributing to the net muscle torque, which is the number of flexors here, and therefore is equal to 4.

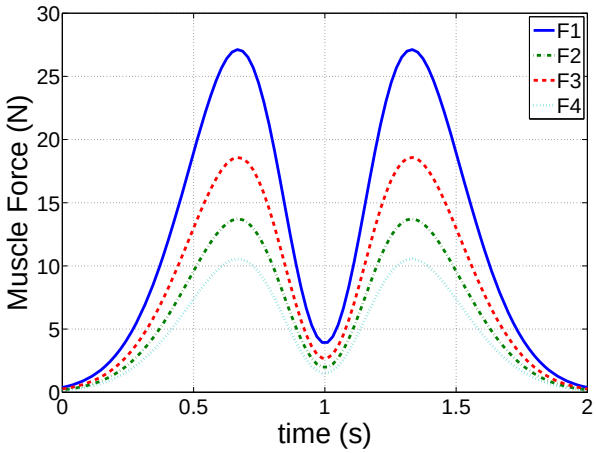


Figure 3.19: Simulated muscle forces using the analytical approach with $P = 2$

### 3.5.3 Discussion

In the expression yielded for $\lambda$, those moment arms which are present are of the muscles with non-zero force values; in this case, the corresponding $\mu$ values will be zero, which is consistent with KKT conditions. For single-articular muscles, this occurs only if the muscles are flexor with positive muscle torque and extensor with negative muscle torque. This proves that in single articular systems with the defined objective function, no antagonistic co-contraction will occur, which is in agreement with [56].

The analytical approach seems to be promising as it finds the optimal solution of the force sharing problem with no iterational computation and no error as in numerical optimization. However, in terms of $n$ inequality constraint, there would be a $2^n$ branches of solutions. For the examples investigated in this section, only considering the lower bound for muscle forces, the optimal solution created four solutions, which was reasonable. For the example in Section 3.5.2, if one would like to add the upper bound for the muscles as well so that the muscle forces do not go beyond the maximum isometric force, there would be four inequality constraints resulting in 16 branches. Therefore, the number of branches of the solutions grows rapidly. For more complicated systems like gait, e.g., in a

system with eight muscles only, the number of branches with lower bound only would be 256, which is practically infeasible to choose as an appropriate approach.

Another major limitation for this approach is that it can only accept those objective functions that are explicit functions of the design variables, e.g., muscle force effort or muscle fatigue criterion. However, even in this type of function, the polynomial exponent $P$ cannot be greater than three; otherwise, it does not have an analytic solution if the lower or upper bounds are imposed to the problem.

The analytical approach works quite efficiently in systems with uni-articular muscles where one can reduce the system to a system with only two muscles, one flexor and one extensor. Then, it is easy to distribute the torque of one side to the muscles of that side in the original problem, based on the unconstrained problem (Section 2.2.6).

Consequently, the major shortcomings of the analytical solution will lead us back to numerical optimization; however, one can use the sub-optimal analytical solution of the system with lower $P$ values as considerably good initial guesses for the numerical optimization.

## 3.6 Chapter Summary

In this chapter different proposed approaches for solving the muscle redundancy and the optimal control problems involved in modelling the human musculoskeletal system were presented and discussed. Each method had advantages and disadvantages and it is the trade-off and conditions of the problem that helps a biomechanist to pick the appropriate technique. If in a low-dimensional system, a sub-optimal solution is required for an application, one can use the analytical approach to find roughly optimal results. If the simulation time does not matter very much, or high quality results are the target, dynamic optimization with high order of parametrization functions might be used. Overall, as mentioned, the choice of a suitable strategy to solve the redundant musculoskeletal system requires knowledge of the problem, required output quality, and also CPU time significance.

The next chapter is devoted to foot contact modelling within gait simulations for the human gait modelling as the final challenge of this thesis.

# Chapter 4

# Foot Contact Modelling within Gait Simulations

An efficient and accurate foot contact model is a crucial piece in forward dynamics of gait. Unlike inverse dynamics, in forward dynamics simulations of gait, a contact model is required to develop ground reaction forces because these forces are not measured a-priori. Ground reaction forces drastically influence the kinetics, kinematics and energetics of human gait.

This chapter introduces the foot contact modelling. Three different contact models and the possibility of applying each in forward gait simulations are investigated here: Kelvin-Voigt, linear volumetric, and nonlinear volumetric. The final model will be employed in the gait modelling, which is presented in Chapter 5.

## 4.1 Model

The foot model is two dimensional with two rigid body segments: the hind-foot, mid-foot, and fore-foot as one rigid body and the phalanges collectively as the second rigid body.

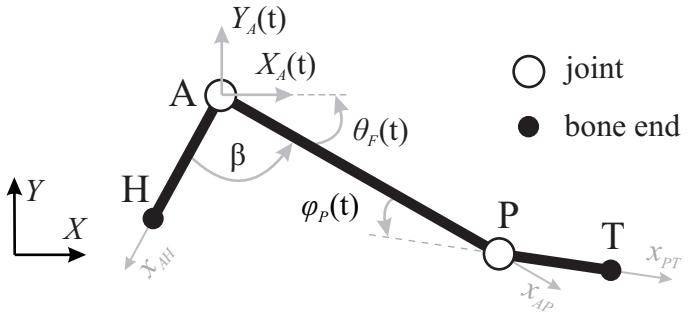


Figure 4.1: Parametric foot geometry

The model has four degrees of freedom: ankle positions $x_A$ and $y_A$, foot orientation $\theta_F$, and phalange orientation $\phi_P$. Both ankle and metatarsal joints are assumed to be revolute joints.

### 4.1.1 Foot Geometry

The parametric geometry of the foot model is depicted in Figure 4.1. $X$ and $x$ designate the horizontal distance in global and local frames, respectively. Points A, H, P, and T represent the ankle, heel, 1st metatarsal joint, and toe, respectively. The lengths in this model were measured on a subject with 1.62 m height; however, in order to have the best foot geometry compatible with the marker positions, a geometry fitting procedure is carried out that is detailed in the following.

In the experimental data presented by Winter [10], marker positions of the 5th metatarsal were provided, but not those of the 1st metatarsal, which is of interest here. Therefore, by measuring the distance from the 5th metatarsal to the 1st metatarsal on a subject with 1.62 m height, which is close to the height of the subject of the experimental data, the kinematics for the 1st metatarsal was generated from those for the 5th metatarsal. While the foot was flat on the ground, the horizontal and vertical distances (in $X$ and $Y$ directions shown in Figure 4.1) were both measured to be 10 mm.

The parametrized foot was driven at all four degrees of freedom to produce a set of

Table 4.1: Optimal parameters of the foot geometry consistent with the marker data.

| Parameter | Optimal Value |
|---|---|
| AH (cm) | 7.4 |
| AP (cm) | 11.0 |
| PT (cm) | 7.3 |
| $\beta$ $(deg)$ | 106 |

kinematics as close as possible to the experimental marker positions within an iterated optimization procedure. $x_A$, $y_A$, and foot orientation $\theta_F$ were taken from the data presented in [10], but as the metatarsal joint angle kinematics is not reported in that reference, this angle was parametrized with an 11-term Fourier series as in Equation 4.1. This implies that the experimental kinematics should be considered in one period of motion, from one toe-off to the next toe-off. The Fourier series functions are suitable choices for joint angles in periodic motions like gait [22]. The coefficients of these functions are treated as parameters in the identification process, which is a typical method in converting an optimal control problem to a parametrized optimization.

$$\phi_P(t) = A_0 + \sum_{k=1}^{5}[A_k \sin(\frac{2\pi kt}{\tau}) + B_k \cos(\frac{2\pi kt}{\tau})] \tag{4.1}$$

where $\tau$ is the motion period. The parameters to be identified are lengths AH, AP and PT, angle $\beta$, and coefficients of the Fourier series representing metatarsal joint angle, resulting in a total of 15 parameters. Geometrical parameters of the best fitted geometry that could follow the experimental marker positions are shown in Table 4.1. The lengths AH, AP and PT are in good agreement with the lengths measured on the subject. The generated metatarsal joint angle is presented in Figure 4.2(g); also simulated positions are plotted against the marker positions for comparison in Figures 4.2(a-f).

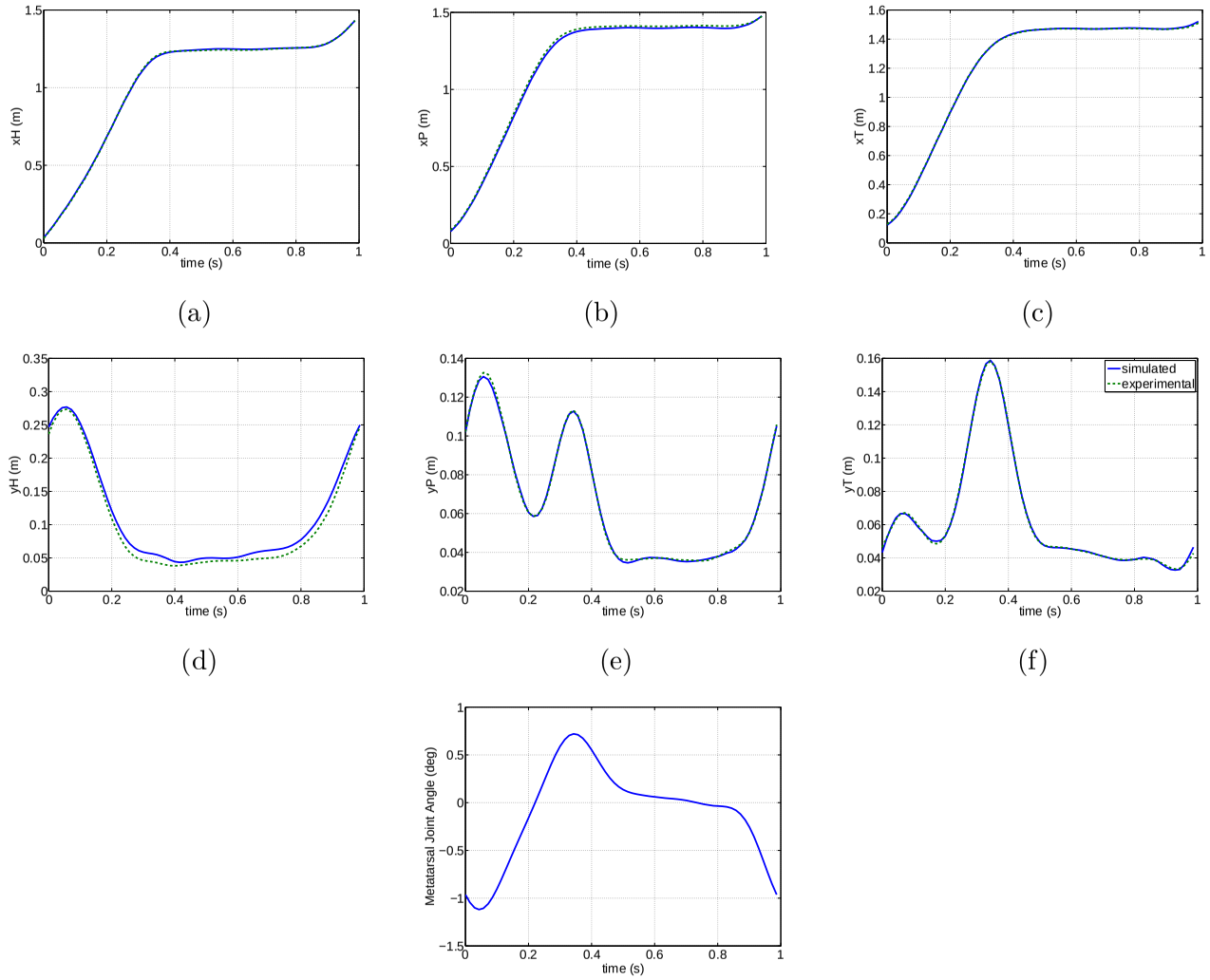


Figure 4.2: Foot geometry fit to the marker positions: (a-f) comparison of the generated point trajectories against the experimental data from [10], (g) optimal metatarsal joint angle

### 4.1.2 Contact Models

Three different contact models were investigated: nonlinear spring and linear damper, linear volumetric sphere, and a nonlinear volumetric sphere. In a foot model, one element of each type is employed at points H, P, and T. Each of the three foot models is presented separately and the corresponding results are discussed. For each case, the model is kinematically driven at the ankle and toe using the experimental position and angle data at the ankle from [10], and the identified angle at the toe. Parameters of each model are then iterated within an optimization procedure so that the generated vertical and friction forces and the centre of pressure position computed by the model match the experimental data as close as possible. The complete form of the objective function to be minimized, of matching non-dimensionalized criteria with equal weighting, is written as:

$$J = \frac{1}{T}\int_0^T \left\{ \left[\frac{f_n^m - f_n^e}{\max(f_n^e)}\right]^2 + \left[\frac{f_f^m - f_f^e}{\max(f_f^e)}\right]^2 + \left[\frac{X_{cop}^m - X_{cop}^e}{\max(X_{cop}^e)}\right]^2 \right\} dt \tag{4.2}$$

where $T$ is the gait cycle period and $f_n$, $f_f$, and $X_{cop}$ are normal force, friction force, and position of the centre of pressure, respectively. In Equation 4.2, superscripts $m$ and $e$ correspond to model and experiment. For the convergence study for each case, three different random initial points were obtained by solving the optimization problem running a Genetic Algorithm (GA) in MATLAB® for a maximum of 100 populations. Afterwards, these three solutions were used to run a Sequential Quadratic Programming (SQP) solver to take advantage of faster gradient-based algorithms. From those three runs, the best one was chosen to be the raw optimum. Using this new solution as a new initial guess, a Pattern Search function as a Direct Search (DS) routine was then run to ensure the globality of the solution. If the objective function value of the DS was less, it was put into the SQP again. This cycle was repeated until the change in the values of the objective function and bound violations were less than 1e-6, where the result was accepted as the global optimum.

**1) Nonlinear Spring-Linear Damper**

The general point contact force can be written as:

$$f_n = K(\delta) + D(\dot{\delta}) \tag{4.3}$$

which includes a stiffness term as a nonlinear function of spring deformation $\delta$ and a damping term as a function of the rate of deformation $\dot{\delta}$. However, this shape of the contact function will result in a spiky contact force at the initial contact instant. The formulation applied here is based on the model proposed by Hunt and Crossley [89], which inhibits the contact element from undergoing a drastic force change at the initial impact due to the velocity of the contact point.

$$f_n = \begin{cases} k_S \mid L - L_0 \mid^{n_S} (1 + a_S v_n) & L \leq L_0 \\ 0 & otherwise \end{cases} \tag{4.4}$$

where $k_S$ and $a_S$ are the spring stiffness and pseudo-damping, respectively, $L_0$ is the rest length, and $n_S$ is the nonlinearity exponent, which form the set of four parameters of this contact model. The variable $L$ is the spring length and $v_n$ is the vertical velocity of the contact point. For this model, the objective function is set to track the vertical contact force only, to examine the efficacy of the normal contact model explicitly. Table 4.2 shows the bounds on the parameters and the optimal values acquired from parameter identification for spring-damper elements at points H, P, and T, respectively. The simulated normal force is shown in Figure 4.3, which implies that this type of point contact model is not sufficient for human foot contact during gait. As can be seen, there is not a smooth transition between peaks present in the contact force. There are some options to improve the results: one is to modify the contact model, and another is to increase the number of contact elements as in [62, 63]. Modification of the contact model is chosen here.

**2) Linear Volumetric Contact Model**

In this part, three spring/dampers are replaced with three spheres, as shown in Figure 4.4, to supply wider contact areas and therefore produce smoother normal contact forces. The

Table 4.2: Optimal contact parameters of the spring-damper elements

| Parameter | Spring | Optimal Value | Lower Bound | Upper Bound |
|---|---|---|---|---|
| $k_S$ $(N/m^n)$ | H | 1.2e4 | 0 | - |
| | P | 1.9e3 | 0 | - |
| | T | 6.4e4 | 0 | - |
| $a_S$ $(s/m)$ | H | 64.6 | 0 | - |
| | P | 1.4e3 | 0 | - |
| | T | 3e-3 | 0 | - |
| $L_0$ $(mm)$ | H | 52 | 1 | 55 |
| | P | 48 | 1 | 50 |
| | T | 43 | 1 | 45 |
| $n_S$ | H | 0.95 | 0.1 | 10 |
| | P | 0.96 | 0.1 | 10 |
| | T | 0.96 | 0.1 | 10 |

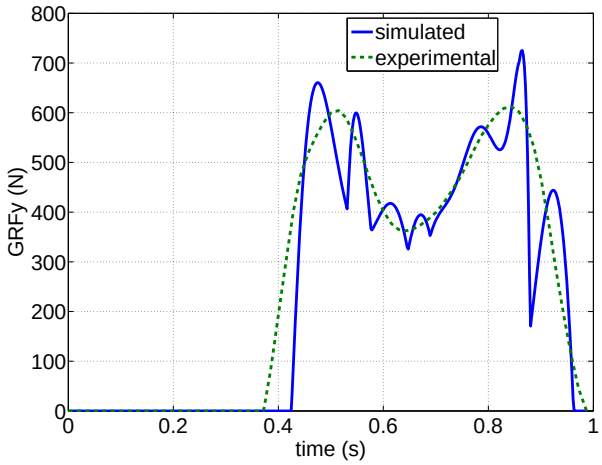


Figure 4.3: Simulated results from the spring-damper contact model versus experimental vertical GRF

contact model is based on a volumetric approach [65, 90]. This model assumes a linear elastic foundation for the material. The authors of [26] did some in-vivo measurements of the heel pad deformation and force, and they concluded that the volumetric contact could be a suitable candidate for human foot contact modelling.

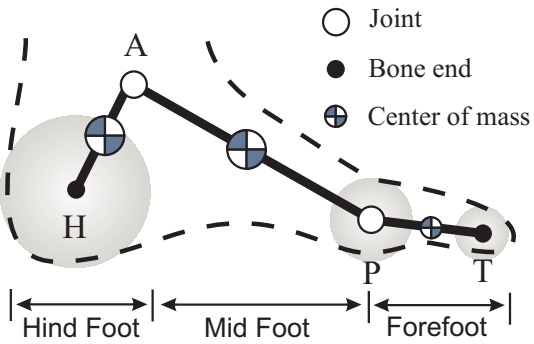


Figure 4.4: Schematic foot with three spherical volumetric contact elements

The idea, instead of using a point contact as in the previous model, assumes a linear pressure distribution $p(s)$, which is a function of the location $s$ on the contact patch $\mathbf{S}$, as shown in Figure 4.5.

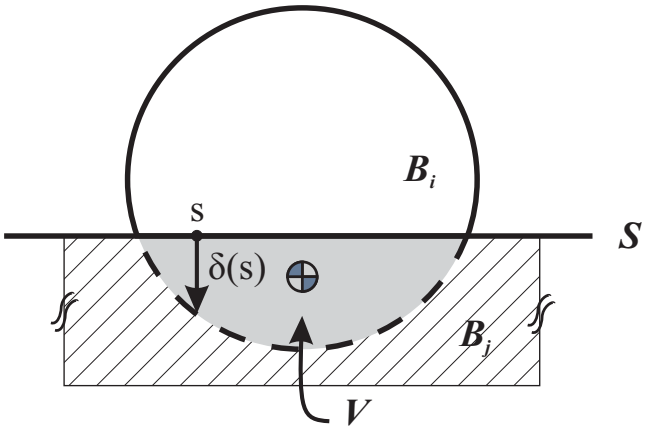


Figure 4.5: Schematic of the volume of the interpenetration between two bodies in contact

Consider the schematic representation of a sphere interacting with the ground. The body $\mathbf{B}_i$ is the deformable body (foot), whereas $\mathbf{B}_j$ is the rigid and fixed body (ground). Therefore the interpenetration volume $V$ is written as:

$$V = \int_S \delta(s) dS = \int_V dV \tag{4.5}$$

where $\delta$ is the deformation at location $s$. The pressure distribution is defined using the theory proposed by Hunt and Crossley [89] with $n = 1$ as below:

$$p(s) = k_V \delta(s)(1 + a_V \dot{\delta}(s)) \tag{4.6}$$

where $k_V$ and $a_V$ are stiffness and pseudo-damping of the foundation, respectively, and $\dot{\delta}(s)$ is the rate of deformation at point $s$. Then the total normal contact force will be given by:

$$f_n = \int_S p(s) dS \tag{4.7}$$

which can be written in the form of a vector function of the deformed volume as:

$$\vec{f_n} = k_V V (1 + a_V v_{cn}) \hat{\mathbf{n}} \tag{4.8}$$

where $\vec{f_n}$ is the normal force, $V$ is the interpenetration volume, $\hat{\mathbf{n}}$ is the unit normal vector to $S$, and $v_{cn}$ is the normal velocity at the center of mass of the deformed volume. The optimal parameters of the linear volumetric contact model for spheres at points H, P, and T are presented in Table 4.3, respectively.

As depicted in Figure 4.6, the total contact force is much closer to the experimental value than the one shown in Figure 4.3. However, the results are not satisfying as oscillatory behaviour is still observed in the contact force. These can be related to lack of fidelity of the contact model, the low number of contact spheres, or due to the errors in the kinematic data. The aspect here is not to question the kinematic data, and not to increase the number of contact elements, so the focus remains on modifying the contact model.

Table 4.3: Optimal contact parameters of the linear volumetric elements

| Parameter | Sphere | Optimal Value | Lower Bound | Upper Bound |
|---|---|---|---|---|
| | H | 2.21e6 | 0 | - |
| $k_V$ $(N/m^3)$ | P | 1.87e6 | 0 | - |
| | T | 2.51e5 | 0 | - |
| | H | 1.2 | 0 | - |
| $a_V$ $(s/m)$ | P | 0.45 | 0 | - |
| | T | 0.1 | 0 | - |
| | H | 51 | 1 | 55 |
| $R_V$ $(mm)$ | P | 49 | 1 | 50 |
| | T | 44 | 1 | 45 |

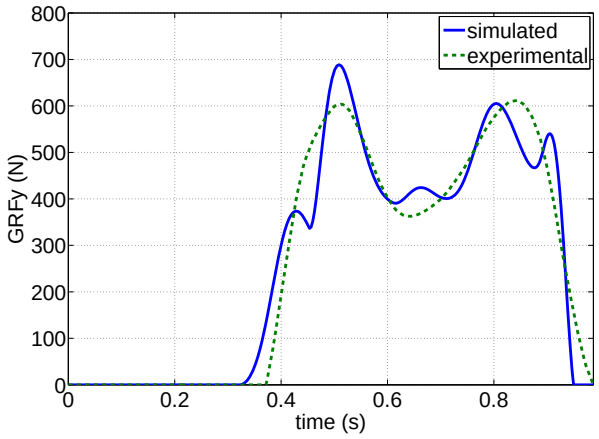


Figure 4.6: Simulated results from the linear volumetric model versus experimental vertical GRF

### 3) Nonlinear Volumetric Contact Model

The principal shortcoming of the previous model is the linearity assumption in the material model. Boos and McPhee [91] assumed a linear elastic foundation model, which is suitable for small deformation ranges, as they initiated the technique for metal on metal contact; however, the soft heel tissue undergoes a maximum deformation of 53.6% reported by [26] considering a 22.8 mm thickness for the heel pad and 12 mm of the maximum deformation. Therefore, the linear foundation assumption is likely not valid for a foot. Alternatively, the foundation can be modelled as a hyper-elastic material [92]. Consider a hyper-elastic foundation with no damping. The normal force can be written as:

$$\vec{f_n} = (k_V V_h)\hat{\mathbf{n}} \tag{4.9}$$

where the hypervolume $V_h$ is expressed as the following:

$$V_h = \iint_S \delta^\eta(s)\ dS = c_v(V) \iint_S \delta(s)\ dS = c_v(V)V \tag{4.10}$$

with

$$c_v(V) = \frac{\iint_S \delta^\eta(s)\ dS}{\iint_S \delta(s)\ dS}$$

It was shown in [92] that the hypervolume $V_h$ is a linear function of the penetration volume $V$ in a double logarithmic scale. Therefore the hypervolume coefficient $c_v(V)$ can be written as:

$$c_v(V) = e^{a_0 + a_1 \ln(V)} \tag{4.11}$$

where $a_0$ and $a_1$ are parameters that depend on the foundation nonlinearity $\eta$ and geometrical properties. In other words, for a given contact geometry and foundation hyper-elasticity exponent, there exist unique values for $a_0$ and $a_1$. For more details, see [92]. Therefore, the normal force can be written as:

$$\vec{f_n} = (k_V c_v(V)\ V)\hat{\mathbf{n}} = (k_V e^{a_0 + a_1 \ln(V)}\ V)\hat{\mathbf{n}} \tag{4.12}$$

which can be further simplified as:

$$\vec{f_n} = (k_h V^{\mathcal{H}})\hat{\mathbf{n}} \quad \text{where} \quad k_h = k_V e^{a_0} \quad \text{and} \quad \mathcal{H} = 1 + a_1 \tag{4.13}$$

The pressure distribution assumed for the hyper-elastic foundation in the foot, including damping, is the following:

$$p(s) = k_V \delta^{\eta}(s) + k_V \delta(s) a_V v_n \tag{4.14}$$

which implies that there is a nonlinear stiffness term, but the damping term is still linear. Then the normal force can be written as:

$$\vec{f_n} = (k_h V^{\mathcal{H}} + a_h V v_{cn})\hat{\mathbf{n}} \tag{4.15}$$

where $k_h$, which is called a hyper-volumetric pseudo-stiffness here, and exponent $\mathcal{H}$ depend on both the volumetric stiffness and geometrical properties; $a_h$ is the foundation stiffness $k_V$ multiplied by the damping $a_V$ as in the linear volumetric formulation.

### 4.1.3 Friction Model

An approximation of the dry Coulomb model is used to compute the force of friction between the contact spheres in the foot model and the ground:

$$f_f = -\mu(v_{ct}) f_n \tag{4.16}$$

where $f_f$ is the friction force for the sphere, $v_{ct}$ is the tangential speed of the centroid of the deformed volume, and $\mu(v_{ct})$ is the friction coefficient function defined to guarantee the differentiability of the expression as follows:

$$\mu(v_{ct}) = \mu_f \arctan(v_{ct}/v_s) \tag{4.17}$$

where $\mu_f$ is the asymptotic friction coefficient and $v_s$ is a shape parameter. The smaller the shape factor $v_s$, the closer the approximation to the dry Coulomb friction.

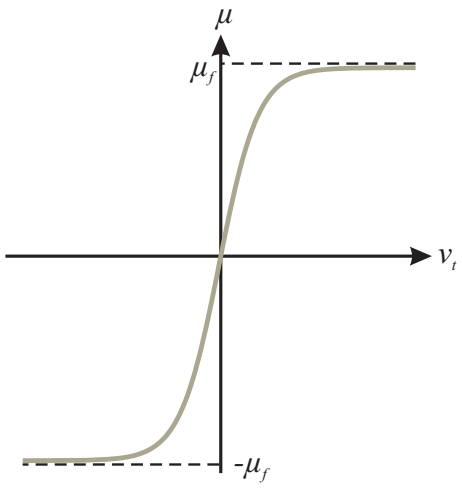


Figure 4.7: Plot of the friction coefficient function versus tangential speed

### 4.1.4 Relaxing the Contact Characteristic Points

Although the motions of the model characteristic points (H, P, and T) match the experimental marker kinematics very well as shown in Figure 4.2, placing the spheres exactly at these points is a restricting assumption. To remove this restriction, the position of the centre of volumetric spheres are relaxed within a certain range. For this goal, the location of the sphere centres are allowed to move within $\pm 15$ mm in both $x$ and $y$ directions, which is within the amount of "skin stretch" during gait [93]. The schematic configuration of this model is shown in Figure 4.8 where $H^*$, $P^*$, and $T^*$ are the relaxed locations of the contact spheres. Finally, the optimal relaxation parameter values $dx$ and $dy$, which are relative displacements in local frames of the segment (see Figure 4.1) for each contact spheres from the characteristic points resulting in a total of 6 more parameters, are determined within the parameter identification procedure for the nonlinear volumetric contact model.

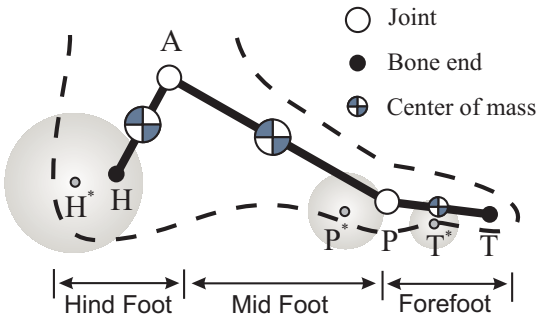


Figure 4.8: Schematic configuration of the volumetric spheres on the foot model with relaxed locations

## 4.2 Results and Discussion

Results of the nonlinear volumetric model are presented in Figures 4.9 and 4.10. As can be observed from the plots, the ground reaction forces are smoother than those of the linear volumetric model, which implies that a nonlinear model is a more accurate representation of the foot/ground interaction. The comparison of the centre of pressure position also shows a quite good match. The friction force comparison in Figures 4.9(b,d) however show some room for improvement. It should be noted that there were only two parameters in the tangential force for model Coulomb friction. Given that, by looking at the simulated and experimental tangential ground reaction forces, a reasonable match can be interpreted.

The results of the hyper-volumetric model with relaxed sphere centre locations are depicted in Figures 4.9(c,d) and 4.10(b) and the optimal parameters for the three spheres of this model are listed in Table 4.4. As can be observed, a significant improvement is made to the friction force compared to the case without relaxation. Although the normal force beginning and end time instants are matching those of the experimental data better, which can also be observed in the centre of pressure plot, a considerable progress in the overall normal force was not seen.

Although the volumetric approach was previously utilized by [26] for foot contact modelling, this study had significant differences: the toe was driven with independent kinemat-

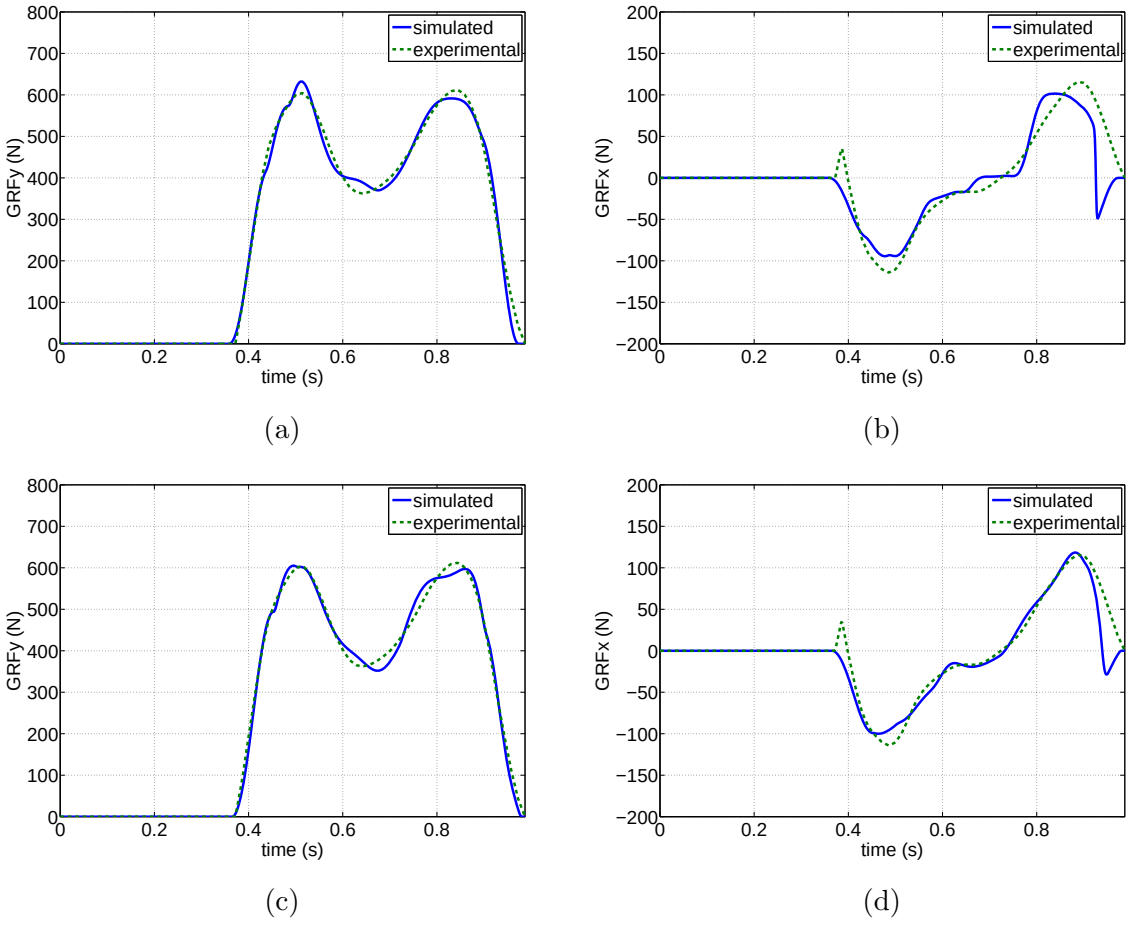


Figure 4.9: Simulated results of the hyper-volumetric model compared to experimental data without relaxing the contact sphere centres: (a) vertical GRF and (b) horizontal GRF, and with relaxing the contact sphere centres: (c) vertical GRF and (d) horizontal GRF

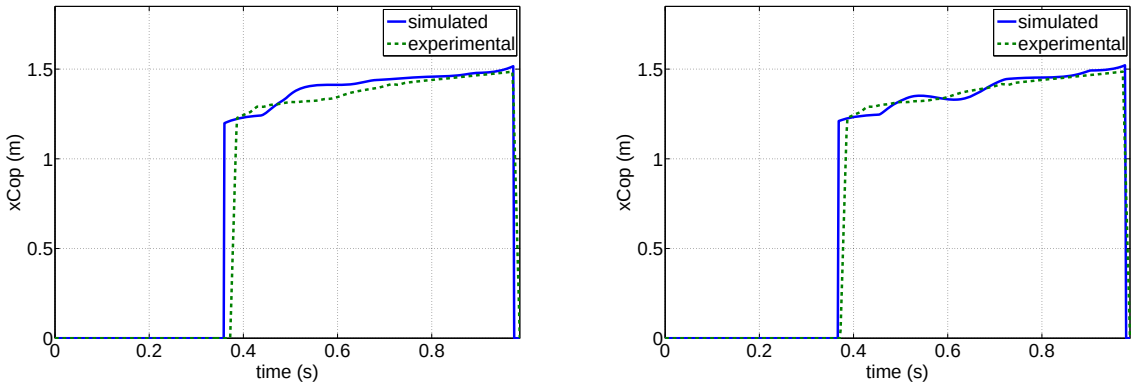


(a) (b)

Figure 4.10: Simulated results for the centre of pressure location of the hyper-volumetric model without relaxing the contact sphere centres (a) and with relaxing the contact sphere centres (b)

ics to provide a smoother transition at toe-off, and the volumetric contact model used in this study was nonlinear. These two changes improved the contact forces significantly.

Additionally, the proposed hyper-volumetric model had a different concept than that presented by Sandhu and McPhee [13]. Their model was nonlinear, but they did not compute any closed-form volume. In other words, they discretized the foundation to finite Kelvin-Voigt elements, and then calculated the contact forces by adding the forces of those elements, which is more similar to the study by Gilchrist and Winter [62] than a volumetric approach.

To examine the sensitivity of the foot contact model to the optimal parameters shown in Table 4.4, as an example, the stiffness of the three contact spheres are increased one at a time by 10% and the perturbation of the total normal contact force is examined. Figures 4.11(a,b,c) show how the normal force is influenced by varying the optimal stiffness of points H, P, and T, respectively by +10%. As can be observed, the normal force is more sensitive to the stiffness of the sphere under the phalangeal joint. This is because that sphere contributes to both humps at the beginning and at the end of mid-stance. However,

Table 4.4: Optimal contact parameters of the hyper-volumetric elements. Parameters $dx$ and $dy$ for characteristic points H, P, and T are expressed in local frames AH, AP, and PT, respectively.

| Parameter | Sphere | Optimal Value | Lower Bound | Upper Bound |
|---|---|---|---|---|
| $k_h$ $(N/m^h)$ | H | 8.0e5 | 0 | - |
| | P | 1.4e6 | 0 | - |
| | T | 7.5e5 | 0 | - |
| $a_h$ $(Ns/m^4)$ | H | 52.3e6 | 0 | - |
| | P | 1.2e5 | 0 | - |
| | T | 13e6 | 0 | - |
| $R_V$ $(mm)$ | H | 50 | 1 | 55 |
| | P | 49 | 1 | 50 |
| | T | 44 | 1 | 45 |
| $\mathcal{H}$ | H | 0.74 | 0.1 | 10 |
| | P | 0.80 | 0.1 | 10 |
| | T | 0.79 | 0.1 | 10 |
| $\mu_f$ | H | 0.20 | 1e-3 | 1 |
| | P | 0.22 | 1e-3 | 1 |
| | T | 0.34 | 1e-3 | 1 |
| $v_s$ $(m/s)$ | H | 0.005 | 1e-6 | 0.1 |
| | P | 0.050 | 1e-6 | 0.1 |
| | T | 0.034 | 1e-6 | 0.1 |
| $dx$ $(mm)$ | H | 1.89 | 0 | 20 |
| | P | 12.85 | 0 | 20 |
| | T | 14.07 | 0 | 20 |
| $dy$ $(mm)$ | H | 3.80 | 0 | 20 |
| | P | 4.19 | 0 | 20 |
| | T | 0.05 | 0 | 20 |

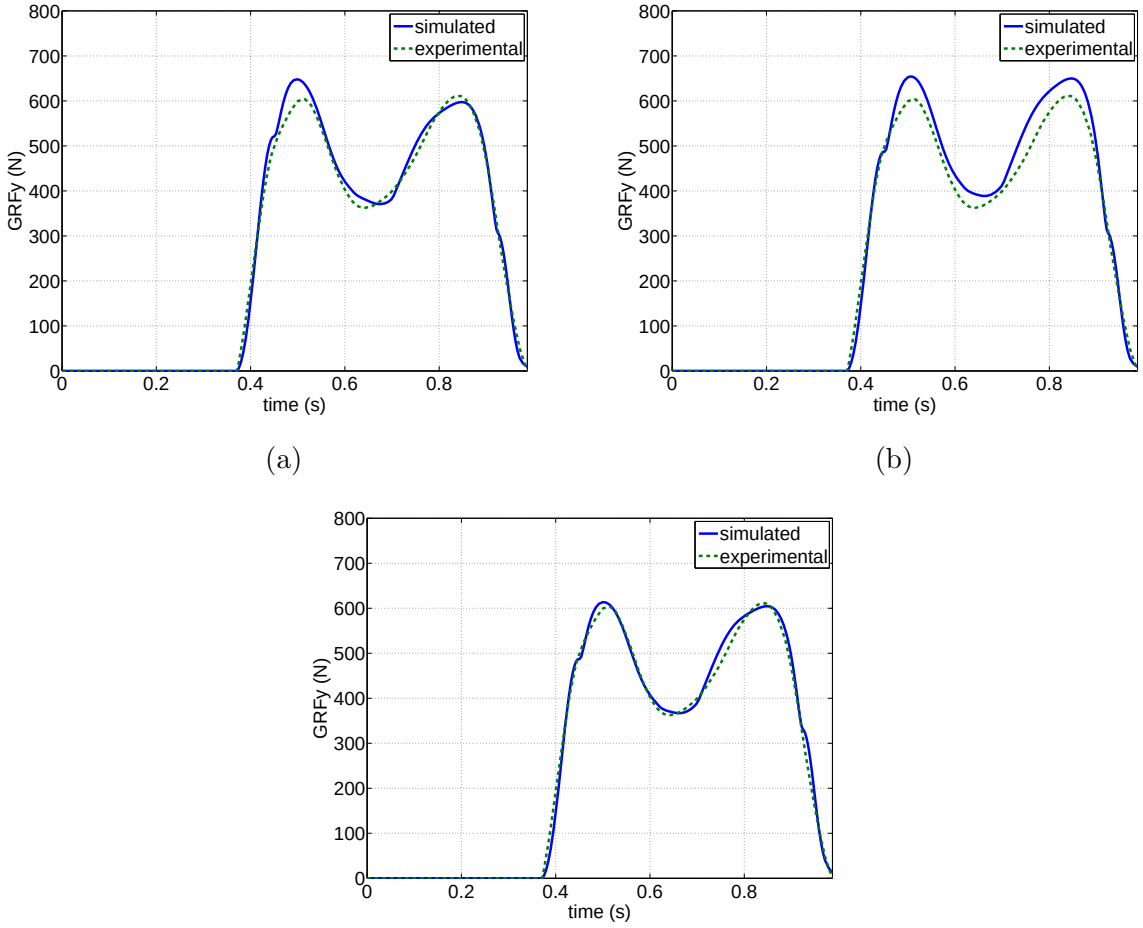


Figure 4.11: Effect of increasing the stiffness of the final foot contact model on the normal force: (a) 110%$k_h$ at H$^*$, (b) 110%$k_h$ at P$^*$, and (c) 110%$k_h$ at T$^*$

the influence of the first sphere is only on the first peak in the normal force, which makes sense. Furthermore, the normal force is less sensitive to the stiffness of the sphere at the toes. Quantitatively speaking, by increasing the stiffness at points H, P, and T by 10%, the total increase in the normal force is 2.4%, 6.3%, and 1.3%, respectively. This implies that ground reaction forces are more sensitive to the perturbation of the optimal parameters of

the 2nd contact sphere; however, even the corresponding relative effect of 6.3% is still less than the 10% perturbation on the model parameter.

The conclusion for this sensitivity analysis above is that the model still works for these parameter changes; therefore, the model is capable of "what-if" simulations in which the foot contact parameters are varied, e.g., for different subjects.

## 4.3 Chapter Summary

A dynamic foot model was developed and validated within a gait simulation. The simulation was performed on an entire period of a gait cycle to ensure the efficiency of the model over the whole cycle, and that it does not produce any unrealistic early contact forces. Three different types of contact scenarios were modelled: point contact, linear volumetric, and hyper-volumetric. The transition from a point contact to a volumetric model showed a promising progress in generating the contact force in agreement with experimental data. For the hyper-volumetric model, the vertical and horizontal ground reaction forces and the center of pressure of the hyper-volumetric foot contact model showed excellent correlations with the experimental data. This means that a hyper-volumetric contact element is a suitable choice for human foot contact modelling.

The next chapter will present the gait modelling using the ultimate foot contact model created here. It is expected that this good foot contact model will help to acquire reasonable gait simulation results.

# Chapter 5

# Forward Dynamics of Gait Simulations

> "Walking is for moving from one place to another to go to table for breakfast, to climb stairs to bed, to meet a friend, to walk the aisles at the food mart" [20].

Walking is a fundamental human motion that is repeated in a human's daily activity. Gait (walking and running) has an undeniable role in a human's life. Although gait seems to be basic, it is one of the most complex and challenging human movements. It is the most common of human movements, and it has been studied more than any other motion [20].

From the modelling point of view, gait is a highly nonlinear dynamic activity, which includes nonlinear multibody equations, nonlinear muscle dynamics and coordination, and nonlinear foot/ground interaction. It consists of various phases for which the major events are graphically presented in Figure 5.1 for right and left legs and are detailed in the following:

- **stance**: this phase defines the interval of time that the foot is fully or partially on the ground. In walking, there is a double-stance phase in which both feet have contact

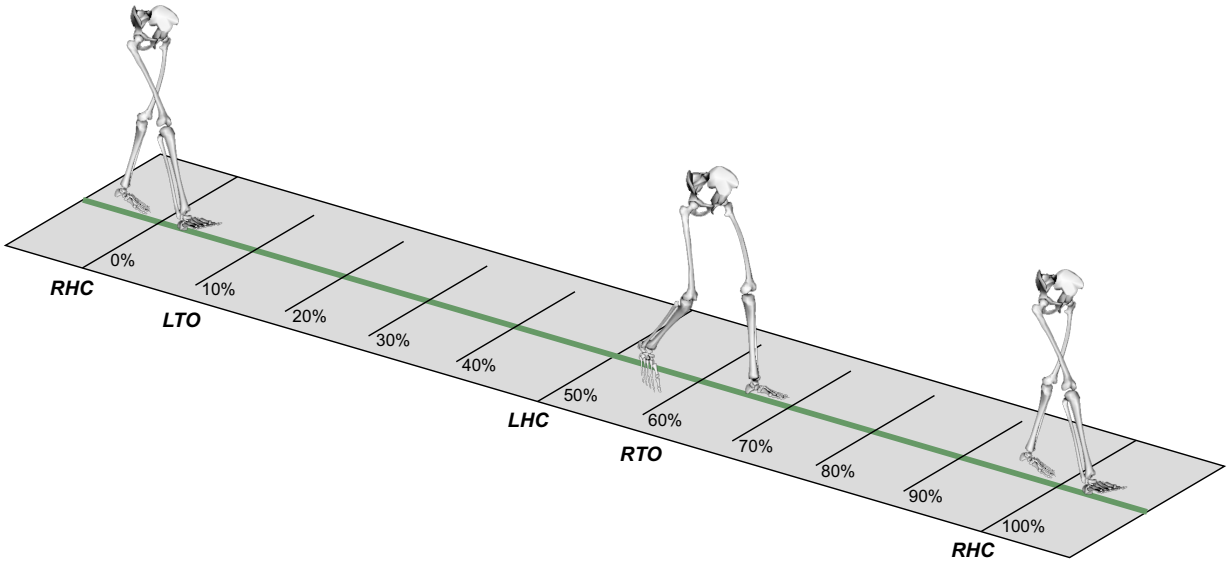


Figure 5.1: Schematic of the major phases of human gait

with the ground; this phase is not present in running. Stance (or support) has several events such as heel-contact (HC), mid-stance (or foot-flat), and toe-off (TO).

- **swing**: the phase that the foot is not connected to the ground. This phase also consists of three events: acceleration, mid-swing, and deceleration.

In normal walking, the swing and stance phases form 38% and 62% of the whole gait cycle, respectively [94]. In addition to the terms defined above, there are two concepts that are extensively used throughout this chapter: stride and step. Stride is the distance from the HC of one foot to the next HC of the same foot. In terms of time, one stride is equal to one gait cycle. On the other hand, step is defined as the distance from HC of one foot to the HC of another foot. In a normal and nearly periodic gait, this time frame represents 50% of the gait cycle [94].

There are very few studies on forward dynamics of gait in which foot contact models are explicitly simulated [22, 95] which are required for the simulation of an entire stride (two steps). In Peasgood et al.'s model [22], joints were kinematically driven, and muscles were

ideal force actuators. Gilchrist and Winter [95] implemented a forward dynamics model with no optimization or feedback control leading the model to fall down; their model did not include any muscles. Millard et al. [26] simulated human gait for multiple steps with a torque-actuated model.

In this chapter, a two-dimensional model for the forward dynamic simulation of human normal gait is presented. The model is implemented in the symbolic multibody package MapleSim® and then the highly efficient code is exported to Matlab® for optimization. A global parametrization approach is applied based on Section 3.3. The novel foot contact model detailed in Chapter 4 is used in this gait study, in which the foot/ground interaction is modelled by means of three spheres. The contact expressions are based on hyper-volumetric contact modelling, which is inspired from considering a non-linear material foundation. The foot contact model is already validated within a gait simulation cycle.

## 5.1 Methods

The model is assumed to move in the sagittal plane where the walking pattern is presumed to be bilaterally symmetric, i.e., the right and left legs perform similar motions but with a time shift. The multibody model has nine segments as shown in Figure 5.2: right and left toes, feet, shanks, thighs, and the HAT (Head, Arms and Trunk), leading to eleven degrees of freedom (dof) as:

$$\{\boldsymbol{q}\} = [X_{tor}, Y_{tor}, \phi_T, \phi_{RH}, \phi_{LH}, \phi_{RK}, \phi_{LK}, \phi_{RA}, \phi_{LA}, \phi_{RP}, \phi_{LP}]^T \tag{5.1}$$

where $\{\boldsymbol{q}\}$ denotes the column matrix of generalized coordinates, and subscripts $RH$, $LH$, $RK$, $LK$, $RA$, $LA$, $RP$, $LP$ represent the right hip, left hip, right knee, left knee, right ankle, left ankle, right phalange orientation, and left phalange orientation, respectively, $X_{tor}$, $Y_{tor}$, and $\phi_T$ are torso center of mass $X$ and $Y$ position, and torso orientation, respectively. Combining head and arms with the trunk is a common approach in gait modelling [93]. A study by [96] shows that the influence of lumping arms into the trunk on kinematics, kinetics, and energetics of human gait is less than 10%.

Table 5.1: Conventional anthropometric data [10] where BM and BH denote the body mass and height, respectively, dP is the location of the center of mass (assumed to lie on line joining distal and proximal heads) from the proximal head divided by segment length, and RoG is the radius of gyration around the center of mass divided by segment length. HAT length (*) is defined as the vertical distance between the glenohumeral joint and the greater trochanter

| BM=64.740 kg and BH=1.696 m | | | | |
|---|---|---|---|---|
| **Segment** | **Mass** | **dP** | **RoG** | **Length** |
| Shank | 0.0465 BM | 0.433 | 0.302 | 0.246 BH |
| Thigh | 0.100 BM | 0.433 | 0.323 | 0.245 BH |
| HAT | 0.678 BM | 0.626 | 0.496 | 0.288* BH |

The model is muscle-actuated at the hip, knee, and ankle joints, and the toe joints are driven by the kinematics computed in Chapter 4. The goal is to solve the optimal control problem for this gait model so that it predicts the optimal lower extremity motions without falling down in one stride (two steps). In this way, the forward dynamic model can be used in predictive "what-if" simulations.

The model contains eight muscle groups per leg based on [15]: Iliopsoas (Ilio), Rectus Femoris (RF), Glutei (Gl), Hamstrings (Hams), Vasti (Vas), Gastrocnemius (Gast), Tibialis Anterior (TA), and Soleus (Sol). The schematic of the model geometry and the recruited muscles is illustrated in Figure 5.2.

All anthropometric data except for the foot, listed in Table 5.1, are adopted from [10]. These are the conventional anthropometric properties in the literature and are similar to those used in [93]. There is not a conventional anthropometric data set for foot segments [93]; data presented in Table 5.2 are used as foot properties, which are similar to those employed by [12, 13]. For foot model geometry, refer to Figure 4.1 and Table 4.1.

There are three different approaches for simulating the forward dynamics of a muscu-

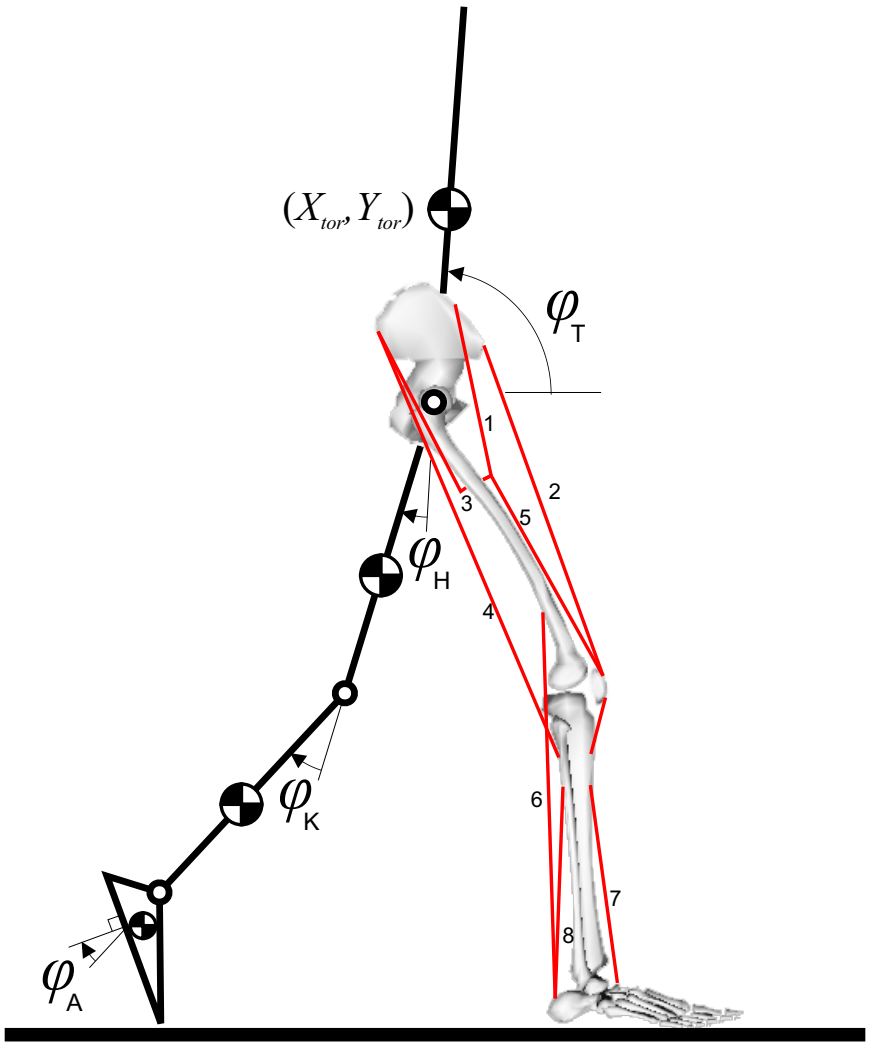


Figure 5.2: Two dimensional gait model with nine segments, eleven dof, and eight muscle groups per leg: 1-Ilipsoas, 2-Rectus Femoris, 3-Glutei, 4-Hamstrings, 5-Vasti, 6-Gastrocnemius, 7-Tibialis Anterior, and 8-Soleus

loskeletal system: Fully Forward, Inverse-Forward starting at joint torques, and Inverse-Forward beginning with muscle forces. These three simulation architectures are introduced below, and pros and cons of each are discussed.

Table 5.2: Foot anthropometric data from [11] and also used in [12,13], where Izz denotes the moment of inertia around the segment center of mass

| **Foot Segment** | **Mass** (kg) | **dP** (m) | **Izz** (kg.m$^2$) |
|---|---|---|---|
| Hind-foot | 0.6 | 0.5 | 0.0013 |
| Fore-foot | 0.6 | 0.5 | 0.0013 |
| Toes | 0.2 | 0.5 | 0.0001 |

**Design 1: Fully Forward (FF)**

The schematic framework is displayed in Figure 5.3. The neural excitations $u(t)$ is the control signal in this design, and due to the muscle redundancy, the optimal patterns of these controls must be obtained via dynamic optimization (see Chapter 3). This design is entitled Fully Forward here as it serves forward dynamics; also the activation and contraction dynamics are solved in the forward dynamics manner, i.e., the differential equations of muscles as well as the multibody system will be integrated together [55, 75].

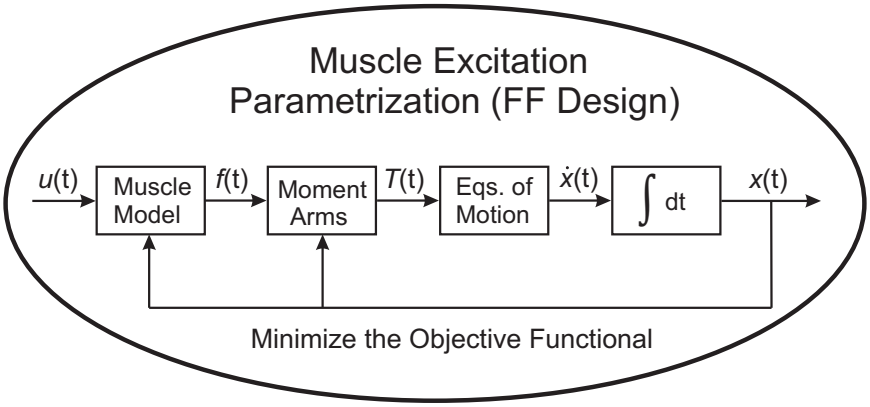


Figure 5.3: Schematic of the FF design work flow in the DO framework

The design of this approach is straight forward in terms of programming; however, it has the following drawbacks:

1. In the activation dynamics (AD), the initial activation value is required to solve the corresponding ODE (see Equations A.1 and A.2). In predictive forward dynamics, such information does not exist. Usually, studies assume zero values for initial activations, which will cause initial jumps in the activation values. Alternatively, the initial values can enter the optimization problem as new parameters, e.g, as in [55], which cause longer convergence time, and an increase in the number of local minima. In periodic motions, one can pick an arbitrary value for the initial activation and run the model for a couple of periods; as the transients fade, the results of the final period can be accepted as the simulation results. Although this circumvents the mentioned limitation, it is inefficient.

2. A similar issue exists in the contraction dynamics (CD); the initial muscle length is required to solve the corresponding ODE. Similar to item 1, in a predictive forward dynamics simulation, such information does not exist and only in periodic motions can the workaround described above be used.

3. This approach involves integration of the full dynamic system, i.e., as well as integrating the equations of motion for the mechanical system, it requires the integration of the activation and contraction dynamics. Therefore, this approach is excessively time-consuming as many iterations will be performed within the dynamic optimization process, with each iteration requiring a forward dynamic simulation.

**Design 2: Inverse-Forward starting at joint Torques (IFT)**

In both designs of the Inverse-Forward approach (IFT and IFM), no ODEs for activation and contraction dynamics will be solved. This speeds up the simulation considerably. The other positive feature of this approach is that it does not need the unknown values for the initial muscle activations and lengths as in FF.

Design 2 solves the multibody mechanical system within forward dynamics, and the rest of the model in the form of inverse dynamics. The schematic work flow of this IFT design

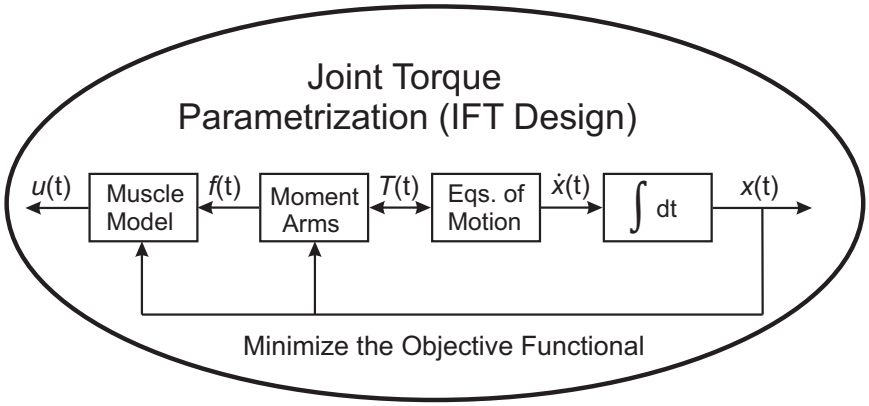


Figure 5.4: Schematic of the IFT design in DO framework

is displayed in Figure 5.4. The optimal control problem here is solved for joint torques $T(t)$. Joint torques are fed into the multibody equations and the states are integrated to compute the motion of the system. At the same time, the force distribution procedure finds individual muscle forces from the joint torques and then, knowing the muscle force and the kinematics, muscle activations can be calculated. Given the activations and the rate of muscle activations, muscle excitations are computed.

If parametrization is the target approach for the optimal control problem, joint torques are parametrized and then the muscle forces, after solving the muscle redundancy problem, have numerical values rather than being mathematical expressions. To solve the muscle model inversely, muscle force rates are required as in Equation 5.4; therefore, a numerical differentiation is required. Also, to calculate the activation rates, another numerical derivative will be required. The numerical differentiation introduces truncation errors, and numerical instabilities.

**Design 3: Inverse-Forward starting at Muscle Forces (IFM)**

The IFM performs the forward dynamics starting from muscle forces, for which the joint torques and then the kinematics are computed. The schematic work flow of this case is

displayed in Figure 5.5. At each iteration, when muscle force is determined, muscle activations are calculated through inverse contraction dynamics and then the muscle excitations are computed via inverse activation dynamics. If a parametrization approach is utilized with this design, there is no need for numerical differentiation to solve the muscle model and acquire the activation rates. Muscle forces can be differentiated symbolically and then the activation rates are acquired, given the muscle force and its derivative. The symbolic differentiation of the forces, compared to numerical differentiation, avoids numerical errors and also saves computation time. The flowchart in Figure 5.6 shows the procedure of computing activation $a(t)$ from a given muscle-tendon force and length for the inverted Hill muscle model employed here. To calculate the activation rate, the following equations must be considered:

$$f^{ce} = f(l^{ce}, \dot{l}^{ce}, a) \tag{5.2}$$

where $f^{ce}$ and $l^{ce}$ are the force and length of the contractile element (CE), respectively. Differentiating,

$$\dot{f}^{ce} = \frac{\partial f}{\partial l^{ce}} \dot{l}^{ce} + \frac{\partial f}{\partial \dot{l}^{ce}} \ddot{l}^{ce} + \frac{\partial f}{\partial a} \dot{a} \tag{5.3}$$

Rearranging Equation 5.3, the activation rate can be written as:

$$\dot{a} = \frac{\dot{f}^{ce} - \frac{\partial f}{\partial l^{ce}} \dot{l}^{ce} - \frac{\partial f}{\partial \dot{l}^{ce}} \ddot{l}^{ce}}{\frac{\partial f}{\partial a}} \tag{5.4}$$

Note that in Equation 5.4, $\dot{f}^{ce}$, $\frac{\partial f}{\partial l^{ce}}$ , and $\frac{\partial f}{\partial \dot{l}^{ce}}$ are the symbolic derivatives of the CE force with respect to time, and CE force function with respect to CE length and velocity, respectively. Also, given $l^{tm}$ (length of the tendon-muscle unit), $\dot{l}^{tm}$, and $\ddot{l}^{tm}$ (from the multibody kinematics) and $f^{tm}$ (force of the tendon-muscle unit), $\dot{f}^{tm}$, and $\ddot{f}^{tm}$, the variables CE length $l^{ce}$, velocity $\dot{l}^{ce}$ and acceleration $\ddot{l}^{ce}$ can be computed through the flowchart depicted in Figure 5.6.

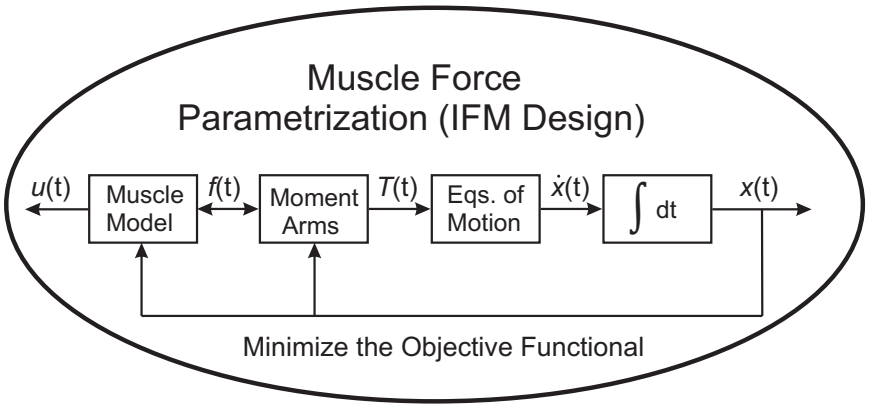


Figure 5.5: Schematic of the IFM design in DO framework

Based on the analyses above, an IF design with force parametrization is chosen for gait modelling. The tendon-muscle force is parametrized by the following Fourier series:

$$f^{tm}(t) = A_0 + \sum_{k=1}^{K}[A_k \sin(\frac{2\pi k(t+\Delta)}{\tau}) + B_k \cos(\frac{2\pi k(t+\Delta)}{\tau})] \tag{5.5}$$

where $\tau$ denotes the gait cycle and $\Delta$ is equal to zero and $\tau/2$ for muscles of the right and left limbs, respectively. This expression is the same as that used in Section 3.3 for periodic forearm simulations. Thereby, similar muscles of the right and left legs have the same forces, but with a time shift. As discussed in Section 3.3, the Fourier series provides several positive features for solving the optimal control problem, which is why it is selected here.

The muscle and tendon models are based on [5] and [4], respectively. The muscle model includes the contractile element (CE) and series elastic element (SE) only; the parallel elastic element (PE) is left out because a passive torque is added to the joints to account for muscle passive properties as well as joint and skin passive properties, which is presented later. The simulation framework used here is depicted in Figure 5.5, which requires an inverse tendon and contraction dynamics.

The objective function employed for solving the muscle coordination is the normalized

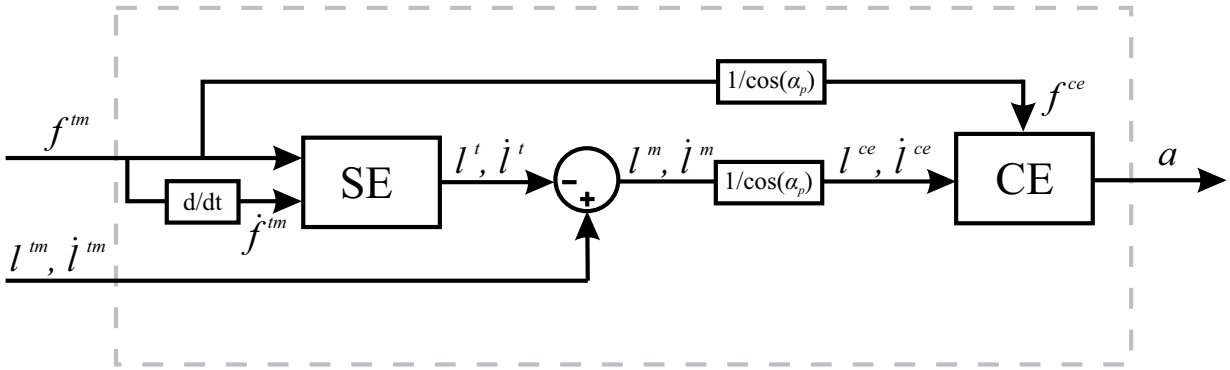


Figure 5.6: Schematic of inverse muscle model: $l^t$ is the tendon length, $l^m$ is the muscle length, and $\alpha_p$ is the muscle pennation angle.

metabolic energy expenditure per distance travelled as follows:

$$J = \frac{1}{\sum \max(\dot{E}_i)} \frac{1}{\tau} \frac{\sum_{i=1}^{n} \int_0^\tau \dot{E}_i dt}{L_r + L_l} \tag{5.6}$$

where $n$ is the total number of muscles, $\dot{E}$ is the muscle metabolic energy rate, and $L_r$ and $L_l$ are the simulated right and left step lengths, respectively. In a fully symmetrical gait, the right and left steps will be equal. The objective function computes the total metabolic energy consumed by the musculoskeletal system from time 0 to $\tau$ of the motion (one gait cycle), as used in [22, 76, 97–99]. An optimization process then solves for the Fourier series coefficients of Equation 5.5 that give muscle forces that minimize $J$, while satisfying certain constraints on the motion.

The focus here is on the muscle coordination and not the design of a complicated balance controller. The strategy to keep the balance of the gait model is to control the torso kinematics. Therefore, the center of mass position and orientation of the torso are parametrized by means of a 6th-order polynomial for the longitudinal $X_{tor}$ and 11-term Fourier series for $Y_{tor}$ and $\phi_T$. Using this approach, torso vertical displacement $y_{tor}$ and orientation $\phi_T$ will be periodic, as desired. In order to have torso trajectories similar to

the experimental data, a tracking constraint can be defined as follows:

$$\begin{aligned} C_{tr1} &\triangleq \|x^s_{tor} - x^e_{tor}\|_\infty \leq \epsilon_{tr1} \\ C_{tr2} &\triangleq \|y^s_{tor} - y^e_{tor}\|_\infty \leq \epsilon_{tr2} \\ C_{tr3} &\triangleq \|\phi^s_T - \pi/2\|_\infty \leq \epsilon_{tr3} \end{aligned} \tag{5.7}$$

where superscripts $s$ and $e$ denote simulated and experimental results, respectively. Values of 0.1 m, 0.1 m, and 0.1 rad are chosen for $\epsilon_{tr1}$, $\epsilon_{tr2}$, and $\epsilon_{tr3}$, respectively, which implies a fairly loose tracking. It should be noted that this tracking could be added to the physiological objective function; however, in that case, the optimization would not remain single-criterion. Note that the third tracking constraint accounts for the deviation of torso angle from upright posture based on [100].

Also to satisfy the conditions of bilateral symmetry, ankle position data are checked to be similar with a 50% of gait cycle time shift, represented by $\delta_t$:

$$\begin{aligned} C_{sym1} &\triangleq \|y_{RK}(t) - y_{LK}(t+\delta_t)\|_\infty \leq \epsilon_{symP} \\ C_{sym2} &\triangleq \|y_{RA}(t) - y_{LA}(t+\delta_t)\|_\infty \leq \epsilon_{symP} \\ C_{sym3} &\triangleq \|y_{RP}(t) - y_{LP}(t+\delta_t)\|_\infty \leq \epsilon_{symP} \\ C_{sym4} &\triangleq \|\dot{x}_{RK}(t) - \dot{x}_{LK}(t+\delta_t)\|_\infty \leq \epsilon_{symV} \\ C_{sym5} &\triangleq \|\dot{x}_{RA}(t) - \dot{x}_{LA}(t+\delta_t)\|_\infty \leq \epsilon_{symV} \\ C_{sym6} &\triangleq \|\dot{x}_{RP}(t) - \dot{x}_{LP}(t+\delta_t)\|_\infty \leq \epsilon_{symV} \end{aligned} \tag{5.8}$$

In Equation 5.8, the first three terms are at the position level, whereas the second three expressions are in terms of velocities. This is because the horizontal positions of right and left legs are not comparable as the step length is not specified. As muscle forces of right and left legs are symmetrical already, $\epsilon_{symP}$ is set to 1e-3 m, and $\epsilon_{symV}$ 1e-3 m/s for the symmetry constraints at $y$ and $\dot{x}$ levels, respectively, which are fairly tight symmetry constraints.

It should be noted that as the gait model is a nonlinear dynamical system, periodic inputs do not necessarily lead to periodic motions, unless a tight tracking of a periodic

motion is performed or periodicity constraints are added. In this predictive gait study, a set of constraints is imposed to the problem to satisfy the periodicity of the simulated motions as follows:

$$
\begin{aligned}
C_{per1} &\triangleq \|\phi_{RH}(0) - \phi_{RH}(\tau)\|_\infty \leq \epsilon_{perP} \\
C_{per2} &\triangleq \|\phi_{RK}(0) - \phi_{RK}(\tau)\|_\infty \leq \epsilon_{perP} \\
C_{per3} &\triangleq \|\phi_{RA}(0) - \phi_{RA}(\tau)\|_\infty \leq \epsilon_{perP} \\
C_{per4} &\triangleq \|\dot{\phi}_{RH}(0) - \dot{\phi}_{RH}(\tau)\|_\infty \leq \epsilon_{perV} \\
C_{per5} &\triangleq \|\dot{\phi}_{RK}(0) - \dot{\phi}_{RK}(\tau)\|_\infty \leq \epsilon_{perV} \\
C_{per6} &\triangleq \|\dot{\phi}_{RA}(0) - \dot{\phi}_{RA}(\tau)\|_\infty \leq \epsilon_{perV}
\end{aligned} \tag{5.9}
$$

where $\epsilon_{perP}$ and $\epsilon_{perV}$ are the tolerances for periodicity violation, which are set to 1e-3 rad and 1e-3 rad/s, respectively. The initial conditions in Equation 5.9 enter the optimization problem as new parameters.

A separate set of constraints are put on muscle neural excitations to keep them within the physiological bounds, i.e., $0 \leq u \leq 1$. The error tolerance for these constraints is 1e-6.

The last constraint is on knee joint angle to avoid any hyper-extension, written as:

$$C_{HE} \triangleq \phi_K \geq -\epsilon_{HE} \tag{5.10}$$

where $C_{HE}$ designates the hyper-extension constraint, and knee joint angle $\phi_K$ is defined as knee flexion angle (see Figure 5.2). The constraint violation for knee angle $\epsilon_{HE}$ is considered to be 1e-6 rad.

In musculoskeletal system modelling, usually the passive moments produced at the joints are ignored; however, these moments exist and affect the dynamics of the system. The sources of the passive moments at the joints are the muscle passive properties, ligaments, skin, and also the joint dissipative moment. For the gait model here, the expressions presented by Riener and Edrich [101] are deployed. They measured the passive joint moments of ten healthy subjects, and found that these moments can be expressed as

functions of the joint angles.

$$
\begin{aligned}
T^{A}_{Passive} =& e^{(2.1016-0.0843\phi_A-0.0176\phi_K)} - e^{(-7.9763+0.1949\phi_A+0.0008\phi_K)} - 1.792 \\
T^{K}_{Passive} =& e^{(1.800-0.0460\phi_A-0.0352\phi_K-0.0217\phi_H)} - e^{(-3.971-0.0004\phi_A+0.0495\phi_K+0.0128\phi_H)} \\
& -4.820 + e^{(2.220-0.150\phi_K)} \\
T^{H}_{Passive} =& e^{(1.4655-0.0034\phi_K+0.0750\phi_H)} - e^{(1.3403-0.0226\phi_K-0.0305\phi_H)} + 8.072
\end{aligned}
\tag{5.11}
$$

where joint angles are in deg and torques are in Nm. These equations reflect all the passive properties of the lower extremity joints and, if used with a three-element Hill muscle model, the passive properties of the muscle will be duplicated. Therefore, using these expressions, the muscle model must exclude the PE element.

The convention here is such that extensor muscles (and ankle plantar flexors) take positive moment arms. Therefore, based on [14, 15] the muscle-tendon lengths can be written as the following:

$$
l^{tm} = l^{tm}_0 - r_H\phi_H + r_K\phi_K - r_A(\phi_A - \pi/2) \tag{5.12}
$$

where $r_A$, $r_K$ and $r_H$ are the muscle moment arms around ankle, knee, and hip joints, respectively. The data for the moment arms are presented in Table 5.3. It should be noted that based on Equation 5.12 and the convention for the signs of moment arms, the positive sign for hip and ankle angles implies joint extension, but for knee, the angle is positive when the joint is flexed (see Figure 5.2).

## 5.2 Experimental Data

The experimental data used in this chapter for validation is from [20], in which the kinematic data, ground reaction forces, and muscle EMGs of nineteen healthy young adults with ages $24.9 \pm 1.9$ years, weights $70.8 \pm 8.8$ kg, and heights $1.75 \pm 0.08$ m were measured.

The reported ground reaction forces are normalized to body mass (BM). The presented linear envelope EMGs are divided by the maximum of MVCs reported in the same reference

Table 5.3: Muscle parameters for the gait model. All parameters are presented in [14]. These parameters are taken from [15] except pennation angles, which are adopted from [16].

| **Muscle Group** | $F^m_{max}$ (N) | $l^{ce}_{opt}$ (m) | $l_{slack}$ (m) | $\alpha_p$ (deg) | $f_{fast}$ (m) | $r_A$ (m) | $r_K$ (m) | $r_H$ (m) | $l^{tm}_0$ (m) | $width$ - |
|---|---|---|---|---|---|---|---|---|---|---|
| Illio | 821 | 0.102 | 0.142 | 7.5 | 0.50 | 0 | 0 | -0.050 | 0.248 | 1.298 |
| RF | 663 | 0.081 | 0.398 | 5.0 | 0.65 | 0 | 0.050 | -0.034 | 0.474 | 1.443 |
| Gl | 1705 | 0.200 | 0.157 | 3.0 | 0.45 | 0 | 0 | 0.062 | 0.271 | 0.625 |
| Hams | 1770 | 0.104 | 0.334 | 7.5 | 0.35 | 0 | -0.034 | 0.072 | 0.383 | 1.197 |
| Vas | 7403 | 0.093 | 0.223 | 4.4 | 0.50 | 0 | 0.042 | 0 | 0.271 | 0.627 |
| Gast | 1639 | 0.055 | 0.420 | 14.3 | 0.50 | 0.053 | -0.020 | 0 | 0.404 | 0.888 |
| TA | 1528 | 0.082 | 0.317 | 6.0 | 0.25 | -0.037 | 0 | 0 | 0.464 | 0.442 |
| Sol | 3883 | 0.055 | 0.245 | 23.6 | 0.20 | 0.053 | 0 | 0 | 0.201 | 1.039 |

[20]. Although this might not scale those signals accurately, it provides a consistent range [0,1] for comparison with the simulated activations.

## 5.3 Results and Discussion

The optimization routine applied and the convergence study performed for gait simulation are the same as those described in Section 3.3.4.

In this section, simulation results are validated against experimental data taken from Winter [20], which provides kinematics, ground reaction forces, and muscle EMGs, expressed in mean±one standard deviation ($\mu \pm \sigma$), acquired from several subjects and trials.

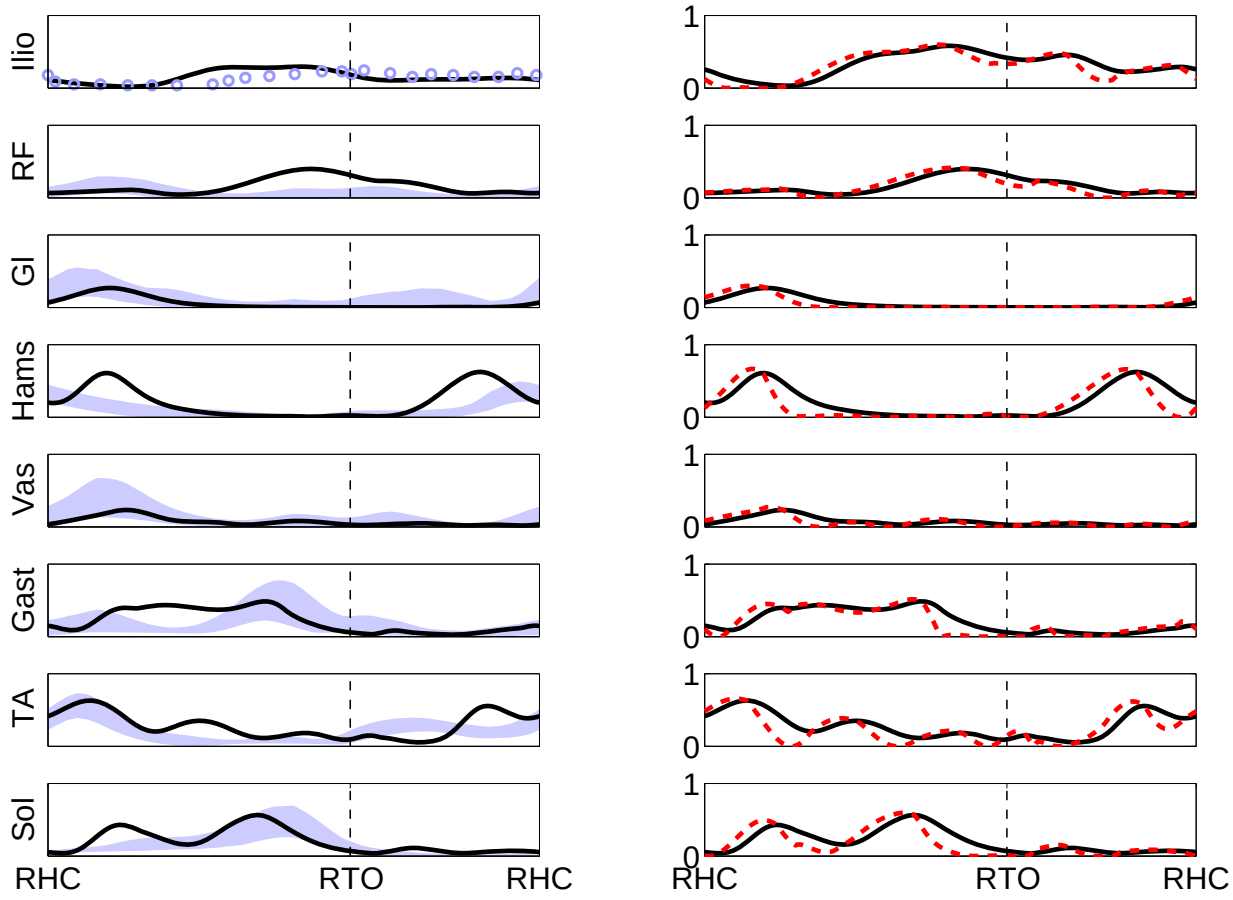


Figure 5.7: On the left: comparison of the simulated muscle activations (solid line) against the muscle EMGs ($\mu \pm \sigma$) from [20] except for the Iliopsoas group where the simulated normalized force is compared against that of [21] (circles). On the right: simulated muscle activations (solid line) plotted against the muscle excitations (dashed line). The vertical axis bounds for the left side is the same as the right side.

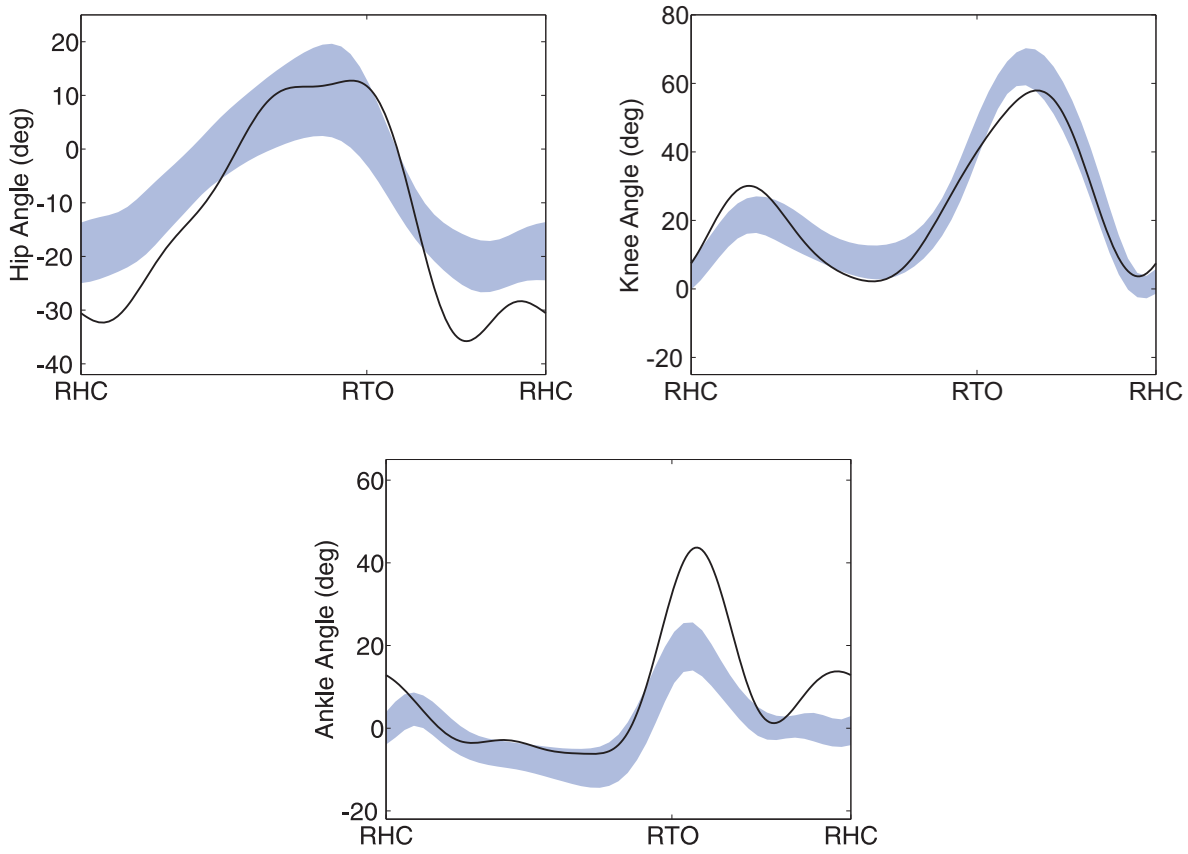


Figure 5.8: Simulated joint angles (hip extension, knee flexion, and ankle plantarflexion) against the experimetal data (shaded area, $\mu \pm \sigma$).

The EMGs of [20] were linear enveloped; once normalized to muscle EMG of maximum voluntary contractions, those can be compared to muscle activations. Maximum and minimum value of MVCs of each muscle group are reported in Winter's book; however, the individual MVCs of the trial are not specified. Therefore, the linear enveloped EMGs are normalized to maximum MVC value reported for each muscle group. Otherwise, muscle activations will have values greater than unity. Figure 5.7 depicts the comparison of muscle activations and experimental EMGs of eight muscle groups. Both the activations and excitations have satisfied the lower and upper bounds within the specified tolerance. Over-

all, the activation patterns agree with the EMGs fairly well. Although the antagonistic coactivation of single-articular muscles increases the cost of motion, since the optimization is over time and since muscles cannot be switched on and off rapidly, some amounts of antagonistic coactivation are observed. Although no EMG data is reported for the Ilipsoas group in [20], the simulated force of this muscle matches that of the simulated muscle force (normalized to maximum isometric force) reported in the work by Anderson and Pandy [21], in which this muscle group is slightly active at heel contact, then its value decreases to nearly zero, and afterwards the activation rises again and stays active until the end of the gait cycle. It must be noted that Anderson and Pandy [21] used the same objective function for simulating gait.

Simulated joint angles are plotted against the experimental data in Figure 5.8. Knee angle shows a close match to the measured data. Not only are the values approximately in the range of data reported, but also the timing of the pattern is quite satisfactory. Furthermore, no knee hyper-extension is observed in the simulation results. Even though the pattern of simulated hip and ankle joint angles is in good agreement with the experimental data, the peak values show some differences. For instance, ankle angle right after toe-off is considerably more than the shaded experimental area. This means that the ankle of the model is plantar-flexed more than that of measured subjects. This can be related to the existence of a finite number of foot contact spheres and the fact that the model has to push the entire foot off the ground in a short period of time. Also, this model is 2D that does not include pelvis yaw rotation to avoid tripping by greater plantarflexion.

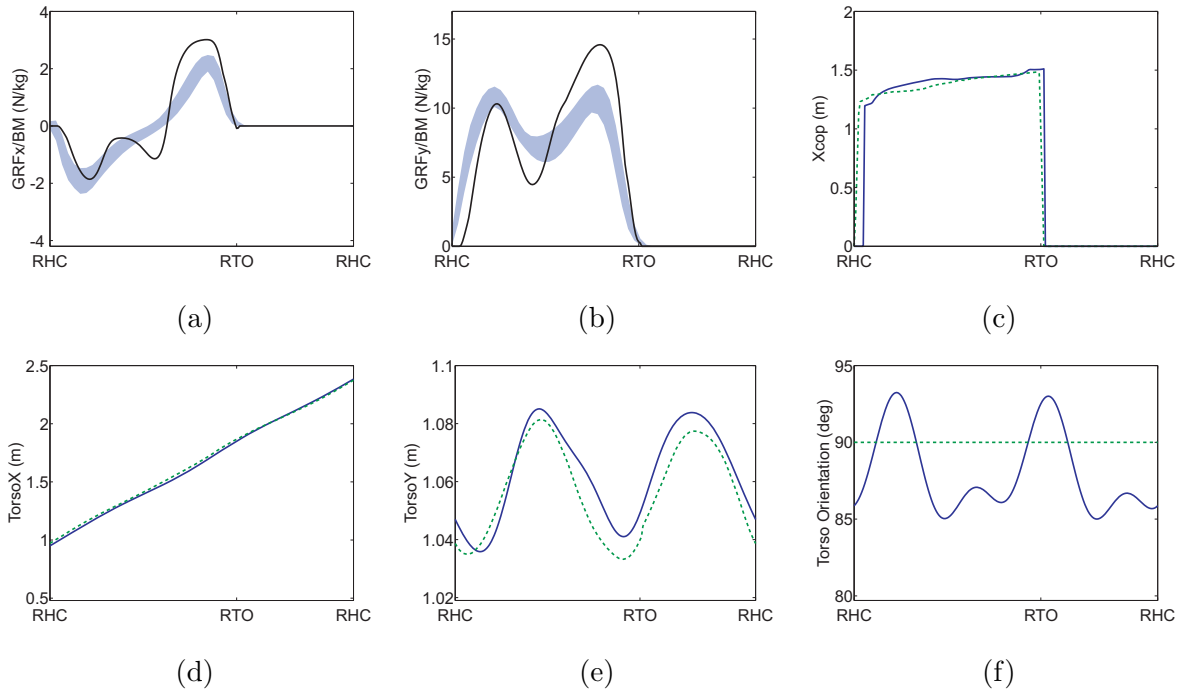


Figure 5.9: Simulated and experimental ground reaction forces divided by body mass ($\mu \pm \sigma$) and center of pressure location (a,b,c). Comparison of optimal torso kinematics (solid) against the reference (dashed), torsoX (d), torsoY (e), and torso orientation (f)

Comparing the simulated contact forces and ground reaction forces indicates a good match in general (see Figures 5.9(a,b)). However, the second peak of the model normal contact force has higher value, which is also reflected in the friction force, but with a different relative amount. Although the foot contact had been validated already, since the ankle kinematics are now different, the excellent match that was observed in Chapter 4 is not seen here.

The differences between the target and simulated kinematics of torso show that the maximum deviation for horizontal and vertical quantities are 5 cm and 1 cm, respectively. Also, the maximum torso leaning forward and backward angles from the vertical posture are 5 deg and 3.2 deg, respectively, which are more than the literature [102] values of 3.5 deg

and 2 deg, respectively. Ruder [102] measured the torso angle variation over the gait cycle averaged on nine separate strides. Note that the maximum torso backward angle occurs at right and left toe-off phases. It should be added that all deviations of torso kinematics from the given references are within the specified tolerances.

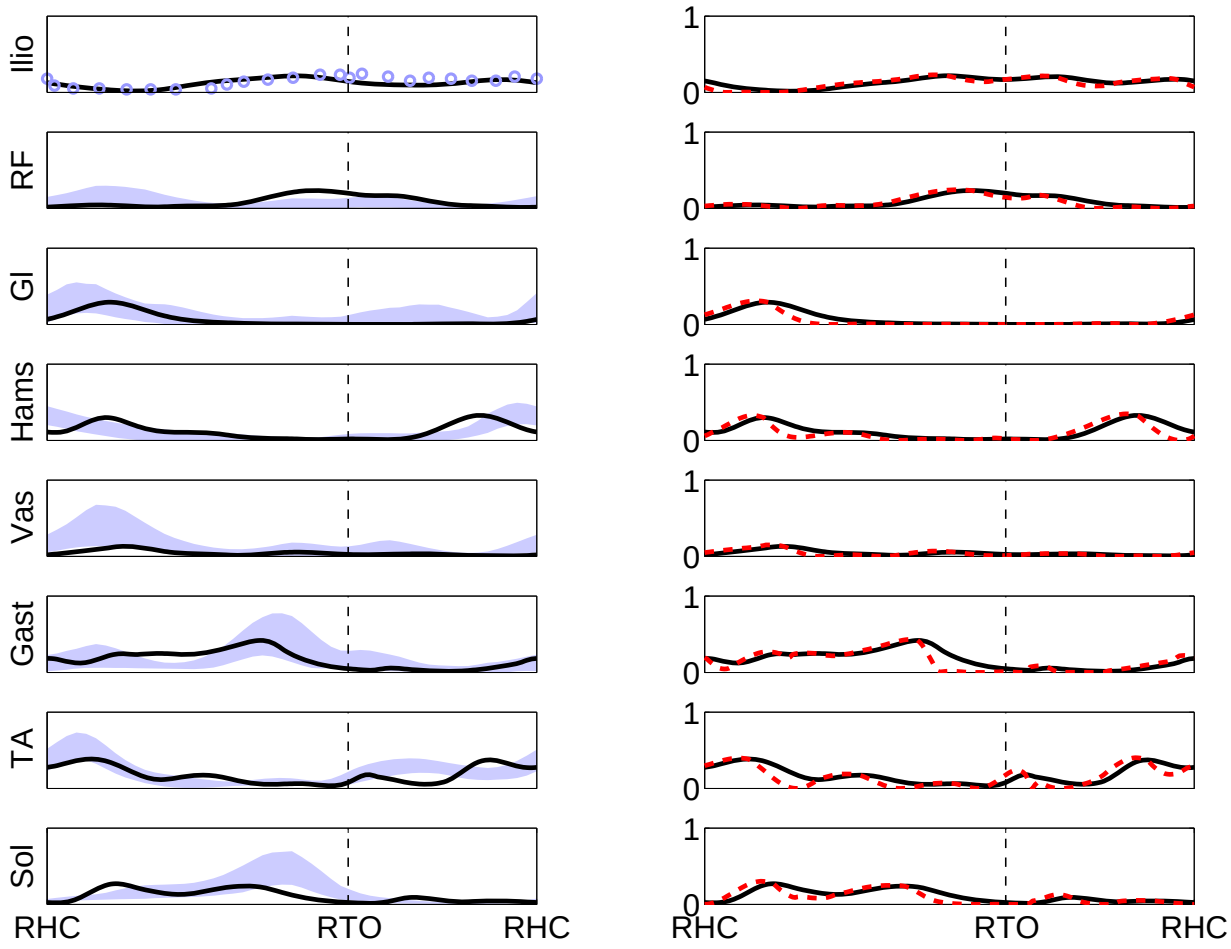


Figure 5.10: Optimal simulation results of the gait model with foot mass reduced to 67%

As mentioned earlier, the foot inertial properties are adopted from [11], whereas other anthropometric data are taken from [10]. To investigate the effect of parameter variations, one sample study is performed. As the foot mass in [11] is nearly 1.5 times of that in [10],

here the foot mass in the gait model is lowered to 67% and the whole gait simulation is rerun. To be brief, optimal muscle activations and excitations are presented only and illustrated in Figure 5.10. These results are comparable to those shown in Figure 5.7. By comparing these two sets of plots, one can conclude that the patterns of the muscle activations have not changed considerably; however, the values of muscle activities are less for the case that foot mass is less. Overall, one can interpret that the activations for this case match the mean±std of the EMGs better. The objective function in this case is 8.8% less, which is due to the fact that muscles are consuming less metabolic energy because of the smaller foot mass.

In addition to inertial properties, muscle parameters affect the simulation results. A thorough sensitivity analysis was done by Scovil and Ronsky [17] in which different muscle parameters are perturbed by ±50% and the relative perturbation of the simulation outputs are calculated. Scovil and Ronsky have reported not only the sensitivity of muscle outputs, but also that of walking and running simulations to the muscle parameters. For the walking study, they simulated forward dynamics of a gait model based on [103] that was driven kinematically at pelvis; the optimal control involved pattern parametrization based on the work by Neptune [104]. The outputs of the model from most to least sensitive are joint angles, joint torques, GRF, and muscle force. The sensitivity averages are partially presented in Table 5.4. Based on that, in a walking simulation, the most sensitive parameters are the tendon slack length and then the optimal fiber length, both of which should be chosen very carefully.

## 5.4 Chapter Summary

This chapter presented a two-dimensional gait model that used the optimal control approach detailed in Section 3.3, and the foot contact model discussed in Chapter 4. The model was simulated for an entire gait stride. As Fourier series were utilized to represent muscle forces, the produced motions of left and right legs were periodic and symmetrical.

Table 5.4: Hill muscle sensitivity by Scovil and Ronsky [17]. Average sensitivity results in terms of ±50% change of muscle parameters. Small: change from 0.01-0.99 of parameter perturbation, Large: change from 1-25 of parameter perturbation, and Extreme: change greater than 25 of parameter perturbation

| **Parameter** | **Muscle Sensitivity** | **Walking Sensitivity** | **Running Sensitivity** |
|---|---|---|---|
| $\hat{f}$ | Large | Small | Small |
| $F^m_{max}$ | Large | Small | Large |
| $l^{ce}_{opt}$ | Large | Large | Large |
| $l_{slack}$ | Extreme | Extreme | Large |

Comparison of simulated muscle activations and experimental EMGs showed a reasonably good agreement.

The next chapter provides a conclusion of the whole thesis, reviews the contributions of the work, and discusses the extension of this thesis for future work.

# Chapter 6

# Conclusions

## 6.1 Summary

In this thesis, the topic of optimal control and multibody dynamic modelling of human musculoskeletal systems was explored. Two new approaches for solving the muscle redundancy as well as the optimal control problems were presented. Global parametrization as a category of dynamic optimization was introduced, and the proposed functions to be used for finger tapping, forearm flexion/extension, and gait were showcased. Forward static optimization as an optimal control approach based on static optimization was also introduced.

The first optimal control example was the finger tapping motion, in which the goal was to find the maximum frequency of index finger tapping. The muscle excitation patterns were globally parametrized with polynomials, and good agreement between the simulated maximum frequency and that reported in the literature was found. The contributions of the finger tapping study were: 1) globally parametrizing the neural excitations with polynomial functions and 2) successfully simulating the maximum frequency of the index finger tapping capacity.

The second dynamic optimization was the forearm flexion/extension simulation for which a global parametrization was again applied, but with Fourier series (FS) for muscle excitations. The model could follow the experimental motion quite well, but the simulated excitations did not match the measured EMGs that well. The contributions of the forearm study were: 1) implementation of the musculoskeletal forearm model in the symbolic multibody MapleSim® environment and 2) globally parametrizing the muscle neural excitations by means of FS terms for forearm simulations.

Forward Static Optimization (FSO) was introduced as a new approach to solve the optimal control of musculoskeletal systems efficiently. FSO is similar to the idea of nonlinear model predictive control (NMPC), with control and prediction horizons of unity [105]. This approach was able to produce remarkable results, comparable to the inverse dynamics results, as reference solutions. Compared to the dynamic optimization approach, the FSO solved the same forearm simulation with considerably less CPU time. As FSO uses instantaneous objective functions, unlike DO, it is prone to result in unphysiological sudden changes in the control variables. Nevertheless, it can still provide a reasonable sub-optimal solution of the system.

In Chapter 4, the hyper-volumetric foot contact model was introduced to the biomechanics field for the first time. This novel model predicted the vertical and horizontal ground reaction forces very well. Before this model, the point contact and the linear volumetric models had not been able to simulate the contact forces with this level of fidelity. The hyper-volumetric foot contact model is also efficient, as it includes only three contact elements.

Finally, the gait model, simulated for two steps, was able to predict the lower-extremity kinematics, the muscle activations, and the ground reaction forces with acceptable agreement to experimental results. This shows that the model, the chosen optimal control approach, and the foot contact model were working reasonably well. The contributions of the gait study include 1) implementation of the musculoskeletal gait model using symbolic programming (MapleSim®), 2) globally parametrizing the muscle forces by FS terms for

gait simulations, and 3) applying the efficient hyper-volumetric foot contact model in a forward dynamic gait simulation.

## 6.2 Recommendations for Future Research

Although the results of the presented models showed strong potential and capability, there is still room for improvement in both modelling and validation aspects. The recommended future research for each part is separately mentioned in the following:

**Finger Tapping**

1. Adding contact elements that account for a piano key or a key of keyboard. If so, the model can be more realistically applied for piano playing or typing.
2. Experimental validation of the model: although the maximum frequency was compared to those reported in the literature, it would be informative to experimentally measure the maximum frequency of the finger tapping under various conditions, such as piano playing and typing for different subjects with diverse typing or piano playing skills.

**Forearm Modelling**

The future work for this model include the following:

1. Collecting more data for various cases, such as the elbow flexion/extension while holding different weights in the hand. This helps to compare the muscle excitations and the EMGs more quantitatively.
2. Extending the two-dimensional (2D) model to 3D would be another future work. In this way, one can see the influence of other degrees of freedom, such as supination/pronation at the elbow.

**Forward Static Optimization**

1. Adding muscle contraction dynamics: in this case, the physiological objective function can be formed based on activation effort rather than force. This can be done through forward or inverse contraction dynamics.

2. The proposed FSO approach is very similar to an NMPC approach with control and prediction horizons of unity [105]. It would be interesting to try larger prediction and control horizons and investigate the effects on the quality of the results as well as the CPU time.

**Foot Contact Modelling**

1. Although the spherical volumetric elements produced reasonable results, which were much better than the point contact models as they provide a wider contact patch, more complicated shapes like an ellipsoid can be employed in the future.

2. The contact model was a sphere on surface, which is three-dimensional per se; however, the forces of the third dimension were not validated. Thus, in the future, it would be interesting to measure the friction forces of the lateral direction to compare the simulated and experimental quantities of this force as well.

3. More sets of experimental data will be required to fully validate the foot contact model. In other words, provided different experimental conditions like slow and fast walking, jogging, and running, and also with different footwear conditions, the model can be validated in a more general and therefore robust way.

4. A more complicated friction model such as the bristle model proposed By Gonthier et al. [91] can replace the Coulomb friction model. There is an obvious room for improving the friction model by looking at the simulated and experimental results.

### Gait Modelling

1. Extending the model to three dimensions. Other degrees of freedom of the human skeletal system such as pelvis yaw can be included, and the effects can be studied.

2. A more complicated balance controller can be designed for the gait model, ideally one that is independent of any a priori torso kinematic measurements.

3. In this thesis, gait motion was assumed to be bi-laterally symmetrical. In future, non-symmetrical gait will also be investigated, which is a more general case.

4. Although gait is a motion with a moderate range of joint angles for which constant moment arms for the muscles worked fine, in the future adding variant moment arms, including origins, insertions, via and wrapping points, will add more fidelity to the model.

### Systematic Sensitivity Analysis

Musculoskeletal models include a great many parameters, including muscle model, foot contact, and anthropometric parameters. A large future project can be to investigate the sensitivity of the simulation outputs, such as predicted limb motions, muscle excitations, and ground reaction forces, to all parameters of the model. A systematic sensitivity analysis is necessary for these models, which can be done through different approaches explained in [106].

# References


[1] He, J., Levine, W. S., and Loeb, G. E., 1991. "Feedback gains for correcting small perturbations to standing posture". *IEEE Transactions on Autonomic Control,* **36**, pp. 322–332.

[2] Winters, J. M., and Stark, L., 1988. "Estimated mechanical properties of synergistic muscles involved in movements of a variety of human joints". *Journal of Biomechanics,* **21**(12), pp. 1027–1041.

[3] Thelen, D. G., 2003. "Adjustment of muscle mechanics model parameters to simulate dynamic contractions in older adults". *Journal of Biomechanical Engineering,* **125**(1), pp. 70–77.

[4] Winters, J. M., 1990. "Hill-based muscle models: a system engineering perpective". *In: J. M.Winters and S. L.-Y.Woo (eds.): Multiple Muscle Systems. Springer-Verlag, Chapt. 5*, pp. 69–93.

[5] Nagano, A., and Gerritsen, K., 2001. "Effects of neuromuscular strength training on vertical jumping performance - a computer simulation study". *Journal of Applied Biomechanics,* **17**, pp. 113–128.

[6] Bhargava, L. J., Pandy, M. G., and Anderson, F. C., 2004. "A phenomenological model for estimating metabolic energy consumption in muscle contraction". *Journal of Biomechanics,* **37**(1), pp. 81–88.

[7] Umberger, B. R., Gerritsen, K. G., and Martin, P. E., 2003. "A model of human muscle energy expenditure". *Computer Methods in Biomechanics and Biomedical Engineering,* **6**(2), pp. 99–111.

[8] Garner, B. A., and Pandy, M. G., 2001. "Musculoskeletal model of the upper limb based on the visible human male dataset". *Computer Methods in Biomechanics and Biomedical Engineering,* **4**, pp. 93–126.

[9] Veeger, H. E. J., Yu, B., An, K.-N., and Rozendal, R. H., 1997. "Parameters for modeling the upper extremity". *Journal of Biomechanics,* **30**(6), pp. 647–652.

[10] Winter, D. A., 2005. *Biomechanics and Motor Control of Human Movement*, 3rd ed. John Wiley & Sons.

[11] Anderson, F. C., and Pandy, M. G., 1999. "A dynamic optimization solution for vertical jumping in three dimensions". *Computer Methods in Biomechanics and Biomedical Engineering,* **2**(3), pp. 201–231.

[12] Erdemir, A., and Piazza, S. J., 2004. "Changes in foot loading following plantar fasciotomy: A computer modeling study". *Journal of Biomechanical Engineering,* **126**(2), pp. 237–243.

[13] Sandhu, S., and McPhee, J., 2010. "A two-dimensional nonlinear volumetric foot contact model". In ASME International Mechanical Engineering Congress & Exposition, Vancouver, Canada.

[14] Ackermann, M., 2007. "Dynamics and energetics of walking with prostheses". PhD Thesis, University of Stuttgart, Germany.

[15] Gerritsen, K. G. M., van den Bogert, A. J., Hulliger, M., and Zernicke, R. F., 1998. "Intrinsic muscle properties facilitate locomotor control - a computer simulation study". *Motor Control,* **2**(3), pp. 206–220.

[16] Menegaldo, L., Fleury, A. T., and Weber, H. I., 2003. "Biomechanical modeling and optimal control of human posture". *Journal of Biomechanics,* **36**(11), pp. 1701–1712.

[17] Scovil, C. Y., and Ronsky, J. L., 2006. "Sensitivity of a hill-based muscle model to perturbations in model parameters". *Journal of Biomechanics,* **39**(11), pp. 2055 – 2063.

[18] Ambrosio, J. A., and Kecskemethy, A., 2007. "Multibody dynamics of biomechanical models for human motion via optimization". *J.C. Garciaa Orden et al. (eds), Multibody Dynamics. Computational Methods and Applications*, pp. 245–272.

[19] Murray, W. M., Delp, S. L., and Buchanan, T. S., 1995. "Variation of muscle moment arms with elbow and forearm position". *Journal of Biomechanics,* **28**(5), pp. 513–525.

[20] Winter, D. A., 1991. *Biomechanics and Motor Control of Human Gait: Normal, Elderly and Pathological*, 2nd ed. University of Waterloo Press.

[21] Anderson, F. C., and Pandy, M. G., 2001. "Static and dynamic optimization solutions for gait are practically equivalent". *Journal of Biomechanics,* **34**(2), pp. 153–161.

[22] Peasgood, M., Kubica, E., and McPhee, J., 2007. "Stabilization of a dynamic walking gait simulation". *Journal of Computational and Nonlinear Dynamics,* **2**(1), pp. 65–72.

[23] Kuo, A. D., 2001. "A simple model of bipedal walking predicts the preferred speed–step length relationship". *Journal of Biomechanical Engineering,* **123**(3), pp. 264–269.

[24] Kuo, A. D., 2002. "Energetics of actively powered locomotion using the simplest walking model". *Journal of Biomechanical Engineering,* **124**(1), pp. 113–120.

[25] Cavagna, G. A., 1977. "Mechanical work in terrestrial locomotion: two basic mechanisms for minimizing energy expenditure". *American journal of physiology,* **233**(5), pp. R243–R261.

[26] Millard, M., McPhee, J., and Kubica, E., 2009. "Multi-step forward dynamic gait simulation". *Bottasso C., editor. Multibody Dynamics: Computational Methods and Applications,* **12**, pp. 25–43.

[27] Hansen, M., Otis, J., Kenneally, S., and Deland, J., 2001. "A closed-loop cadaveric foot and ankle loading model". *Journal of Biomechanics,* **34**(4), pp. 551 – 555.

[28] Hill, A. V., 1938. "The heat of shortening and the dynamic constants of muscle". *Proceedings of the Royal Society of London, Series B, Biological Sciences,* **126**(843), pp. 136–195.

[29] Winters, J., and Stark, L., 1987. "Muscle models: What is gained and what is lost by varying model complexity". *Biological Cybernetics,* **55**, pp. 403–420.

[30] Stark, L., 1968. *Neurological control systems.* Plenum Press, New York.

[31] Agarwal, G. C., Berman, B. M., and Stark, L., 1970. "Studies in postural control systems part i: Torque disturbance input". *Systems Science and Cybernetics, IEEE Transactions on,* **6**(2), pp. 116–121.

[32] Zajac, F. E., 1989. "Muscle and tendon: properties, models, scaling, and application to biomechanics and motor control". *CRC Critical Reviews in Biomedical Engineering,* **19**(4), pp. 359–411.

[33] Close, R., 1972. "Dynamic properties of mammalian skeletal muscle". *Physiol. Rev.,* **52**, pp. 129–197.

[34] Winters, J., 1985. "Generalized analysis and design of antagonistic muscle models: effect of nonlinear properties on the control of human movement". PhD Thesis, University of California, Berkeley, USA.

[35] Glantz, S., 1974. "A constitutive equation for the passive properties of muscle". *Journal of Biomechanics,* **7**, pp. 137–145.

[36] Buchanan, T. S., 2004. "Neuromusculoskeletal modeling: estimation of muscle forces and joint moments and movements from measurements of neural command". *Journal of applied biomechanics,* **20**(4), pp. 367–395.

[37] van Soest, A. J., and Bobbert, M. F., 1993. "The contribution of muscle properties in the control of explosive movements". *Biological Cybernetics,* **69**(3), pp. 195–204.

[38] Cole, G. K., Nigg, B. M., van den Bogert, A. J., and Gerritsen, K. G. M., 1996. "Lower extremity joint loading during impact in running". *Clinical Biomechanics,* **11**(4), pp. 181–193.

[39] Hill, T. "Theoretical formalism for the sliding filament model of contraction of striated muscle, part ii.". In Progress in Biophysics and Molecular Biology, Vol. 29, pp. 105–159.

[40] Wood, J., and Mann, R., 1981. "A sliding-filament cross-bridge ensemble model of muscle contraction for mechanical transients". *Math. Biosci.,* **57**, pp. 211–263.

[41] Zahalak, G., 1981. "A distribution-moment approximation for kinetic theories of muscular contraction". *Math. Biosci.,* **55**, pp. 89–114.

[42] Silva, M., 2003. "Human motion analysis using multibody dynamics and optimization tools". PhD Thesis, Technical University of Lisbon , Lisbon, Portugal.

[43] Crowninshield, R. D., and Brand, R. A., 1981. "A physiologically based criterion of muscle force prediction in locomotion". *Journal of Biomechanics,* **14**(11), pp. 793–801.

[44] Tsirakos, D., B. V., and Bartlett, R., 1997. "Inverse optimization: functional and physiological considerations related to the force-sharing problem". *Critical Reviews in Biomedical Engineering,* **25**(4-5), pp. 371–407.

[45] Dul, J., Johnson, G., Shiavi, R., and Townsend, M., 1984. "Muscular synergism-i. on criteria for load sharing between synergistic muscles". *Journal of Biomechanics,* **17**, pp. 663–673.

[46] van Bolhuis, B., and Gielen, C., 1999. "A comparison of models explaining muscle activation patterns for isometric contractions". *Biological Cybernetics,* **81**, pp. 249–26.

[47] Rohrle, H., Scholten, R., Sigolotto, C., Sollbach, W., and Kellner, H., 1984. "Joint forces in the human pelvis-leg skeleton during walking". *Journal of Biomechanics,* **17**, pp. 409–424.

[48] Pedotti, A., K. V., and Stark, L., 1978. "Optimization of muscle force sequencing in locomotion". *Mathematical Biosciences,* **38**, pp. 57–76.

[49] Herzog, W., 1987. "Individual muscle force estimations using non-linear optimal design". *Journal of Neuroscience Methods,* **21**, pp. 167–179.

[50] Happee, R., 1994. "Inverse dynamic optimization including muscular dynamics, a new simulation method applied to goal directed movements". *Journal of Biomechanics,* **27**(7), pp. 953–960.

[51] Rasmussen, J., Damsgaard, M., and Voigt, M., 2001. "Muscle recruitment by the min/max criterion a comparative numerical study". *Journal of Biomechanics,* **34**(3), pp. 409–415.

[52] Davy, D. T., and Audu, M. L., 1987. "A dynamic optimization technique for the muscle forces in the swing phase of the gait". *Journal of Biomechanics,* **20**(2), pp. 187–201.

[53] Hatze, H., 1976. "The complete optimization of a human motion". *The complete optimization of a human motion, Mathematical Biosciences,* **28**, pp. 99–135.

[54] Pandy, M. G., Anderson, F. C., and Hull, D. G., 1992. "A parameter optimization approach for the optimal control of large-scale musculoskeletal systems". *Journal of Biomechanical Engineering,* **114**(4), pp. 450–460.

[55] Anderson, F. C., and Pandy, M. G., 2001. "Dynamic optimization of human walking". *Journal of Biomechanical Engineering,* **123**(5), pp. 381–390.

[56] Kerwin, J., and Challis, D., 1993. "An analytical examination of muscle force estimations using optimization techniques". *Journal of Engineering in Medicine,* **207**, pp. 139–148.

[57] Raikova, R. T., and Prilutsky, B. I., 2001. "Sensitivity of predicted muscle forces to parameters of the optimization-based human leg model revealed by analytical and numerical analyses". *Journal of Biomechanics,* **34**(10), pp. 1243–1255.

[58] Thelen, D. G., Anderson, F. C., and Delp, S. L., 2003. "Generating dynamic simulations of movement using computed muscle control". *Journal of Biomechanics,* **36**(3), pp. 321–328.

[59] Zajac, F. E., Neptune, R. R., and Kautz, S. A., 2002. "Biomechanics and muscle coordination of human walking, part i: Introduction to concepts, power transfer, dynamics and simulations". *Gait & Posture,* **16**(3), pp. 215–232.

[60] Zajac, F. E., Neptune, R. R., and Kautz, S. A., 2003. "Biomechanics and muscle coordination of human walking: Part ii: Lessons from dynamical simulations and clinical implications". *Gait & Posture,* **17**(1), pp. 1–17.

[61] Zhou, X., Draganich, L. F., and Amirouche, F., 2002. "A dynamic model for simulating a trip and fall during gait". *Medical Engineering & Physics,* **24**(2), pp. 121–127.

[62] Gilchrist, L. A., and Winter, D. A., 1996. "A two-part, viscoelastic foot model for use in gait simulations". *Journal of Biomechanics,* **29**(6), pp. 795–798.

[63] Neptune, R. R., Wright, I. C., and Den Bogert, A. J. V., 2000. "A method for numerical simulation of single limb ground contact events: Application to heel-toe running". *Computer Methods in Biomechanics and Biomedical Engineering,* **3**(4), pp. 321–334.

[64] Wojtyra, M., 2003. "Multibody simulation model of human walking". *Mechanics Based Design of Structures and Machines,* **31**(3), pp. 357–379.

[65] Gonthier, Y., McPhee, J., Lange, C., and Piedboeuf, J.-C. "A contact modeling method based on volumetric properties". In ASME Conference Proceedings, Vol. 2005, pp. 477–486.

[66] Samin, J., and Fisette, P., 2003. *Symbolic Modeling of Multibody Systems.* Kluwer Academic Publishers.

[67] Morency, K., McPhee, J., and Schmitke, C., 2006. Using graph theory and symbolic computing to generate efficient models for vehicle dynamics. Proceedings of the CSME Forum, Calgary, Alberta.

[68] Uchida, T. K., 2011. "Real-time dynamic simulation of constrained multibody systems using symbolic computation". PhD thesis, University of Waterloo, Canada.

[69] Wittkopf, A., 2008. "Automatic code generation and optimization in maple". *Journal of Numerical Analysis, Industrial and Applied Mathematics (JNAIAM),* **3**(1-2), pp. 167–180.

[70] Ambrosio, J., Lopes, G., Costa, J., and Abrantes, J., 2001. "Spatial reconstruction of the human motion based on images from a single stationary camera". *Journal of Biomechanics,* **34**, pp. 1217–1221.

[71] Allard, P., S. I., and Blanchi, J., 1995. "Three-dimensional analysis of human movement". *Human Kinetics, Champaign, Illinois.*

[72] Kirk, D. E., 2004. *Optimal Control Theory: An Introduction.* Dover Publications Inc., Mineola, New York.

[73] Betts, J., 2001. *Practical Methods for Optimal Control Using Nonlinear Programming.* SIAM, Philadelphia.

[74] Chachuat, B. C., 2007. *Nonlinear and Dynamic Optimization: From Theory to Practice.* Automatic Control Laboratory, EPFL, Switzerland.

[75] Ackermann, M., and van den Bogert, A. J., 2010. "Optimality principles for model-based prediction of human gait". *Journal of Biomechanics,* **43**(6), pp. 1055–1060.

[76] Garcia-Vallejo, D., and Schiehlen, W., 2012. "3d-simulation of human walking by parameter optimization". *Archive of Applied Mechanics,* **82**(4), pp. 533–556.

[77] Shourijeh, M. S., McPhee, J., and Wells, R., 2010. A model for forward dynamic simulation of rapid tapping motion of index finger. Canadian Society for Biomechanics, Kingston, Canada.

[78] Shourijeh, M. S., and McPhee, J., 2012. Dynamic optimization of human forearm simulations by parameterizing the muscle excitations. Canadian Society for Biomechanics, Burnaby, Canada.

[79] Buchner, H., H. M., and Hemami, H., 1988. "A dynamic model for finger interphalangeal coordination". *Journal of Biomechanics,* **21**(6), pp. 459–468.

[80] Unsworth, A., and Alexander, W. J., 1979. "Dimensions of the metacarpophalangeal joint with particular reference to joint prostheses". *Engineering in Medicine,* **8**(2), pp. 75–80.

[81] Kuo, P.-L., Lee, D. L., Jindrich, D. L., and Dennerlein, J. T., 2006. "Finger joint coordination during tapping". *Journal of Biomechanics,* **39**(16), pp. 2934–2942.

[82] Kuboyama, N., Nabetani, N., Shibuya, K., Machida, K., and Ogaki, T., 2004. "The effect of maximal finger tapping on cerebral activation". *Journal of Physiological Anthropology and Applied Human Science,* **23**(4), pp. 105–110.

[83] Morrison, S., H. S., and Newell, K., 2009. "Upper frequency limits of bilateral coordination patterns". *Neuroscience Letters,* **454**, pp. 233–238.

[84] Happee, R., and Van der Helm, F. C. T., 1995. "The control of shoulder muscles during goal directed movements, an inverse dynamic analysis". *Journal of Biomechanics,* **28**(10), pp. 1179–1191.

[85] Thelen, D. G., and Anderson, F. C., 2006. "Using computed muscle control to generate forward dynamic simulations of human walking from experimental data". *Journal of Biomechanics,* **39**(6), pp. 1107–1115.

[86] Shelburne, K. B., and Pandy, M. G., 2005. "A dynamic model of the knee and lower limb for simulating rising movements". *Computer Methods in Biomechanics and Biomedical Engineering,* **5**(2), pp. 149–159.

[87] Baumgarte, J., 1972. "Stabilization of constraints and integrals of motion in dynamical systems". *Computer Methods in Applied Mechanics and Engineering,* **1**(1), pp. 1–16.

[88] Ostermeyer, G.-P., 1990. "On baumgarte stabilization for differential algebraic equations". *Real-time integration methods for mechanical system simulation,* **69**, pp. 193–207.

[89] Hunt, K., and Crossley, F., 1975. "Coefficient of restitution interpreted as damping in vibroimpact". *Journal of Applied Mechanics,* **7**, pp. 440–445.

[90] Boos, M., and McPhee, J., 2013. "Volumetric modeling and experimental validation of normal contact dynamic forces". *Journal of Computational and Nonlinear Dynamics,* **8**(2), p. 021006.

[91] Gonthier, Y., McPhee, J., Lange, C., and Piedbuf, J.-C., 2004. "A regularized contact model with asymmetric damping and dwell-time dependent friction". *Multibody System Dynamics,* **11**(3), pp. 209–233.

[92] Petersen, W., 2013. "A volumetric contact model for planetary rover wheel application". PhD thesis, University of Waterloo, Canada.

[93] Millard, M., 2011. "Mechanics and control of human balance". PhD thesis, University of Waterloo, Canada.

[94] Vaughan, C. L., Davis, B. L., and O'connor, J. C., 1992. *Dynamics of human gait.* Human Kinetics Publishers, Champaign, Illinois.

[95] Gilchrist, L., and Winter, D., 1997. "A multisegment computer simulation of normal human gait". *IEEE Transactions on Rehabilitation Engineering,* **5**(4), pp. 290–299.

[96] Umberger, B. R., 2008. "Effects of suppressing arm swing on kinematics, kinetics, and energetics of human walking". *Journal of Biomechanics,* **41**(11), pp. 2575–2580.

[97] Bullimore, S., and Burn, J., 2006. "Consequences of forward translation of the point of force application for the mechanics of running". *Journal of Theoretical Biology,* **238**, pp. 211–219.

[98] Cavanagh, P., 1999. "Plantar soft tissue thickness during ground contact in walking". *Journal of Biomechanics,* **32**, pp. 623–628.

[99] Carson, M., Harrington, M., Thompson, N., O'Connor, J., and Theologis, T., 2001. "Kinematic analysis of a multi-segment foot model for research and clinical applications: a repeatability analysis". *Journal of Biomechanics,* **34**, pp. 1299–1307.

[100] Kim, H., Wang, Q., Rahmatalla, S., Swan, C., Arora, J., Abdel-Malek, K., and Assouline, J., 2008. "Dynamic motion planning of 3d human locomotion using gradient-based optimization". *Journal of Biomechanical Engineering,* **130**(3), pp. 201–214.

[101] Riener, R., and Edrich, T., 1999. "Identification of passive elastic joint moments in the lower extremities". *Journal of Biomechanics,* **32**(5), pp. 539–544.

[102] Ruder, G., 1989. "Whole body balance during normal and perturbed walking in the sagittal plane". MSc Thesis, University of Waterloo, Canada.

[103] Scovil, C., 2004. "The viability of a 3d forward dynamic model of walking as a research tool to enhance clinical understanding of gait abnormalities". PhD Thesis, University of Calgary, Canada.

[104] Neptune, R. R., 1999. "Optimization algorithm performance in determining optimal controls in human movement analyses". *Journal of biomechanical engineering,* **121**, pp. 249–252.

[105] Grune, L., and Pannek., J., 2011. *Nonlinear Model Predictive Control: theory and algorithms*. Springer-Verlag London Limited.

[106] Banerjee, J. M., and McPhee, J., 2013. "Symbolic sensitivity analysis of multibody systems". *J.-C. Samin, P. Fisette (eds.), Multibody Dynamics, Computational Methods in Applied Sciences 28*, pp. 123–146.

[107] Raasch, C. C., Zajac, F. E., Ma, B., and Levine, W. S., 1997. "Muscle coordination of maximum-speed pedaling". *Journal of Biomechanics,* **30**(6), pp. 595–602.

[108] Elia, M., 1992. "Organ and tissue contribution to metabolic rate". *Kinney, J.M. and Tucker, H.N., eds, Energy Metabolism: Tissue Determinants and Cellular Corollaries (Raven Press, New York)*, pp. 61–77.

# APPENDICES

# Appendix A

# Muscle Model

## A.1 Activation Dynamics by He et al. [1]

$$\dot{a}(t) = (u(t) - a(t))(t_1 u(t) + t_2) \tag{A.1}$$

with

$$t_2 = 1/\tau_{fall}$$

$$t_1 = 1/\tau_{rise} - t_2$$

where $u$ and $a$ are the muscle excitation and activation, respectively, $\tau_{fall}$ is the deactivation time constant (approximately 50 ms), and $\tau_{rise}$ is the activation time constant (approximately 15 ms).

## A.2 Activation Dynamics by Winters and Stark [2]

### A.2.1 Forward

Forward activation dynamics is the case that muscle activation is calculated from known neural excitation. The differential equation for the activation dynamics used in this thesis:

$$\dot{a} = \begin{cases} (u-a)(t_1 u + t_2) & u \geq a \\ (u-a)t_2 & u < a \end{cases} \tag{A.2}$$

where $u$ is muscle excitation, and $t_1$ and $t_2$ are defined in the following [107]:

$$t_2 = \frac{1}{\tau_{fall}} \tag{A.3}$$

$$t_1 = \frac{1}{\tau_{rise}} - t_2 \tag{A.4}$$

where $\tau_{fall}$ and $\tau_{rise}$ are assumed to be 68 ms and 11 ms, respectively [2, 12]. It should be noted that the conditions in Equation A.2, $u \geq a$ and $u < a$, are equivalent to $\dot{a} \geq 0$ and $\dot{a} < 0$, respectively.

### A.2.2 Inverse

In case the goal is to find neural excitation from the activation and activation rate, the relation is called inverse activation dynamics. Rearranging Equation A.2, the excitation can be written as:

$$u = \begin{cases} \dfrac{at_1 - t_2 \pm \sqrt{(at_1 + t_2)^2 + 4\dot{a}t_1}}{2t_1} & \dot{a} \geq 0 \\ \dfrac{\dot{a} + t_2 a}{t_2} & \dot{a} < 0 \end{cases} \tag{A.5}$$

where in the first statement, only the positive value is valid; otherwise, the excitation will be negative.

## A.3 Muscle-Tendon Dynamics by Thelen [3]

### A.3.1 Tendon Dynamics

The tendon force normalized to muscle maximum isometric force $F^m_{max}$ is represented as an exponential function of the tendon strain:

$$\tilde{f}^t = \begin{cases} \frac{\tilde{f}^t_{toe}}{e^{k_{toe}} - 1}(e^{\frac{k_{toe}\epsilon^t}{\epsilon^t_{toe}}} - 1) & \epsilon^t \leq \epsilon^t_{toe} \\ k_{lin}(\epsilon^t - \epsilon^t_{toe}) + \tilde{f}^t_{toe} & \epsilon^t > \epsilon^t_{toe} \end{cases} \tag{A.6}$$

where $\epsilon^t$ is engineering strain of tendon (calculated based on the slack length $l_{slack}$), $\epsilon^t_{toe}$ is a limit after which the tendon relation switches to the linear expression, $k_{toe}$ is a shape factor, $k_{lin}$ is the linear slope of the second condition, and $\tilde{f}^t_{toe}$ is the function value at $\epsilon^t$=$\epsilon^t_{toe}$. Values of the parameters are adopted from [3]: $k_{toe}$=3, $\tilde{f}^t_{toe}$=0.33, $\epsilon^t_0$=0.04, $\epsilon^t_{toe}$=0.609$\epsilon^t_0$, and $k_{lin}$=1.712/$\epsilon^t_0$.

### A.3.2 Parallel elastic element Relation

The relation for muscle passive force normalized to muscle maximum isometric force $F^m_{max}$ is expressed as:

$$\tilde{f}^{pe} = \frac{e^{\frac{k^{pe}(\tilde{l}^{ce} - 1)}{\epsilon^m_0}} - 1}{e^{k^{pe}} - 1} \tag{A.7}$$

where $\tilde{l}^{ce}$ is the muscle fiber length normalized to $l^{ce}_{opt}$, $k^{pe}$ is a shape parameter set to 5, $\epsilon^m_0$ is called the passive muscle strain and adopted to be 0.6 (for young adults) in this thesis.

### A.3.3 Force-Length-Velocity Relation

The force-length relation is written as:

$$f_{isom}^{ce} = e^{-\frac{(\tilde{l}^{ce}-1)^2}{\gamma}} \tag{A.8}$$

where $\gamma$ is a shape factor and is set to be 0.45.

Afterwards, the total force-length-velocity in this muscle model can be formulated as the following:

$$v^{ce} = (0.25 + 0.75a)\, v_{max}^{ce} \frac{\tilde{f}^{ce} - a f_{isom}^{ce}}{b} \tag{A.9}$$

with

$$b = \begin{cases} a f_{isom}^{ce} + \tilde{f}^{ce}/A_f & \tilde{f}^{ce} \leq a f_{isom}^{ce} \\ \dfrac{(2 + 2/A_f)(a f_{isom}^{ce}\hat{f} - \tilde{f}^{ce})}{\hat{f} - 1} & \tilde{f}^{ce} > a f_{isom}^{ce} \end{cases}$$

where $a$ is the muscle activation, $v^{ce}$ is the fiber velocity (velocity of CE element), $\tilde{f}^{ce}$ is the force of CE element normalized to maximum isometric force, $\hat{f}$ is the normalized asymptotic eccentric force (equal to 1.4 for young adults), $A_f$ is a shape parameter (adopted to be 0.25), $v_{max}^{ce}$=10 $l_{opt}^{ce}$ m/s is the maximum contraction velocity of the muscle fiber.

## A.4 Tendon Dynamics by Winters [4]

For studying muscle coordination purposes, the tendon can be modelled as a hyper-elastic component. This model is based on [4] in which tendon force is modelled by means of a quadratic function of the tendon deformation:

$$f^t = \begin{cases} k^t (l^t - l_{slack})^2 & l^t \geq l_{slack} \\ 0 & l^t < l_{slack} \end{cases} \tag{A.10}$$

where $l_{slack}$ is the tendon slack length, which is similar to rest length of a spring, and $k^t$ is the tendon stiffness defined as:

$$k^t = \frac{F^m_{max}}{\left(\epsilon^t_0 l_{slack}\right)^2} \tag{A.11}$$

where $F^m_{max}$ is the maximum isometric force of the muscle and $\epsilon^t_0$ is the tendon characteristic strain, which is reported to be from 3-5 percent. The value of 4% is adopted for this model.

## A.5 Contraction Dynamics by Nagano and Gerritsen [5]

The force-length-velocity relations of the CE element based on the work by [5] are presented here. Similar formulations were also previously presented by [37,38]. Like most contraction dynamics models, this model consists of a piecewise formulation for the contraction velocity. The force-length-velocity relation for two cases of concentric contraction ($v^{ce} \leq 0$) and eccentric contraction ($v^{ce} > 0$) can be expressed as the following:

$$v^{ce} = \begin{cases} -\hat{a}\, l^{ce}_{opt} \left[ \dfrac{(f^{ce}_{isom} + A_{rel})B_{rel}}{\dfrac{f^{ce}}{a\, F^m_{max}} + A_{rel}} - B_{rel} \right] & v^{ce} \leq 0 \\ -l^{ce}_{opt} \left[ \dfrac{c_1}{\dfrac{f^{ce}}{a\, F^m_{max}} + c_2} - c_3 \right] & v^{ce} > 0 \end{cases} \tag{A.12}$$

where $\hat{a} = \min(1, \frac{10}{3}a)$, $A_{rel}$ and $B_{rel}$ are parameters that might depend on the ratio of the fast twitch fibers to all fibers, $f_{fast}$, [7] or training conditions [5] (adopted to be 0.41 and 5.2, respectively from [5, 14]).

The variable $f^{ce}_{isom}$ represents the normalized force-length relation, which can be written

as:

$$f_{isom}^{ce} = c\left(\frac{l^{ce}}{l_{opt}^{ce}}\right)^2 - 2c\left(\frac{l^{ce}}{l_{opt}^{ce}}\right) + c + 1 \tag{A.13}$$

with

$$c = -\frac{1}{width^2}$$

in which values of the parameter *width* are presented in Table 5.3 for eight muscle groups of the lower extremity.

The parameters of the eccentric relation can be formulated as:

$$\begin{aligned} c_1 &= \frac{\hat{a}B_{rel}(f_{isom}^{ce} + c_2)^2}{(f_{isom}^{ce} + A_{rel}\Gamma)} \\ c_2 &= -f_{isom}^{ce}\hat{f} \\ c_3 &= \frac{c_1}{f_{isom}^{ce} + c_2} \end{aligned} \tag{A.14}$$

where $\hat{f}$ is the asymptotic eccentric force, assumed to be 1.4 here based on [3], and $\Gamma$ is the slope of the force-velocity relation at zero velocity, which is 2 in references [5, 37, 38], but is set to be 1 here according to [14, 76]. This avoids difficulties in the convergence of the optimization problem.

# Appendix B

# Metabolic Energy Rate

The equations used for metabolic energy rate are taken from [7]. These equations are presented to phenomenologically model the metabolic energy rate for a muscle. According to the thermodynamics 2nd law, the net decrease rate in the internal energy of a muscle (or total muscle energy expenditure rate) consists of the heat generated and the rate of work done by the muscle, as follows:

$$\dot{E} = \dot{H} + \dot{W} \tag{B.1}$$

where the work rate is written in the form:

$$\dot{W} = -f_{ce}(l^{ce}, v^{ce}, a)v^{ce} \tag{B.2}$$

where $l^{ce}$, $v^{ce}$, and $f_{ce}$ are the length, velocity, and force of the contractile element, respectively in which $f_{ce}$ is always non-negative. It should be noted that this work is the one done by the contractile element only, which is different from the total muscle-tendon work. Muscle mass is calculated as follows:

$$m = \rho_m l^{ce}_{opt} \frac{F^m_{max}}{\sigma_m} \tag{B.3}$$

where $\rho_m$ is the muscle density and assumed to be 1059.7 kg/m$^3$, $l^{ce}_{opt}$ is the optimum length of the muscle fiber, $F^m_{max}$ is the muscle maximum isometric force, and $\sigma_m$ is the muscle specific tension and is assumed to be 0.25 MPa.

## B.1 Heat Rate by [6]

$$\dot{H} = \dot{A} + \dot{M} + \dot{S} + \dot{B} \tag{B.4}$$

where $\dot{A}$ is the activation heat rate, $\dot{M}$ is the maintenance heat rate, $\dot{S}$ is the shortening/lengthening heat rate, and $\dot{B}$ is the basal metabolic rate.

**1) Activation Heat Rate**

$$\dot{A} = \phi_{df} m[f_{fast}\dot{A}_{fast}u_{fast} + f_{slow}\dot{A}_{slow}u_{slow}] \tag{B.5}$$

where $m$ is the muscle mass, $f_{fast}$ and $f_{slow}$ are the ratio of the fast and slow twitch fibers to all fibers, $\dot{A}_{fast}$ and $\dot{A}_{slow}$ are constants and are assumed to be 133 W/kg and 40 W/kg respectively, and $u_{fast}$ and $u_{slow}$ are the contributions of the fast and slow twitch fibers in the total muscle excitation that can be calculated as follows:

$$\begin{aligned} u_{fast}(t) =& 1 - \cos(\pi/2u(t)) \\ u_{slow}(t) =& \sin(\pi/2u(t)) \end{aligned} \tag{B.6}$$

$\phi_{df}$ is called the decay function and is defined as follows:

$$\phi_{df} = 0.06 + e^{-t_{stim}u(t)/\tau_\phi} \tag{B.7}$$

where $\tau_\phi$ is the decay time constant and is set to be 45 ms; $t_{stim}$ is the total time the muscle excitation has been greater than 0.1.

**2) Maintenance Heat Rate**

$$\dot{M} = \psi_H(\tilde{l}^{ce})m[f_{fast}\dot{M}_{fast}u_{fast} + f_{slow}\dot{M}_{slow}u_{slow}] \tag{B.8}$$

where $\psi_H(\tilde{l}^{ce})$ is the following piecewise expression:

$$\psi_H(\tilde{l}^{ce}) = \begin{cases} 0.5\tilde{l}^{ce} & \tilde{l}^{ce} \leq 0.5 \\ \tilde{l}^{ce} & 0.5 \leq \tilde{l}^{ce} \leq 1 \\ -2\tilde{l}^{ce} + 3 & 1 \leq \tilde{l}^{ce} \leq 1.5 \\ 0 & 1.5 \leq \tilde{l}^{ce} \end{cases} \tag{B.9}$$

$\dot{M}_{fast}$ and $\dot{M}_{slow}$ are constants that are assumed to be 111 W/kg and 74 W/kg respectively.

**3) Shortening/Lengthening Heat Rate**

$$\dot{S} = -\alpha v^{ce} \tag{B.10}$$

where $\alpha$ is defined as below:

$$\alpha = \begin{cases} 0.16 f^{ce}_{isom}(a, l^{ce}) + 0.18 f^{ce} & v^{ce} \leq 0 \\ 0.157 f^{ce} & v^{ce} > 0 \end{cases} \tag{B.11}$$

where $f^{ce}$ is the force produced by the contractile element and is a function of muscle activation, contractile element length and velocity, and $f^{ce}_{iso}(a, l^{ce})$ is the $f^{ce}$ when the contraction velocity is zero.

**4) Basal Metabolic Rate**

$$\dot{B} = 0.0225m \tag{B.12}$$

## B.2 Heat Rate by [7]

$$\dot{H} = m\dot{h} \tag{B.13}$$

$$\dot{h} = \dot{h}_M + \dot{h}_{SL} + \dot{h}_A \tag{B.14}$$

where $\dot{h}_M$, $\dot{h}_{SL}$, and $\dot{h}_A$ are the maintenance, shortening/lengthening, and activation heat rates per unit mass, respectively. The final expression for the total mass-specific heat rate is as follows:
if $l^{ce} \leq l^{ce}_{opt}$

$$\begin{aligned} \dot{h} &= \dot{h}_{AM} \beta^{0.6} \xi \\ &+ \begin{cases} -\tilde{v}^{ce} \beta^{0.2} \xi (\alpha_{S(ST)} f_{slow} + \alpha_{S(FT)} f_{fast}) & \tilde{v}^{ce} \leq 0 \\ \alpha_L \tilde{v}^{ce} \beta \xi & \tilde{v}^{ce} > 0 \end{cases} \end{aligned} \tag{B.15}$$

if $l^{ce} > l^{ce}_{opt}$

$$\dot{h} = \dot{h}_{AM}\beta^{0.6}\xi(0.4 + 0.6f^{ce}_{isom}) + \begin{cases} -f^{ce}_{isom}\tilde{v}^{ce}\beta^{0.2}\xi(\alpha_{S(ST)}f_{slow} + \alpha_{S(FT)}f_{fast}) & \tilde{v}_{ce} \leq 0 \\ \alpha_L f^{ce}_{isom}\tilde{v}^{ce}\beta\xi & \tilde{v}^{ce} > 0 \end{cases} \tag{B.16}$$

where $f_{fast}$ and $f_{slow}$ are the ratio of the fast and slow twitch fibers to all fibers, and other variables are defined as follows:

$$\beta = \begin{cases} u & u > a \\ (u+a)/2 & u \leq a \end{cases} \tag{B.17}$$

$$\dot{h}_{AM} = 128f_{fast} + 25 \tag{B.18}$$

$$\alpha_{S(ST)} = \frac{100}{\tilde{v}^{ce}_{max(ST)}} \tag{B.19}$$

$$\alpha_{S(FT)} = \frac{153}{\tilde{v}^{ce}_{max(FT)}} \tag{B.20}$$

$$\alpha_L = 4\alpha_{S(ST)} \tag{B.21}$$

where $\tilde{v}_{ce}$ is the velocity of the CE divided by $l^{ce}_{opt}$, $f^{ce}_{isom}$ is the force-length relation of CE normalized by $F^{m}_{max}$, $\tilde{v}^{ce}_{max(FT)}$ and $\tilde{v}^{ce}_{max(ST)}$ are the maximum shortening velocity of fast twitch and slow twitch fibers divided by $l^{ce}_{opt}$, which are assumed to be 10 $s^{-1}$ and 4 $s^{-1}$, $\xi$ is a scaling factor, where values of 1.0 and 1.5 for $\xi$ are associated with a primarily anaerobic and aerobic movements, respectively. $\xi$=1.0 is adopted for the forearm model, whereas $\xi$ is assumed to be 1.5 for gait modelling. In addition, the term $-\alpha_{S(ST)}f_{slow}\tilde{v}^{ce}$ is not allowed to exceed 100 W/kg, and the total specific heat rate, $\dot{h}$, must be greater than or equal to 1.0 W/kg. This lower bound condition approximates the muscle energy rate when the muscle is least active, i.e., in resting state [108]. It should be noted that the variables $\alpha_{S(ST)}$, $\alpha_{S(FT)}$, and $\alpha_L$ are energy contents of the muscle tissue and are expressed in J/kg.